# Optimization of Multidimensional Equalizers Based on MMSE Criteria for Multiuser Detection


Sangar N.Qader

Electrical and Electronic School

Newcastle University

A thesis submitted for the degree of

*PhilosophiæDoctor (PhD)*

2016

# Abstract

This thesis is about designing a multidimensional equalizer for uplink interleaved division multiple access (IDMA) transmission. Multidimensional equalizer can be classified into centralized and decentralized multidimensional equalizer. Centralized multidimensional equalizer (MDE) have been used to remove both inter-symbol interference (ISI) and multiaccess interference (MAI) effects from the received signal. In order to suppress MAI effects, code division multiple access (CDMA) has been used with MDE to minimize the correlation between users' signals. The MDE structure can be designed using linear equalizer (MLE) or decision feedback equalizer (MDFE). Previous studies on MDE employed adaptive algorithms to estimate filter coefficients during the training mode, i.e. the symbol equalization was not optimal, for two users. In our work, we applied MDE on IDMA receiver for multipath selective fading channels and also derived new equations to obtain the optimal filter taps for both types of MDE equalizers, i.e. MDFE and MLE, based on the minimum mean square error (MMSE) criterion. The optimal filter taps are calculated for more than two users. Moreover, we investigated the performance of the optimal MDFE using both IDMA (MDFE-IDMA) and CDMA (MDFE-CDMA) detectors.

Generally, the MDE equalizer suffers from residual MAI interference effects at low signal-to-noise-ratios (SNR) due to the delay inherent in the convergence of the crossover filter taps. Therefore, a new decentralized multidimensional equalizer has been proposed to IDMA detector. Within design of decentralized equalizer, the convergence

problem has been resolved by replacing the crossover filters with parallel interference canceler (PIC) for removing MAI dispersion. The proposed decentralized multidimensional equalizer shows a higher efficiency in removing MAI interference when compared with existing receivers in the literature. However, this is achieved at the expense of higher computational complexity compared to centralized multidimensional equalization.

To My Family

# Acknowledgements

I would like to thank Dr.Charalampos Tsimenidis for his helpful supervision and enlightening support throughout the development and improvement of this thesis. His support has a valuable significance to reach the end of this thesis. I thank him for being patient and tolerating my weaknesses in written English.

I also give thanks to my supervisors Prof.Bayan Sharif and Dr.Martin Johnston for their continuous support and for sharing their great knowledge and experience.

I'm grateful to Khalid and Sardar families for their lasting support and care.

# Contents

**List of Figures** **xi**

**List of Tables** **xv**

**1 Introduction** **1**

1.1 Introduciton . . . . . 1

1.2 Literature review . . . . . 2

1.2.1 Development of Multiuser Communications . . . . . 2

1.2.2 Equalization . . . . . 4

1.2.3 Adaptive Equalization . . . . . 5

1.2.3.1 Linear Filters . . . . . 5

1.2.3.2 Non-Linear Adaptive Filter . . . . . 7

1.2.4 Multi-Dimensional Equalization . . . . . 8

1.3 Research Contributions . . . . . 9

1.4 Thesis Organization . . . . . 10

**2 Preliminaries: Channel Models, Channel Encoding and Equalization Techniques** **13**

2.1 Communication Channels . . . . . 13

2.1.1 Multipath Fading Channel model . . . . . 14

2.1.2 Shallow-Water Acoustic channel Model . . . . . 17

2.1.2.1 Attenuation . . . . . 18

2.1.2.2 Multipath Propagation . . . . . 20

2.1.2.3 Doppler shift . . . . . 21

2.2 Channel Encoding . . . . . 21

2.2.1 Convolution Coding . . . . . 22
2.2.1.1 Encoder . . . . . 22
2.2.1.2 Decoder . . . . . 24
2.2.2 Soft Input Soft Output Decoding (SISO) . . . . . 26
2.2.3 Turbo Coding . . . . . 30
2.2.3.1 Turbo Encoder . . . . . 30
2.2.3.2 Turbo Decoder . . . . . 30
2.3 Equalization Principles . . . . . 32
2.3.1 Linear Equalizer . . . . . 33
2.3.2 DFE Equalizer . . . . . 36
2.4 Joint Equalization and Decoding in an Iterative system . . . . . 39
2.4.1 Linear MMSE Turbo-Equalization . . . . . 44
2.4.2 Non-Linear MMSE Turbo-Equalization . . . . . 45
2.5 Chapter Summary . . . . . 48

**3 Multiuser Detection Schemes 49**
3.1 Introduction . . . . . 49
3.2 DS-CDMA Detection Schemes . . . . . 50
3.3 Signal Model . . . . . 50
3.4 Non-Iterative DS-CDMA Detection . . . . . 52
3.4.1 Optimal Detector . . . . . 52
3.4.2 Suboptimal Multiuser Detector . . . . . 52
3.5 Iterative CDMA Detection . . . . . 54
3.6 IDMA Detection Algorithm . . . . . 55
3.6.1 Signal Model . . . . . 56
3.6.2 IDMA on AWGN Channels . . . . . 57
3.6.3 IDMA Over Multipath Selective Channels . . . . . 60
3.6.4 Chapter Summary . . . . . 62

**4 Optimization and Analysis of Centralized Multi-dimensional Equalizers 63**
4.1 Introduction . . . . . 63
4.2 Optimal Centralized MDE-IDMA Receiver . . . . . 64
4.2.1 Multi-dimensional LE (MLE) . . . . . 65

4.2.2 Multi-dimensional DFE (MDFE) . . . . . 70
4.3 MDE and Multiuser detection . . . . . 75
4.4 Iterative Channel Estimation for Optimal MDE-MUD Receivers . 77
4.5 Simulation Results and Performance Comparisons . . . . . 78
4.5.1 Selective Fading Wireless Channels . . . . . 80
4.5.1.1 MLE-MUD . . . . . 80
4.5.1.2 MDFE-MUD . . . . . 83
4.5.1.3 Impact of Encoder Type . . . . . 84
4.5.1.4 Impact of Channel Estimation . . . . . 89
4.5.2 Performance Comparison in Underwater Shallow Channels 90
4.6 Chapter Summary . . . . . 93

**5 Decentralized Multi-Dimensional Equalization 95**
5.1 Introdution . . . . . 95
5.2 Iterative DDFE-MUD System . . . . . 96
5.3 Iterative PIC-DDFE-IDMA Detection . . . . . 97
5.3.1 PIC . . . . . 99
5.3.2 APP-DEC . . . . . 100
5.3.3 Optimal DFE Equalizer . . . . . 100
5.4 Iterative Channel Estimation . . . . . 105
5.5 Performance of PIC-DDFE-IDMA and Comparison with MDFE-IDMA . . . . . 107
5.6 Chapter Summary . . . . . 111

**6 Complexity and Performance analysis of Adaptive Multi-dimensional Equalizers 113**
6.1 Adaptive Centralized Mulit-Dimensional Equalizer . . . . . 114
6.2 Adaptive PIC-DDFE-IDMA . . . . . 120
6.3 Complexity Analysis . . . . . 123
6.4 Chapter Summary . . . . . 127

**7 Conclusions 129**

**References 133**

# List of Figures


1.1 A ultiuser transmission scenario in multipath fading channels. . . 2
1.2 Transversal filter structure. . . . . 6

2.1 The forms of wireless channel environments: LOS and NLOS . . . 14
2.2 Transmitted sequence. . . . . 15
2.3 Received sequence. . . . . 15
2.4 Tapped delay line channel model. . . . . 16
2.5 Impulse response of shallow water channel. . . . . 20
2.6 (3,1,3) convolutional encoder. . . . . 22
2.7 The systematic (3,1,3) convolutional encoder. . . . . 23
2.8 (2,1,4) convolutional encoder. . . . . 23
2.9 Trellis diagram of (2,1,4) code. . . . . 25
2.10 Encoding process for input sequence. . . . . 26
2.11 Notation. . . . . 26
2.12 SISO decoder. . . . . 28
2.13 Transitions corresponding to $u_t$. . . . . 29
2.14 Turbo encoder. . . . . 31
2.15 Turbo decoder. . . . . 32
2.16 Transmitter. . . . . 33
2.17 Linear equalizer structure. . . . . 33
2.18 DFE equalizer structure. . . . . 37
2.19 ML turbo equalization. . . . . 40
2.20 Iterative equalization using SISO and MAP decoder. . . . . 42
2.21 SISO-LE equalizer structure. . . . . 43
2.22 SISO-DFE equalizer structure. . . . . 46

## LIST OF FIGURES


3.1 Diagram of an uplink DS-CDMA system with $K$ users. . . . . 51
3.2 Optimum detector for $k$-user CDMA Gaussian channels. . . . . 52
3.3 Transmitter structure of coded CDMA system for $K$ users. . . . . 54
3.4 Structure of iterative CDMA receiver. . . . . 56
3.5 The transmitter components for the K users. . . . . 57
3.6 IDMA Reciever for AWGN channels. . . . . 58

4.1 Centralized MDE structure. . . . . 64
4.2 MLE structure. . . . . 65
4.3 MDFE Structure. . . . . 72
4.4 The IDMA and CDMA transmitter components of the $k$th user. . 75
4.5 The general multiuser MDE structure. . . . . 76
4.6 The iterative channel estimator structure. . . . . 78
4.7 Impulse and frequency response of the channels used in the simulations. . . . . 79
4.8 Optimal MLE-IDMA and MDFE-IDMA performances for various $\Delta$ values, where each 1 delay of $\Delta$ equals one symbol duration (Ts). 80
4.9 Performance of MLE-MUD receiver for different number of users in frequency selective channels. . . . . 81
4.10 The improvement of SINR in crossover feedback filters within MLE-IDMA iterations. . . . . 82
4.11 Performance of MDFE-MUD receiver for different number of users in frequency selective channels. . . . . 84
4.12 The improvement of SINR in crossover feedback filters within centralized MDFE-IDMA iterations. . . . . 85
4.13 Effect of lower coding rate on MDFE performance. . . . . 86
4.14 Performance comparison between optimal MLE-IDMA and MDFE-IDMA receivers employing 1/8 convolution coding. . . . . 86
4.15 Impact of FEC on MLE-IDMA systems performances. . . . . 87
4.16 Impact of FEC on MDFE-IDMA systems performances. . . . . 88
4.17 CLE-IDMA performance for perfect channel assumption and LS channel estimations. . . . . 89

4.18 MDFE-IDMA performance for perfect channel assumption and LS channel estimations. . . . . 90
4.19 Underwater shallow water transmission scenario. . . . . 91
4.20 Normalized channel impulse response for user one. . . . . 91
4.21 Normalized channel impulse response for user two. . . . . 91
4.22 Impact of feedback delay $\Delta$ on MLE-IDMA and MDFE-IDMA performances. . . . . 92
4.23 Impact of FEC on MLE-IDMA and MDFE-IDMA performances. . 93

5.1 The general multiuser DMDE structure. . . . . 96
5.2 BER vs. Eb/N0 performance of optimal DDFE-MUD system for 8 and 16 users in frequency selective channels. . . . . 97
5.3 The proposed iterative PIC-DDFE-IDMA receiver structure. . . . 98
5.4 BER vs. Eb/N0 performance of optimal PIC-DDFE-IDMA system for different number of users in frequency selective channels. . . . 102
5.5 MMSE curve for PIC-DDFE-IDMA for different number of users. 103
5.6 The improvement of SINR in crossover feedback filters within centralized PIC-DDFE-IDMA iterations. . . . . 104
5.7 The iterative channel estimator structure. . . . . 105
5.8 BER vs. Eb/N0 optimal PIC-DDFE-IDMA performance for LS and perfect channel estimations. . . . . 107
5.9 Effect of coding rate on PIC-DDFE-IDMA receiver for 8 users. . 109
5.10 Performance comparison between centralized and decentralized IDMA receivers for 1/8 convolution code. . . . . 109
5.11 mmse vs SNR Performance comparison between centralized and decentralized IDMA receivers for 1/32 convolution code, 8 users. 110
5.12 Performance comparison different coding types for PIC-DFE-IDMA in shallow water channels. . . . . 110

6.1 Adaptive MDFE-IDMA performances for two users. . . . . 115
6.2 Adaptive MDFE-IDMA performances for four users. . . . . 115
6.3 Adaptive MDFE-IDMA performances for eight users. . . . . 116
6.4 MMSE performance of adaptive MDFE-IDMA for two users. . . . 117
6.5 MMSE performance of adaptive MDFE-IDMA for four users. . . . 117

## LIST OF FIGURES


6.6 MMSE performance of adaptive MDFE-IDMA for eight users. . . 118
6.7 Two-user uplink transmission scenario. . . . . 119
6.8 BER vs. $E_b/N_0$ performance for DLE, DDFE, and MDFE in multipath fading channels. . . . . 119
6.9 Average least square error versus iteration number at $E_b/N_0$=10 dB (1 iteration= 1 symbol period). . . . . 121
6.10 Scatter plot of the equalized symbols for both users using MDFE at $Eb/N0$=10 dB. . . . . 121
6.11 BER vs. Eb/N0 performance comparison of PIC-DDFE-IDMA and MDFE-IDMA using optimal and adaptive algorithms. . . . . 122
6.12 Performance of PIC-DDFE-IDMA in underwater acoustic shallow channels . . . . . 122
6.13 BER vs. Eb/N0 of PIC-DDFE-IDMA and MDFE-IDMA for different numbers of users. . . . . 127
6.14 Performance comparison of optimal multiuser detectors for wireless channels. . . . . 128
6.15 Performance comparison of optimal multiuser detectors for two-user underwater acoustic channels. . . . . 128

# List of Tables

2.1 Power delay profile examples of ITU channel models. . . . . 16
2.2 Look up table for the convolutional encoder (2,1,4). . . . . 24

6.1 Complexity comparison between rake IDMA, MDFE-IDMA and PIC-DDFE-IDMA for K=8, L=16, It=8, $\text{It}_c$=4, $N_f$=$N_b$=$N_c$=16 utilizing NLMS algorithm. . . . . 125
6.2 Complexity comparison between rake IDMA, MDFE-IDMA and PIC-DFE-IDMA for K=8, L=16, It=8, $\text{It}_c$=4, $N_f$=$N_b$=$N_c$=16, $N_o = N_f + N_b$, $N_\bullet = (K-1)N_c + N_o$ utilizing RLS algorithm. . . 126

## LIST OF TABLES

# 1

# Introduction

## 1.1 Introduciton

With higher demand of using personal communications utilities, the communications technologies have experienced a significant development in recent years. To support this upswing of communication systems market, the communication systems must cope with the formidable challenges that stem from channel fading, multipath effects and multiaccess interference. The design of channel equalization and multiaccess techniques has a significant effect in developing low complexity systems that can eliminate channel disruptions, and in turn, communicate at high data rate.

Within high-speed transmission in multiaccess communication scenarios, the equalization process for multipath selective channels is an important issue, such that, it needs to be able to remove both intersymbol interference (ISI) and multiple access interference (MAI), simultaneously. The multipath fading characteristic of the communication channel and the multiuser transmission are the main reason behind producing ISI and MAI, respectively. ISI is often neglected for low-rate multiuser systems [1]. However, for high-rate systems, ISI cannot be ignored. In fact, the ISI with MAI represent the main obstacle to the overall system performance [2].

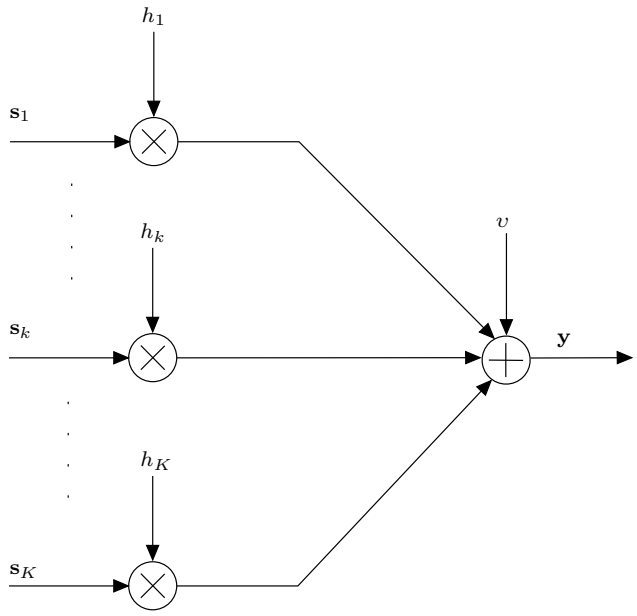


**Figure 1.1:** A ultiuser transmission scenario in multipath fading channels.

## 1.2 Literature review

### 1.2.1 Development of Multiuser Communications

When digital modulated symbols are transmitted through multipath fading channels, the induced ISI of the received signal is the main reason for the high Bit Error Rates (BER). However, in multiuser transmission environments, MAI has an equally significant impact as ISI, thus, both effects should be jointly eliminated at the receiver.

Within multiuser communications, multiple transmitters are enabled to send information simultaneously through multipath fading channels as shown in Fig.1.1. The multiuser communication technique had been firstly invented by Thomas A. Edison in 1873 to transmit two telegraphic messages in the same direction through the same wire [3]. Nowadays, there are many types of multiuser communication systems in which their receivers obtain the superposition of the signals sent by the active different transmitters occur unintentionally owing to non-ideal effects [4].

The basic multiuser techniques are frequency division multiple access (FDMA)[5],

time division multiple access (TDMA), code division multiple access (CDMA), and interleaved division multiple access (IDMA). In FDMA, each user employs a specific frequency band for transmission. This system has been used in 1G mobile phone systems such as advanced mobile phone systems (AMPS). While in TDMA, the users are distinguished employing a specific time slot for each user to prevent interference between users [6]. TDMA is used in 2G mobile communications known as global system for mobile communications (GSM) .

On other hand, in CDMA systems, each user employs specific spreading code with good auto-correlation and cross-correlation properties that enables the receiver to successfully separate the user's data symbols; for this reason, many researchers have used this system as a multiuser detection (MUD) in multipath delay spread channels [7] [8] . This means that all users can utilize the whole bandwidth and time resources at the same time [9].

Interleave division multiple access (IDMA) is a recent multiple access technique for new wireless communication systems, which unlike CDMA, it employs distinct chip-level interleavers to separate each user's data[6]. The IDMA receiver uses a simple chip-by-chip iterative MUD strategy for jointly removing ISI and MAI. Thus the complexity of the MUD in an IDMA system is a linear function of the number of users [10] and is much simpler than the MUD algorithms used in CDMA systems . Moreover, within the coded iterative turbo receiver design, IDMA showed higher performance than CDMA receiver for multipath fading channels [11].

During last few years, many works have been undertaken around IDMA topic in terms of the type of channel coding, detection algorithm and equalization techniques. Generally, within IDMA receiver, the symbol detection taken place by exchanging extrinsic information between Gaussian Chip Detector (GCD) and Soft Input Soft Output (SISO) decoders, while in [12], Probablistic Data Association (PDA) has been employed instead of GCD to provide lower complexity and faster convergence of the turbo receiver. On other hand, the easily integration of IDMA receiver with Orthogonal Frequency Division Multiplexing (OFDM) [13] and Multi Input Multi Output (MIMO) systems [14] to produce parallel flat fading subchannels in frequency selective channels and higher channel diversity,

respectively, have encoraged reserachers to propose more techniques and algorithms that can improve system performance regarding to OFDM-IDMA and MIMO-OFDM-IDMA systems [15] [16].

OFDM-IDMA combines advantes of OFDM and IDMA to jointly mitigating ISI and MAI interferences, however, it also suffers from high sensitivity to carrier frequency offsets (CFO) caused by the Doppler shift or the mismatch between the local oscillators of transmitter and receiver [17]. Especially for uplink OFDM-IDMA transmission, although the desired user's CFO can be compensated by a signle user detector, however, the residual CFOs from other users are still introduce an additional interference. New schemes have been proposed to mitigate CFO and improve detection in OFDM-IDMA system [18] for multipath fading channels, however, for fast fading time selective channels, the effect of CFO interference on the received signal grows significantly. Therefore, applying time domain equalization for jointly removing MAI and ISI in uplink IDMA system is better solution to prevent CFO and provide higher equalization efficiency.

### 1.2.2 Equalization

The speed of data transmission over multipath fading channels is usually limited by channel distortion that causes ISI in single user transmission scenario or both ISI and MAI in multiuser transmission systems. Practically, the channel impulse response is unknown. However, training symbols can be utilized for estimating channel impulse response, and in turn, it could be used to remove channel effects on the received signal by implementing an inverse filter. This is the aim of using equalizers.

When more than one version of the transmitted signals arrive to the receiver with different delay times, it implies that there are several propagation paths between the transmitter and the receiver, which are referred to as multipath phenomenon. This phenomenon can be modeled by a finite impulse response (FIR) filter. The multipath channels have a significant effect on the system performance, thereby providing another good reason for channel equalization [19].

The objective of the equalizer is to calculate the taps of a filter such that the convolution of the impulse response of the equalizer filter and the channel impluse

response results in producing 1 at the center tap and have nulls at the other points within the filter span. The filter coefficients can be formulated by utilizing two main techniques: automatic synthesis and adaptation [20]. In the first method, the error signal is obtained by comparing the received training signal with the stored training signal which is used later to determine the coefficient taps of the inverse filter. However in the second method, the error signal is calculated by subtracting the output of the equalizer and the output of the decision device. Although, the training symbols have benefit in determining channel characteristics, however, it also present main drawback in producing transmission overhead[21].

### 1.2.3 Adaptive Equalization

Adaptive equalization is an effective process that mitigates the received signal dispersion caused by signal propagation in multipath channels [22]. Adaptive filters are the main part within adaptive equalization and they can offer a performance improvement over filter designs when *a priori* knowledge of a process and its statistics are available. Hence, they have been used in many applications such as communications, control, robotics, sonar, radar, seismology and biomedical engineering. In general, the filtering process can be characterized by filtering, smoothing, prediction and deconvolution processes [23], also according to their transfer function types they can be categorized as linear and non-linear filters.

#### 1.2.3.1 Linear Filters

A linear adaptive filter has a linear transfer function such that the input and the output are related with a linear combination at any moment in time between adaptation operations [24]. There are three types of linear adaptive structures commonly used

- Transversal
- Lattice predictor
- Systolic array.

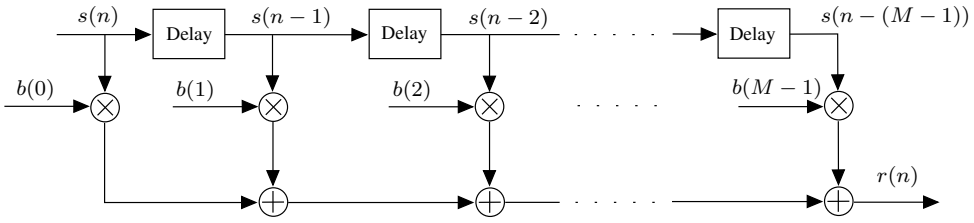


**Figure 1.2:** Transversal filter structure.

Guarantee of stability and global convergence are two good properties of transversal linear filters which made it more popular than the other types. It is sufficient to say that for a given $M$th order FIR filter, given in Fig.1.2, the output sequence $r(n)$ can be defined as follows

$$r(n) = \sum_{k=0}^{M-1} b(k)s(n-k), \tag{1.1}$$

where $b(k)$ are fixed filter coefficients, value $n$ represents the current discrete-time instant, and $(n-k)$ represents the previous $k$th instant. Whenever the filter coefficients are known, then the FIR filter can be completely defined. These coefficients can be determined using optimal solutions or employing adaptive algorithms.

There is no unique adaptive algorithm for linear filtering problems. However, based on the problem requirements, various algorithms and approaches have been proposed such as stochastic gradient approach and least square estimation (LSE) [25].

**Stochastic Gradient Approach** - This approach utilizes a transversal structure. The optimization of transversal weights is taken place by using least mean square (LMS) algorithm. The LMS algorithm is defined by the following equation

$$\mathbf{w}(k+1) = \mathbf{w}(k) + 2\eta e(k)\mathbf{s}(k), \tag{1.2}$$

where

$$\mathbf{w}(k) = [w_1, w_2, \ldots, w_p]^T, \text{ the tap weight vector,}$$

$$\mathbf{s}(k) = [s_1, s_2, \ldots, s_p]^T, \text{ the tap vector,}$$

$\eta$ is the learning rate parameter and the obtained error $e(k)$ is a scalar error which is given by

$$e(k) = s(k) - \hat{s}(k) \tag{1.3}$$

where $\hat{s}(k)$ is the estimated transmitted symbol. The LMS algorithm known to be slow to converge and dependent on the ratio of the largest to smallest eigenvalue of the correlation matrix of the tap inputs. Nevertheless, because of it's simplicity, it is the most popular algorithm and under right conditions can perform very adequately.

**Least Square Estimation (LSE)** - Block estimation and recursive estimation are the two methods used for formulating LSE algorithm which minimizes the sum of square errors between the desired and the actual filter output. In the first method, the blocks of equal time length are constructed from the input data sequence and processing proceeds block by block. While the second method uses the idea of state and it could be seen as a special case of Kalman filter. The general term of Kalman filtering can be defined as follows [25]

$$\mathbf{x}(k+1) = \mathbf{x}(k) + \mathbf{K}(k)\mathbf{i}(k), \tag{1.4}$$

where $\mathbf{K}(k)$ is the Kalman gain matrix at instance $k$, $\mathbf{i}(k)$ is the innovation vector at instance $k$, and $\mathbf{x}(k)$ is the state of instance $k$. The vector $\mathbf{i}(\mathbf{k})$ consists of the new information that is presented to the filter for instance $k$.

#### 1.2.3.2 Non-Linear Adaptive Filter

Non-linearity refers to the lack of linear combination between input and output at any moment in time [26][27]. The applications of signal processing are often assuming system linearity, however, in practice, the system performance is limited by the non-linearity characteristic. Thus, more concern has been given to design non-linear filters. Volterra filter [28] is an example of nonlinear adaptive filter which can be seen as a type of polynomial extension to the linear adaptive

filter. Volterra filter can keep its output linear with respect to high power impulse responses or system coefficients. Although utilizing nonlinear filters will improve the learning efficiency, however, this comes at the expense of more complex mathematical analysis of the problem.

### 1.2.4 Multi-Dimensional Equalization

Within multiuser equalization, in addition to using the previously detected symbols of the user of interest, estimates of the current symbols of the remaining active users are also required to jointly remove both MAI and ISI effects [29] for the current symbol detection. Blind equalization, which only needs a received signal and desired output signature, has been used with DFE in such situations [7].

Multidimensional equalizers are typically proposed to reduce the adjacent channel interference that can often appear in mobile data transmission [30]. This method has been exploited with two user transmission for co-channel interference suppression [8]. In these receivers, referred to as centralized equalizers, the MAI has been subtracted by using crossover filters in conjunction with CDMA or IDMA. On the other hand, decentralized equalizers are obtained by removing the crossover filters.

An IDMA detector with DFE multidimensional equalization has been proposed in [31] for downlink scenarios in underwater acoustic channels. In this system, the summation of the users' data headed by a common sequence of training symbols constructs the transmitted signal frames to be sent through the channel. Since the signal frame arriving at a specific user experiences the same channel characteristics, a single DFE equalizer is sufficient to remove the ISI from the received signal, while the MAI can be cancelled by IDMA detection. However, this approach cannot be applied to uplink scenarios, where the transmission of each user arrives at the base-station via distinct multipath channels.

## 1.3 Research Contributions

This work mainly concentrates on the solution to the equalization problems in multiuser systems for uplink scenario. First we proposed a centralized multi-dimentional equalizer for two user IDMA uplink system in shallow water acoustic channels [32]. Within centralized equalization, ISI is eliminated by using feed-forward and feed-backward filters, while, MAI is removed using crossover filters. A new mathematical derivation has been derived for calculating the optimal filter coefficients. Then, the optimal equalizer is applied to the wireless channel environment for more than two users.

Although the proposed multi-dimensional equalizer provides higher system performance than usual rake IDMA and traditional CDMA receivers, however, it suffers from delay in converging filter taps which results in decreasing system performance, especially, at low SNR values. For this reason, A new decentralized multi-dimensional equalizer has been designed for uplink multiuser systems by replacing cross-over filters with parallel interference canceller (PIC) technique. A comprehensive study on the receiver design, performance analysis, optimization solutions and complexity comparison are also presented for both the proposed receivers. More specifically, the contributions can been listed as follows:

- The centralized multidimensional equalizer structure outlined in Chapter 4. The equalizer was employed with CDMA for two-users in shallow water acqoustic channels and adaptive algorithm has been used for determining filter taps. This thesis designed an iterative centralized multidimensional equalizer that uses IDMA. The two-user uplink scenario for shallow water acoustic channels is considered in [33]. At the receiver, for each user, a DFE equalizer has been used before IDMA detection. The IDMA detector iteratively returned the hard limited symbol to the equalizers to optimize the cost function employed in the adaptive algorithm.

- New derivations for calculating optimal filter taps are also presented in the Chapter 4. The derivations are given for both linear and DFE equaliz-

ers. Moreover, that optimal solution could be applied to both IDMA and CDMA.

- Due to delay in converging filter taps, especially cross-over filters, the centralized equalization provides low performance at low SNR values. Hence, a new decentralized multidimensional equalizer is proposed in Chapter 5. A new IDMA receiver has been applied to wireless multipath fading channels in [34] and shallow water acoustic channels in [35]. The proposed receiver is a mixture between Rake IDMA and decentralized multidimensional equalizer such that it utilizes a PIC to eliminate MAI impairments, while it applies DFE equalization to overcome ISI effects for each user. The design of such a receiver obtain high system performance and lower system complexity compared to the centralized and Rake receivers.

## 1.4 Thesis Organization

The remaining of the thesis is organized as follows.

Chapter 2 provides preliminaries on channel models, channel encoding and fundamentals of equalization techniques. Firstly, the models of both wireless fading and shallow water acoustic channels have been reviewed. Several characteristics of the channels are elaborated. Two types of channel encoding are presented which are convolution and trubo coding. Also the fundamentals of linear and DFE equalization techniques have been described. Moreover, joint equalization and decoding in an iterative system are illustrated for achieving higher system performance in multipath fading channels.

Chapter 3 is devoted to multiuser detection schemes, i.e CDMA and IDMA. The basic structure of both CDMA and IDMA are outlined. The iterative scheme of CDMA detection has been illustrated. The fundamental equations of IDMA for both additive white Gaussian noise (AWGN) and multipath selective channels are also provided.

Chapter 4 develops centralized multidimensional equalizer method to be applied to iterative CDMA and IDMA receivers. The optimization problem for centralized multidimensional equalizers employing linear and DFE principles is

also solved, such that the determined filter coefficients give optimal performance. Comprehensive comparisons between CDMA and IDMA are carried out utilizing the proposed centralized multidimensional equalizer.

Due to delay in converging filter taps in centralized multidimensional equalizer schemes, the IDMA detector suffers in performance due to the remaining MAI effects in crossover filter taps. Thus, Chapter 5 provides a new decentralized multidimensional equalizer for IDMA detection which totaly depends on PIC operation to remove MAI dispersion. The structure of the proposed IDMA receiver is presented and its system performance is compared to the centralized IDMA detector for both wireless and shallow water acoustic channels.

Chapter 6 focuses on applying adaptive algorithms on the two proposed multidimensional equalizers for IDMA detector. The adaptive receivers are also compared with rake IDMA receiver in terms of complexity.

Finally, conclusions are presented in Chapter 7 and the thesis ends with a possible line of future work.

# 2

# Preliminaries: Channel Models, Channel Encoding and Equalization Techniques

This chapter provides a general introduction to channel models, channel encoding, MMSE equalization (LE and DFE) , and turbo equalization techniques. Channel models for both wireless and underwater shallow channels are presented, as the system performance of the proposed systems in later chapters in this thesis are evaluated for both channels. The principles of convolution and turbo coding are then explained. Furthermore, the fundamentals of MMSE equalization are presented for both LE and DFE. Finally, the turbo equalization technique is reviewed and the formulas for finding optimal filter taps are derived for both linear and non-linear MMSE turbo equalizers.

## 2.1 Communication Channels

The purpose of any communication system is to transmit the information signals from one point to another. The medium over which the information signals are transmitted is called communication channel which can be wire line, optical cable, wireless radio channel or acoustic channel. When data information are transmitted through the channel, it is subject to an assortment of changes. These

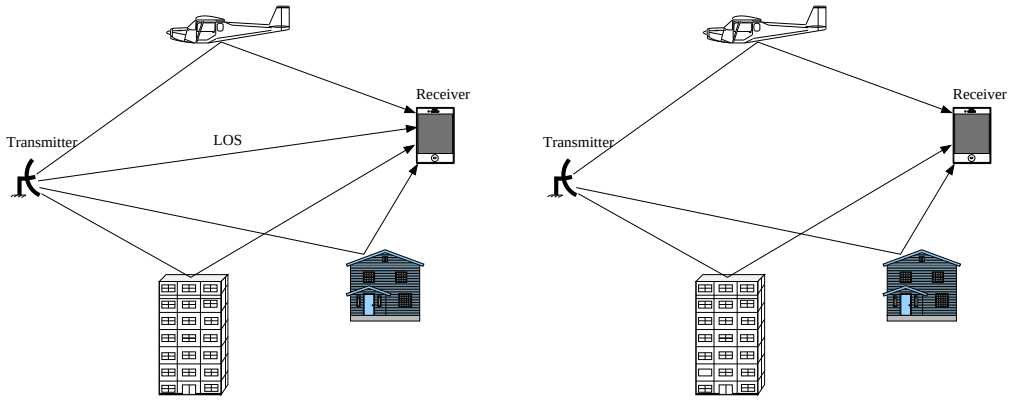


**Figure 2.1:** The forms of wireless channel environments: LOS and NLOS

changes could be deterministic, i.e attenuation, linear and non-linear distortion, or probabilistic, i.e additive noise, multipath fading, etc.

### 2.1.1 Multipath Fading Channel model

Line-of-sight (LOS) and non line-of-sight (NLOS) are two general forms of wireless channels. The absence of the direct line between the transmitter and the receiver in NLOS is the only characteristic that makes it differ from LOS. The pobability density function (PDF) follows Rician and Rayleigh distribution in LOS and NLOS, respectively [36]. Fig. 2.1 depicts these two different environments. In LOS channels, the antennas receive the signal via direct path and also via different propagation paths which are created due to reflections, diffraction and scattering from natural and manmade objects. However, in an urban environment, the absence of a direct line propagation due to surrounding obstacles results in arriving signals only from the multipath propagation paths. These multipath components, have a randomly distributed amplitudes, phases and angles of arrival signal such that their combination at the receiver results in a signal that can vary widely in both amplitude and phase. This phenomenon is called fading.

The signal reflections, changing of Doppler shifts and delays of multipath propagation are generally the three main effects of the fading multipath channels on the transmitted signal . During arrival of a number of the attached symbols

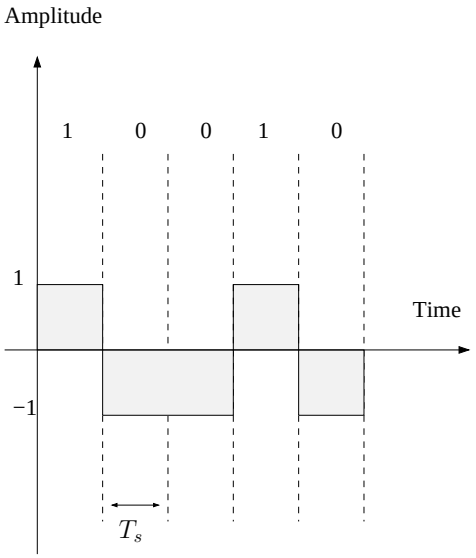


**Figure 2.2:** Transmitted sequence.

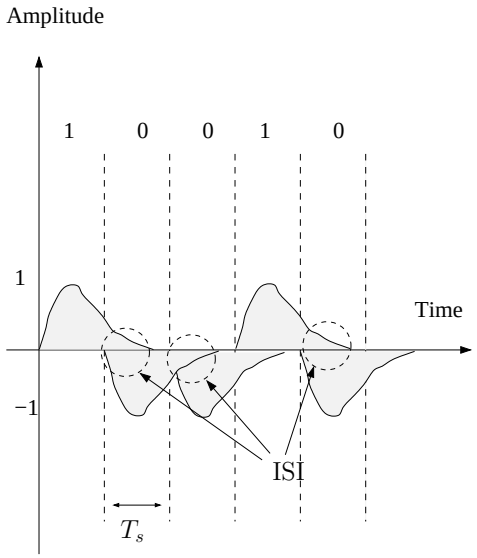


**Figure 2.3:** Received sequence.

at the same time to the receiver via various multipath propagation, the receiver simply adding them together at every time instants, which inturn, results in producing inter symbol interference (ISI). Fig. 2.3 illustrates the effect of ISI on the transmitted data sequence 10010 shown in Fig. 2.2 over a fading multipath channel.

A tapped delay line (TDL) can be employed to model the multipath channels as given in Fig. 2.4 and its characteristics are often specified by a power delay profile (PDP). The pedestrian and vehicular PDP by ITU are given in Table 2.1, in which each path is distinguished by its relative delay and average power. The relative delay is an excess delay with respect to the reference time while the average power for each path is normalized by that of the first path [37].

Several small scale multipath channel parameters such as mean excess delay, root mean square (RMS) delay spread and excess delay spread which define the channel time dispersive properties can be obtained from the PDP. *Mean Excess Delay* ($\overline{\tau}$) is the first moment of PDP and is defined as [38]

$$\overline{\tau} = \frac{\sum_l a_l^2 \tau_l}{\sum_l a_l^2} = \frac{\sum_l \tau_l P(\tau_l)}{\sum_l P(\tau_l)}, \tag{2.1}$$

where $\tau_l$ denotes the channel delay of the $l^{th}$ path while $a_l$ and $P(\tau_l)$ denote the amplitude and power, respectively.

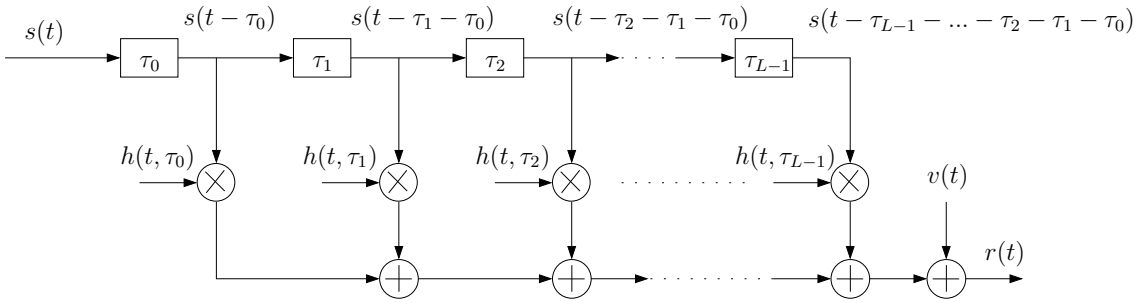


**Figure 2.4:** Tapped delay line channel model.

**Table 2.1:** Power delay profile examples of ITU channel models.

| Tap | Pedestrian | | Vehicular | |
|---|---|---|---|---|
| | Relative Delay (ns) | Average Power (db) | Relative Delay (ns) | Average Power (db) |
| 1 | 0 | 0 | 0 | 0 |
| 2 | 110 | -9.7 | 310 | -1 |
| 3 | 190 | -19.2 | 710 | -9 |
| 4 | 410 | -22.8 | 1090 | -10 |
| 5 | - | - | 1730 | -15 |

While, the root of second central moment of PDP is called RMS delay ($\sigma_\tau$) and its defined as

$$\sigma_\tau = \sqrt{\overline{\tau^2} - (\overline{\tau})^2}, \tag{2.2}$$

where

$$\overline{\tau^2} = \frac{\sum_l a_l^2 \tau_l^2}{\sum_l a_l^2} = \frac{\sum_l \tau_l^2 P(\tau_l)}{\sum_l P(\tau_l)}. \tag{2.3}$$

The characterization of the channel in time domain is defined by employing delay spread parameters. However, in frequency domain the channel is characterized by the coherence bandwidth ($B_c$) which is the range of frequencies over which the signal strength remains more or less unchanged. In general, the relation between $B_c$ and RMS delay is an inverse proportion, that is [38]

$$B_c \approx \frac{1}{\sigma_\tau}. \tag{2.4}$$

If a bandwidth with correlation of 0.9 or above is defined for presenting the

coherence bandwidth, then

$$B_c \approx \frac{1}{50\sigma_l}, \tag{2.5}$$

while if a correlation of 0.5 or above is taken, then the coherence bandwidth is given as

$$B_c \approx \frac{1}{5\sigma_l}. \tag{2.6}$$

The characteristics of the transmitted signal and the properties of the channel are the two main factors for identifying the type of channel fading. The channel is called frequency selective fading channel when the bandwidth of the transmitted signal is greater than bandwidth over which the frequency response of a mobile channel has a constant gain and linear phase, i.e $B_c < B_s$ or $T_s < \sigma_\tau$ where $T_s$ and $B_s$ are the symbol period and bandwidth of the transmitted signal. Thus, frequency selective fading is a result of the time dispersion of the transmitted symbol within the channel.

On the other hand, the movement of the transmitter or reciever results in changing the channel response within a symbol period transmission, thus the signals transmit through a time-selective fading channel. The rapid variation of impulse response leads to a spread in the frequency domain which is known as a Doppler shift. If maximum Doppler shift denotes as $(f_m)$, then the Doppler bandwidth is given as $B_d = 2f_m$. In general, the coherence time is related to Doppler spread as

$$T_c \approx \frac{1}{f_m}. \tag{2.7}$$

The channel behaves as fast fading under the following conditions:

$$T_s > T_c \qquad \text{and} \qquad B_s < B_d,$$

while, it behaves as slow fading when

$$T_s \ll T_c \qquad \text{and} \qquad B_s \gg B_d.$$

### 2.1.2 Shallow-Water Acoustic channel Model

The underwater acoustic channel is another example of multipath medium where the signal transmits through reflections from the surface and the bottom of the

sea. In addition, it can be a time-varying channel due to the motion of the transmitter or the receiver during transmission or due to medium variability. The wave propagation in an underwater channel is mainly affected by channel variations, multipath propagation and Doppler shift with an adverse impact on achieving high data rates and transmission robustness. Furthermore, the usable bandwidth of an underwater channel is typically a few kHz at large distances. In order to achieve high data rates it is natural to employ bandwidth efficient modulation.

Most researches on underwater acoustic channels are focused on mathematical models which are mainly characterized as shallow water multipath and deep vertical channels [39]. Shallow water channels are presented into two models: random time-varying filter and random statistical channel model [40], based on ray theory [41][42]. Most practical applications are preferred ray theory model over random statistical channel model due to the independency of ray trajectories on the interested used frequency [43][44].

In a shallow water channel, the acoustic waves travel through a LOS path also by bouncing from the surface and bottom [45]. The propagation of acoustic signals can be roughly estimated over a shallow water by simplifying the environment parameters. If the surface and bottom of the water are assumed to be smooth, then the expected propagation paths for the acoustic waves can be geometrically calculated. In general, the parameters which are mainly affecting the underwater communications are

#### 2.1.2.1 Attenuation

The spreading and absorption are the main losses that attenuate the transmitted signal in shallow water channels. According to inverse square law, the attenuation is proportional to $\frac{1}{L^2}$, where $L$ is the distance between the transmitter and the receiver, for LOS propagation. As $L$ increases, propagation occurs via reflection at the sea surface and floor boundaries where the attenuation is proportional to $\frac{1}{L}$, and this is called cylindrical spreading. The total transmission losses (TL) for cylindrical spreading can be expressed as [46]

$$\mathrm{TL}(f) = 10\log_{10}(L) + a(f)L \times 10^{-3}, \tag{2.8}$$

where $a(f)$ is the attenuation coefficient in dB/km and can be computed as [47]

$$a(f) = Af^2 + \frac{Bf_o}{1 + \left(\frac{f_o}{f}\right)^2} + \frac{Cf_1}{1 + (f_1/f)^2}, \tag{2.9}$$

where

$$A = 2.1 \times 10^{-10}(T - 38)^2,$$

$$B = 2S \times 10^{-5}$$

and

$$C = 1.2 \times 10^{-4}$$

are fresh water attenuation, magnesium sulphate relaxation and boric acid relaxation, respectively, $S$ is the salinity in parts per thousand and $f$ is the operating frequency in KHz. Additionally

$$f_o = 50(T + 1),$$

$$f_1 = 10^{\frac{T-4}{100}},$$

where $T$ is the temperature in Celsius. In practice, absorption losses can be determined by [48]

$$a(f) < 10\text{dB}. \tag{2.10}$$

On the other hand, another factor in shallow water channels that has a great impact on the system performance is ambient noise. The ambient noise exists in specific places in the background of the sea such as snapping shrimp in warm waters, and also it comes from rain, breaking waves and distant shipping. The spectral density of ambient noise decreases significantly over a range of operating frequencies, hence, it is not white. The comprehensive analysis of different underwater channels can be found in [49].

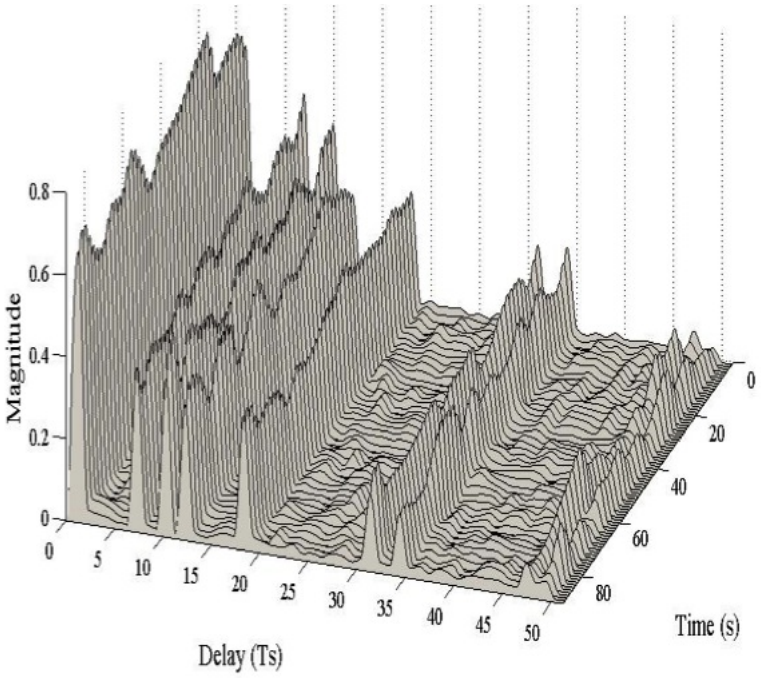


**Figure 2.5:** Impulse response of shallow water channel.

#### 2.1.2.2 Multipath Propagation

The phenomenon of multipath within an underwater acoustic channel is mainly produced by the geometry of the water environments. The water environments include different reflectors and scatters, bottom boundaries, surface reflectors, and heterogeneity of sea water. The multipath underwater channels are usually time-varying channels, thus it is impulse responses can be characterized as doubly spread. Doubly spread referred to delay and Doppler spread. Frequency selective fading and time dispersion are the two main effects of the delay spread, while Doppler spread results in creating frequency dispersion and time-selective fading effects. The multipath delay profile of a shallow water channel depicted in Fig.2.5 is experimentally obtained by sea-trials conducted by Newcastle University in the North Sea.

#### 2.1.2.3 Doppler shift

Doppler shift is produced by the movement of the transmitter or receiver and varying reflections at the surface and bottom of the sea. The reflection and scattering of sound waves on the surface of the sea is based on the Rayleigh parameter [47]. Rayleigh parameter can be calculated as

$$R = \frac{2\pi\rho sin\phi}{\lambda}, \tag{2.11}$$

where $\lambda$ is the wavelength of the sound wave, $\rho$ is the rms roughness wave height, and $\phi$ is the grazing angle. For $R << 1$ indicates the surface is perfectly smooth and behaving principally as reflector. In contrast, for rough surface, the Rayleigh coefficient $R >> 1$, and the surface acts as a scatterer. The reflection loss can be computed as

$$\mu_R = 20\log_{10}R. \tag{2.12}$$

In general, there is a vast difference in complexity between the signal reflections on the surface of the sea and the seabed. The high changing of the acoustic properties in the bottom and the gradual changing of the sound velocity and density due to layered bottom makes seabed more complex than the sea surface.

## 2.2 Channel Encoding

Within communication systems, the prime requirement of transmitting information over multipath channels is reliability. Hence, the channel encoding techniques have occupied a high interesting by the researchers in modern communication systems. The detection capability and error correction are the main two characteristics for good coding schemes. In this section, we will give a brief introduction into the field of channel coding. To this end, we will describe two common channel encoders which are widely used in communication systems. These encoders are based on convolution coding and turbo coding which are mainly employed in our proposed receivers in the following chapters.

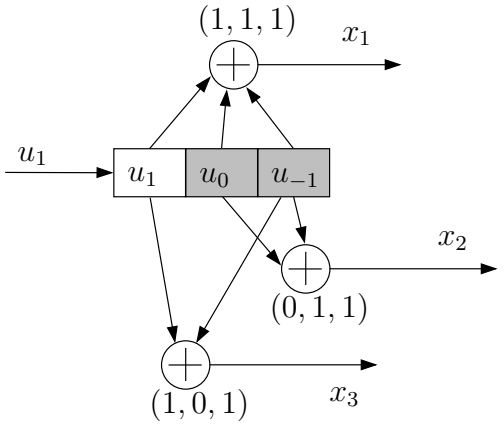


**Figure 2.6:** (3,1,3) convolutional encoder.

## 2.2.1 Convolution Coding

### 2.2.1.1 Encoder

The convolutional codes generally are specified by

$$N = \text{number of output bits},$$
$$K = \text{number of input bits},$$
$$M = \text{number of memory registers}.$$

The efficiency of the code can be measured by the code rate $(K/N)$. Fig. 2.6 depicts a (3,1,3) convolutional encoder with rate 1/3. The module-2 adders are the generators for the three outputs, and their inputs are selected by a specific generator polynomial (g) for each output bits, that is

$$x_1 = \text{mod2}(u_1 + u_0 + u_{-1}),$$
$$x_2 = \text{mod2}(u_0 + u_{-1}),$$
$$x_3 = \text{mod2}(u_1 + u_{-1}).$$

The polynomials can create codes having completely different properties. For any $M$ order code, there are many choices for polynomial which will not all result in output codes with good error protection properties. The complete list of these polynomials can be found in [50].

States are referred to the number of combination bits in the shaded registers and are defined by

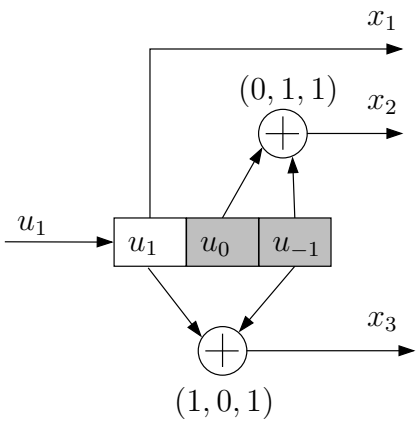


**Figure 2.7:** The systematic (3,1,3) convolutional encoder.

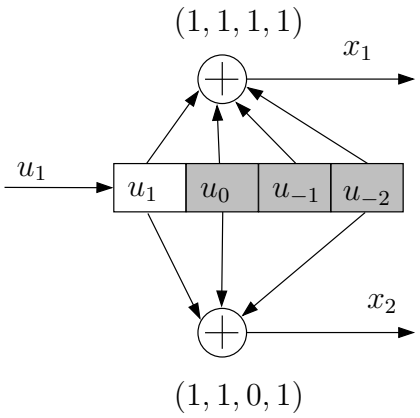


**Figure 2.8:** (2,1,4) convolutional encoder.

$$\text{Number of states} = 2^{\text{L}},$$

where L represents the constraint length of the code and it is equal to $K(M-1)$. The shaded registers in Fig. 2.6 have a constraint length of 2. The convolutional code could be systematic or non-systematic. In systematic convolution coding, the known sequence of the input bits are forwarded with the output bits. The systematic version of Fig. 2.6 is shown in Fig. 2.7. Even though both types of convolution codes have the same protection properties, however, systematic codes are preferred over non-systematic due to less hardware requirement for encoding, quick looking permission and the absence of catastrophically error propagation. Thus, systematic convolution codes are used in Trellis Coded Modulation (TCM) and turbo codes.

Table lookup mechanism is usually employed for encoding purpose which consists of the input bits, the output bits and the state of the encoder. Table 2.2 gives the look up table for (2,1,4) convoultional code shown in Fig. 2.8.

State, tree and trellis diagrams are three ways to look at the encoder and understand the operation of encoding. Trellis diagram is the most preferred over the others because it represents linear time sequencing of events. Within the trellis diagram, the x-axis is discrete time and all possible states are shown on the y-axis. Each horizontal transition indicates arrived bits, and each transmitted code word has its own trellis diagram. The trellis diagram always starts at state

**Table 2.2:** Look up table for the convolutional encoder (2,1,4).

| **Input Bit** | Input State | | | Output Bits | | Output State | | |
|---|---|---|---|---|---|---|---|---|
| 0 | 0 | 0 | 0 | 0 | 0 | 0 | 0 | 0 |
| 1 | 0 | 0 | 0 | 1 | 1 | 1 | 0 | 0 |
| 0 | 0 | 0 | 1 | 1 | 1 | 0 | 0 | 0 |
| 1 | 0 | 0 | 1 | 0 | 0 | 1 | 0 | 0 |
| 0 | 0 | 1 | 0 | 1 | 0 | 0 | 0 | 1 |
| 1 | 0 | 1 | 0 | 0 | 1 | 1 | 0 | 1 |
| 0 | 0 | 1 | 1 | 0 | 1 | 0 | 0 | 1 |
| 1 | 0 | 1 | 1 | 1 | 0 | 1 | 0 | 1 |
| 0 | 1 | 0 | 0 | 1 | 1 | 0 | 1 | 0 |
| 1 | 1 | 0 | 0 | 0 | 0 | 1 | 1 | 0 |
| 0 | 1 | 0 | 1 | 0 | 0 | 0 | 1 | 0 |
| 1 | 1 | 0 | 1 | 1 | 1 | 1 | 1 | 0 |
| 0 | 1 | 1 | 0 | 0 | 1 | 0 | 1 | 1 |
| 1 | 1 | 1 | 0 | 1 | 0 | 1 | 1 | 1 |
| 0 | 1 | 1 | 1 | 1 | 0 | 0 | 1 | 1 |
| 1 | 1 | 1 | 1 | 0 | 1 | 1 | 1 | 1 |

000 and it becomes fully populated after L bits. The transitions then repeat from this point as it is shown in Fig. 2.9. The encoding process of the incoming bits is easy using trellis diagram, basically branching up for a 0 and down for a 1 bit. An example of encoding the sequence (10100) is depicted in Fig. 2.10. The path taken by the bits of the sequence determines the output code sequence.

#### 2.2.1.2 Decoder

The main objective of the decoder operation is to provide the highest possibility of estimation for the uncoded transmitted bits from the received coded bits. The decoder type depends on the type of the demodulator output such that the decoder is referred to as *hard-decision decoding* when the demodulator carries out a binary decision concerning the received bit (i.e *hard-decision demodulation*). While, the decoder is referred to as *soft-decision decoding* when the demodulator

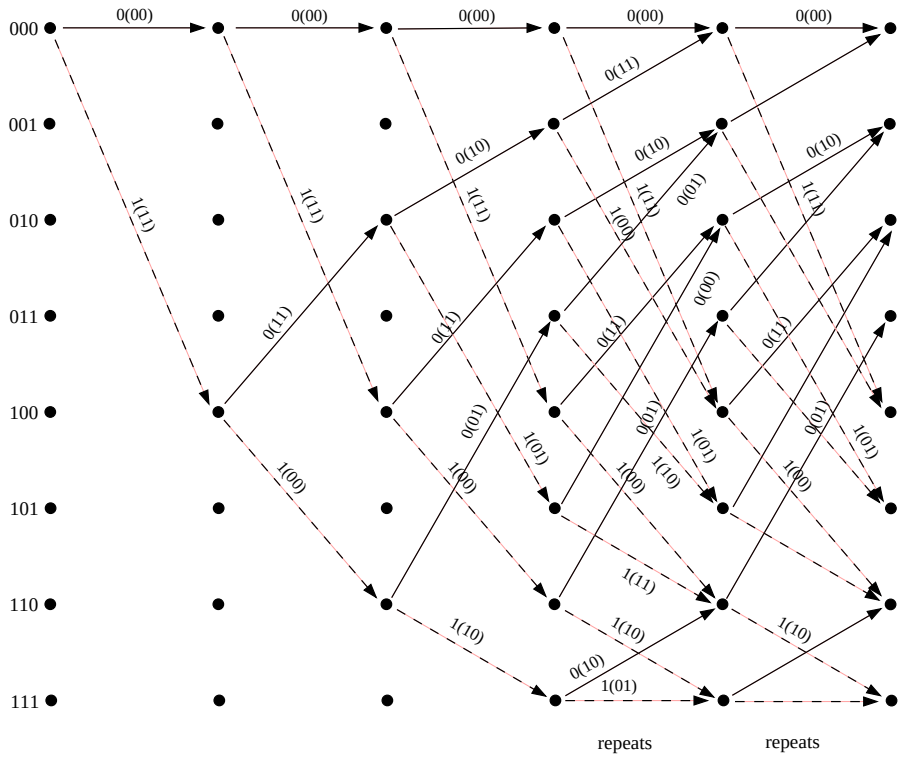


**Figure 2.9:** Trellis diagram of (2,1,4) code.

outputs includes multilevel confidence measures concerning the probability of a binary one and zero (i.e *soft-decision demodulation*) .

In general, the soft decoder is used in iterative detection due to it's higher efficiency than hard decoder. Soft decoding relies on symbol probability decoding algorithms for the iterative processes. The well-known and widely used algorithm for soft decoding is called *a posteriori* probability (APP). The APP algorithm is also known as BCJR or the forward-backward algorithm. The APP algorithm was originally invented by [51] to provide the maximum probability of correction for each symbol, and this referred to as the maximum *a posteriori* probability (MAP) algorithm. With the invention of turbo codes, the APP became the prime representative of the so called soft-in soft-out (SISO) algorithms which is used for obtaining probability information on the symbols of a trellis code.

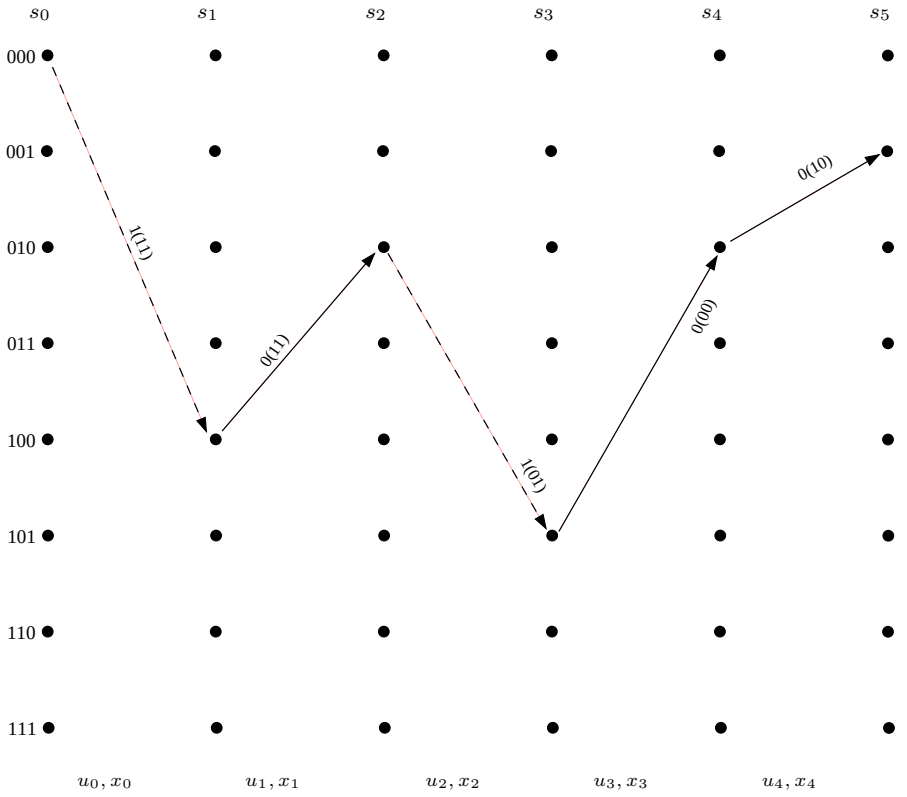


**Figure 2.10:** Encoding process for input sequence.

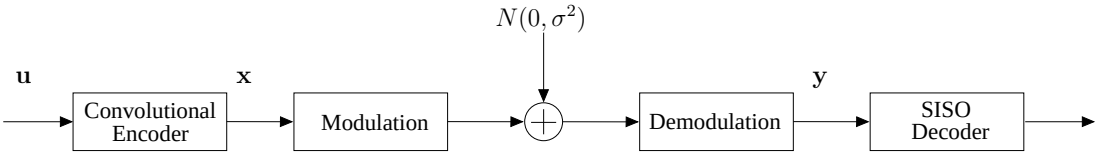


**Figure 2.11:** Notation.

### 2.2.2 Soft Input Soft Output Decoding (SISO)

In order to simplify SISO decoding description, we establish a notational convention as in Fig. 2.11. The trellis code shown in Fig. 2.10 consists of five sections. The transmitted code signal is $\mathbf{x} = [x_0, ..., x_4]$, and the data symbols are $\mathbf{u} = [u_0, ..., u_4]$. The purpose of SISO decoder is to compute the *a posteriori* probabilities, such as $\Pr[u_r|\mathbf{y}]$ or $\Pr[x_t|\mathbf{y}]$, where $\mathbf{y}$ is the output of the demodu-

lator. In general, the SISO decoders have three inputs and generate two outputs. Regarding the notation shown in Fig. 2.12, the systematic part, parity part of the received codeword and *a priori* probabilities on information symbols are the three inputs of the SISO decoder. The outputs of a SISO decoder are APP($u_t$) which is an estimate of $u_t$ given all observations and given all *a priori* probabilities, and Ext($u_t$), is a type of APP($u_t$) independent of $r_t^p$ and $\Pi(u_t)$, where $\Pi$ denotes the interleaving operation. The *a priori* probability input is used for iterative decoding, whereas for non-iterative decoding its values are zeros.

### MAP algorithm

Conceptually, the MAP algorithm calculates the probability that the encoder crossed a specific transition in the trellis, i.e. $\Pr[s_t = i, s_{t+1} = j|\mathbf{y}]$, where $s_t$ is the state at time $t$, and $i$ and $j$ are the previous and present states, respectively [52]. This probability can be computed as the product of three terms

$$\Pr[s_t = i, s_{t+1} = j|\mathbf{y}] = \frac{1}{\Pr(\mathbf{y})}\alpha_{t-1}(i)\gamma_t(i,j)\beta_t(j). \tag{2.13}$$

The internal variables of the algorithm are given by the values of $\alpha$ and can be determined by the forward recursion

$$\alpha_{t-1}(i) = \sum_{\text{states } l} \alpha_{t-2}(l)\gamma_{t-1}(i,l). \tag{2.14}$$

Employing previously calculated $\alpha$ values at time $t-2$ and the sum over all states $l$ at time $t-2$ that connect with state $i$ at time $t-1$, the estimation of the $\alpha$ values are obtained during forward recursion at time $t-1$. The initial values for $\alpha$ are

$$\alpha(0) = 1, \alpha(1) = \alpha(2) = \alpha(3) = 0.$$

On other the hand, the values of $\beta$ are calculated by using backward recursion

$$\beta_t(j) = \sum_{\text{states } l} \beta_{t+1}(l)\gamma_{t+1}(l,j), \tag{2.15}$$

and initialized as $\beta(0) = 1, \beta(1) = \beta(2) = \beta(3) = 0$ which enforces the terminating condition of the trellis code. The overall states $l$ summation takes place


**Figure 2.12:** SISO decoder.

at time $t+1$ to which state $j$ at time $t$ connects. The values of $\gamma$ are the conditional probabilities which are the inputs to the algorithm, while, $\gamma(j,i)$ is the joint probability that the state at time $t+1$ is $s_{t+1}=j$ and that $y_t$ is received. This can be calculated as

$$\gamma_t(j,i) = \Pr(s_{t+1}=j, y_t | s_r = i) = \Pr[s_{t+1}=j | s_t = i]\Pr(y_t|x_t). \tag{2.16}$$

where the first term $\Pr[s_{t+1}=j|s_t=i]\Pr$ is the a priori transition probability which is related to the probability of $u_t$. Hence, this transition probability can be abbreviated as

$$p_{ij} = \Pr[s_{t+1}=j|s_t=i] = \Pr[u_t]. \tag{2.17}$$

While the second term in (2.16) is the conditional channel transition probability, given that symbol $x_t$ is transmitted. Hence, (2.16) can be rewritten as follows

$$\gamma_t(j,i) = \Pr[u_t]\Pr(y_t|x_t). \tag{2.18}$$

The output of the iterative decoder can be derived to calculate a priori probability $\Pr(u_t)$, while, the joint probability can be computed as

$$\begin{aligned} \Pr(y_t/x_t) &= \prod_{l=1}^{n} \Pr(y_{tl}/x_{tl}) \\ &= \prod_{l=1}^{n} \frac{1}{\sqrt{2\pi\sigma^2}} e^{\frac{-1}{2\sigma^2}(y_{tl}-x_{tl})^2} \end{aligned} \tag{2.19}$$

where $x_{tl}$ and $y_{tl}$ are single transmitter and receiver bits within codewords, respectively; $n$ is the number of bits in each codeword; and $\sigma^2$ is the noise variance, for binary phase shift keying (BPSK) modulation and Gaussian channel. The

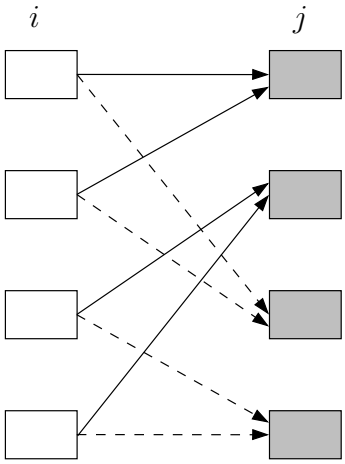


**Figure 2.13:** Transitions corresponding to $u_t$.

summation over all transitions of the *a posteriori* transition probabilities (2.13) can be used to compute the *a posteriori* symbol probabilities $\Pr[u_t|\mathbf{y}]$ regarding to $u_t = 1$ and $u_t = 0$, separately, that is

$$p[u_t = 1|\mathbf{y}] = \frac{1}{\Pr(\mathbf{y})} \sum_{solid} \alpha_{t-1}(i)\gamma_t(i,j)\beta_t(j), \tag{2.20}$$

$$p[u_t = 0|\mathbf{y}] = \frac{1}{\Pr(\mathbf{y})} \sum_{dashed} \alpha_{t-1}(i)\gamma_t(i,j)\beta_t(j), \tag{2.21}$$

where solid transition correspond to $u_t = 1$, and the dashed transitions correspond to $u_t = 0$ as illustrated in Fig. 2.13. Hence, the output *a posteriori* LLR can be determined as

$$\begin{aligned} L(u_t|\mathbf{y}) &= \log\left[\frac{p[u_t = 1|\mathbf{y}]}{p[u_t = 0|\mathbf{y}]}\right] \\ &= \log\left[\frac{\sum_{(i,j)\in A(u)} \alpha_{t-1}(i)\gamma_t(i,j)\beta_t(j)}{\sum_{(i,j)\in B(u)} \alpha_{t-1}(i)\gamma_t(i,j)\beta_t(j)}\right], \end{aligned} \tag{2.22}$$

where $A(u)$ and $B(u)$ denote the solid and dash transition states, respectively.

The mathmatical operations of the real numbers involved in the MAP algorithm results in a high complexity in the hardware implementations [51]. Transferring the algorithm to the logarithm domain leads to reduce the algorithm

complexity which is called *Max-log-MAP* algorithm [53][54]. This technique utilizes an approximation which drastically reduces the complexity however, at a cost of performance degradation. The lower performance problem of *Max-log-MAP* algorithm can be solved by using Log-MAP algorithm [55] that corrected the approximation used in the Max-Log-MAP algorithm.

### 2.2.3 Turbo Coding

#### 2.2.3.1 Turbo Encoder

According to Shannon, when a message is sent infinite times, each time shuffled randomly, then the ultimate code can be obtained. This means that the receiver has infinite copies of the message, which can be used by the decoder to decode the message sent with near error-free probability. Turbo code, aims to achieve this performance, albeit with messages being sent only two or three times.

Fig. 2.14 shows the turbo encoder which consists of two recursive systematic convolutional (RSC) encoders. The output of the two encoders are approximately statistically independent of each other due to using the interleaver between them. Although, its possible to utilize more than two components in turbo codes, however, we concentrate on the standard turbo encoder structure which is using two RSC codes. Each half rate RSC encoder generated a systematic output which includes the original and parity information. Half of the parity output bits from the encoders are punctured so as to produce one half of the overall coding rate. Hence, after puncturing, the output of the turbo encoder is a multiplexing of the systematic bits with the punctured parity bits.

#### 2.2.3.2 Turbo Decoder

The turbo decoder employs maximum likelihood detection (MLD), where the received signal after modulation is fed to the decoders which work on the signal amplitude to output soft decision bits. The MLD is known as maximum MAP when it is used by turbo decoding [56]. Within turbo decoding, the MAP algorithm works iteratively to improve the system performance, where the number of iterations depends on the SNR value. The higher the SNR, the less iterations are required.

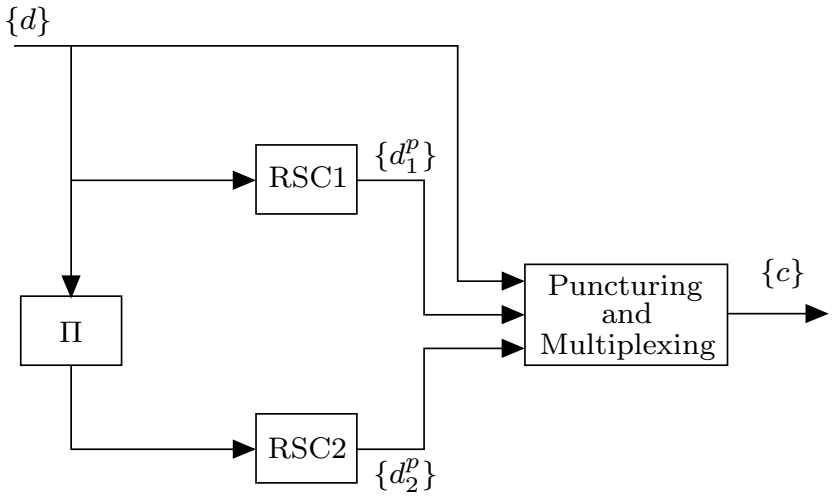


**Figure 2.14:** Turbo encoder.

The SISO decoder is the most important component in turbo decoder, because it computes *a posteriori* probabilities on bits. Corresponding to the two RSC encoders at the transmitter, the turbo decoder includes two SISO decoders that are connected by interleaver as shown in Fig. 2.15. The number of SISO decoders is equal to the number of RSC encoder components. During processing of the received signal, each SISO decoder computes the information about the data bits and extrinsic information about the coded bits, which in turn is sent to the other SISO decoder. The key idea of exchanging soft extrinsic bits between these two SISO decoders can greatly improve the system performance.

The channel output values are taken by the first SISO decoder which produces the soft output as its estimate of the data bits during the first iteration. Then the soft output bits are interleaved and taken as a *priori* information for the second SISO decoder. The second decoder employs this a *priori* data and the received data bits to obtain the estimate of the data bits. Similarly, the estimated output bits of the second decoder are deinterleaved, which are treated as a *priori* information by the first SISO decoder during second iteration. The exchanging of a *priori* information between the SISO decoders in each iteration leads to improve BER of the system at the next iteration.

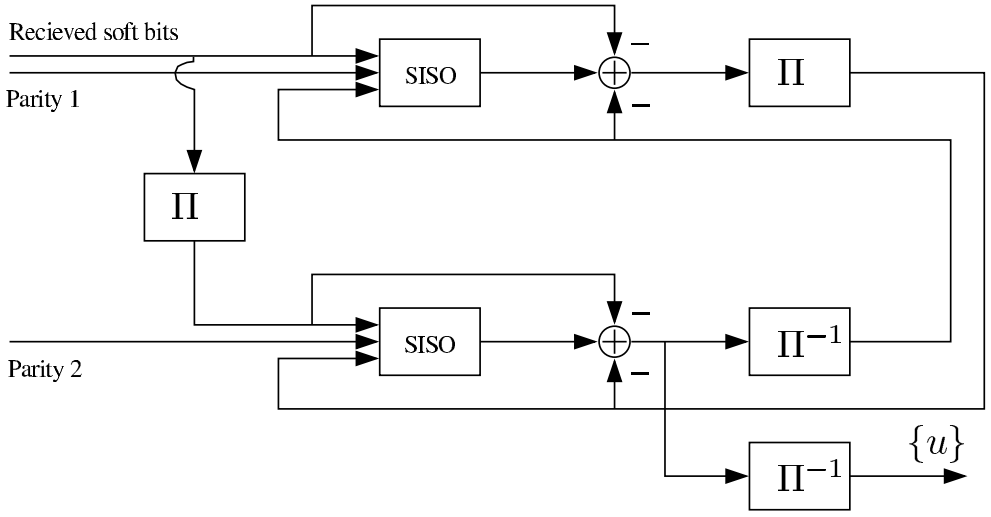


**Figure 2.15:** Turbo decoder.

## 2.3 Equalization Principles

The amplitude and phase dispersion of the channels leads to a very high BER at the receiver due to the effects of ISI. In order to solve the problem of ISI caused by the multipath channels, in spite of utilizing channel encoders, equalizers are also required. The receiver design depends on the fact that the channel transfer function is known. However, in practical communications applications, the channel transfer function is not known to the receiver to eliminate channel effects.

The optimum equalizer can be obtained by using maximum likelihood sequence detection (MSLE) which depends on the criterion of minimum probability of error. However, MSLE has high complexity. Alternatively, employing linear combinations of the received signal symbols to remove ISI is a suboptimal method of equalization and it is called Linear Equalizer (LE). LE has a good performance in slow fading channels, however, it has limited performance in fast fading channels. Therefore, the decision feedback equalizer (DFE) has been designed to mitigate fast fading through using feedback filter to remove the effect of the ISI caused by previous transmitted symbols.

Having a transmitter as shown in Fig. 2.16, $\{c\}_{i=0}^{N_d R_c - 1}$ denote the user's


**Figure 2.16:** Transmitter.

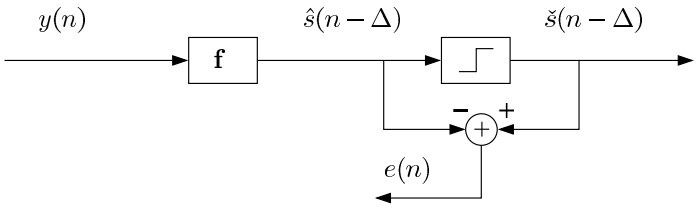


**Figure 2.17:** Linear equalizer structure.

data after error control encoding with $R_c$ and $N_d$ representing the code rate and number of transmitted data bits, respectively. After encoding, the codeword bits are mapped to symbols $\{s_k\}_{n=0}^{N_s-1}$, where $N_s$ is the number of the transmitted symbols, which are taken from a $M$-ary symbol alphabet: $\chi \triangleq \{\alpha_1, ..., \alpha_M\}$ with $E\{\chi\} = 0$ and $E\{|\alpha_q|^2\} = 1$.

We assume $L$ paths channel model, with complex-valued fading coefficients $\{h(l)\}_{l=0}^{L-1}$. The received signal can then be represented as

$$y(n) = \sum_{l} h(l)s(n-l) + \upsilon(n), \tag{2.23}$$

where $\upsilon(n)$ are complex-valued samples of zero-mean AWGN with variance $\sigma_v^2 = N_0/2$.

### 2.3.1 Linear Equalizer

The simplest suboptimum solution to remove ISI in the received signal is through the use of LE as shown in Fig. 2.17. This method generally incorporates a transversal filter (**f**), and the complexity of the filter linearly depends on the channel's transfer function.

Within communication systems, the transmitted data symbols $s(n)$ are received in the presence of multipath channel effects and additive noise $\upsilon(n)$. The signals $s(n)$ and $\upsilon(n)$ are assumed uncorrelated. Due to channel memory, each received symbol $y(n)$ contains contributions form both $s(n)$ and prior transmitted symbols. Hence, the received data symbols in (2.23) can be rewritten as follows:

$$y(n) = h(0)s(n) + \underbrace{\sum_{l=1}^{L} h(l)s(n-l)}_{ISI} + \upsilon(n), \tag{2.24}$$

where the second term on the right hand side describes the ISI caused by the prior transmitted symbols.

Assuming that the detected symbols $\check{s}(n)$ after the decision device are free of errors, *i.e* the $\check{s}(n-\Delta)$ can be replaced with $s(n-\Delta)$, then the criterion for determining transversal filter coefficients ($\mathbf{f}$) is obtained by minimizing the variance of the error signal, which can be given as

$$e(n-\Delta) = s(n-\Delta) - \hat{s}(n-\Delta). \tag{2.25}$$

where $s(n-\Delta) = \check{s}(n-\Delta)$ by assuming the correct detection of the equalized symbol. The received observed symbols can be expressed in column form as

$$\mathbf{y} = \begin{bmatrix} y(n) \\ y(n-1) \\ y(n-2) \\ . \\ . \\ . \\ . \\ y(n-N_f+1) \end{bmatrix}, \tag{2.26}$$

where $N_f$ is the length of transversal filter taps. Moreover, the process $s(n-\Delta)$ is jointly wide-sense stationary with $\mathbf{y}$, hence the covariance quantities

$$\mathbf{R}_{\mathbf{y}} = E\left[\mathbf{y}\mathbf{y}^H\right] = \mathbf{H}\mathbf{R}_{\mathbf{s}}\mathbf{H}^H + \mathbf{R}_v, \tag{2.27}$$

$$\mathbf{r}_{s\mathbf{y}} = E\left[s(n-\Delta)\mathbf{y}^H\right] = \lambda_s \mathbf{H}^H, \tag{2.28}$$

are independent of $n$, where

$$\lambda_s = [\underbrace{0 \quad 0 \quad \dots}_{\Delta} \sigma_s \quad \dots \quad 0 \quad 0],$$

is a vector of length $N_f$ which all its element are zeros except element with position $\Delta$, $\sigma_s = E[s(n-\Delta)s(n)^*]$, $(.)^H$ denotes the conjugate transpose operation, $\mathbf{H} \in \mathbb{C}^{N_f \times (L+N_f-1)}$ is the channel matrix constructed from the estimated channel taps during training mode, i.e.

$$\mathbf{H} = \begin{bmatrix} h(0) & \dots & h(L-1) & 0 & \dots & 0 \\ \vdots & \ddots & \ddots & \ddots & \ddots & \vdots \\ 0 & \dots & 0 & h(0) & \dots & h(L-1) \end{bmatrix}, \tag{2.29}$$

and $\mathbf{R}_s \in \mathbb{C}^{(N_f+L-1)\times(N_f+L-1)}$ is the covariance matrix.

The covariance matrix

$$\mathbf{R} \triangleq \begin{bmatrix} \sigma_s & \mathbf{r}_{s\mathbf{y}} \\ \mathbf{r}_{s\mathbf{y}}^H & \mathbf{R}_{\mathbf{y}} \end{bmatrix}, \tag{2.30}$$

is assumed to be positive-definite and invertible. The positive-definiteness of $\mathbf{R}$ guarantees that both $\mathbf{R}_{\mathbf{y}}$ and the Schur complement of $\mathbf{R}$ are positive-definite matrices too, i.e.

$$\mathbf{R}_{\mathbf{y}} > 0, \quad \mathbf{R}_\delta \triangleq \sigma - \mathbf{r}_{s\mathbf{y}}\mathbf{R}_{\mathbf{y}}^{-1}\mathbf{r}_{s\mathbf{y}}^H > 0,$$

where the Schur complement is denoted by $\mathbf{R}_\delta$ [25]. The optimal filter taps can be determined by solving

$$\Delta J = \min_{\mathbf{f}} E|e_k(n-\Delta)|^2. \tag{2.31}$$

Moreover, (2.25) can be rewritten as

$$\begin{aligned} e(n-\Delta) &= s(n-\Delta) - \hat{s}(n-\Delta) \\ &= s(n-\Delta) - \sum_{l_f=0}^{l_f=N_f-1} f(l_f)y(n-l_f). \end{aligned} \tag{2.32}$$

By collecting the coefficients of $f(l_f)$ in row form

$$\mathbf{f}^H \triangleq [f(0) \quad f(1) \quad \cdots \quad f(N_f-1)], \tag{2.33}$$

the expression in (2.32) can be rewritten in vector form as follows

$$e(n) = s(n-\Delta) - \mathbf{f}^H\mathbf{y}. \tag{2.34}$$

By substituting (2.34) in (2.31), the optimization problem can be written as follows

$$\Delta J = \min_{\mathbf{f}} E|s(n-\Delta) - \mathbf{f}^H\mathbf{y}|^2. \tag{2.35}$$

The right hand-hand side of (2.35) can be expanded as follows

$$\begin{aligned} \Delta J &= \min_{\mathbf{f}} E\left[\left(s_k(n-\Delta) - \mathbf{f}^H\mathbf{y}\right)\left(s(n-\Delta) - \mathbf{f}^H\mathbf{y}\right)^H\right] \\ &= \min_{\mathbf{f}} E\left[\left(s(n-\Delta) - \mathbf{f}^H\mathbf{y}\right)\left(s(n-\Delta)^H - \mathbf{y}^H\mathbf{f}\right)\right] \\ &= \min_{\mathbf{f}} E[s(n-\Delta)s(n-\Delta)^H - s(n-\Delta)\mathbf{y}^H\mathbf{f} \\ &\quad - \mathbf{f}^H\mathbf{y}s(n-\Delta)^H + \mathbf{f}^H\mathbf{y}\mathbf{y}^H\mathbf{f}]. \end{aligned} \tag{2.36}$$

In turn, with the aforementioned definitions, (2.36) can be rewritten as follows

$$\Delta J = \min_{\mathbf{f}}(1 - \mathbf{r}_{s\mathbf{y}}\mathbf{f} - \mathbf{f}^H\mathbf{r}_{s\mathbf{y}}^H + \mathbf{f}^H\mathbf{R}_{\mathbf{y}}\mathbf{f}) \tag{2.37}$$

.

The optimal $\mathbf{f}^H$ is determined by differentiating $\Delta J$ with respect to $\mathbf{f}$ and setting it to be equal to zero.

$$\frac{\partial \Delta J}{\partial \mathbf{f}} = -\mathbf{r}_{s\mathbf{y}} + \mathbf{f}^H\mathbf{R}_{\mathbf{y}}, \tag{2.38}$$

hence,

$$\mathbf{f}^H = \mathbf{r}_{s\mathbf{y}}\mathbf{R}_{\mathbf{y}}^{-1}. \tag{2.39}$$

By substituting (2.39) into (2.37), we can find the minimum mean square error of linear equalizer ($\mathbf{MMSE}_{LE}$), that's

$$\mathbf{MMSE}_{LE} = 1 - \mathbf{r}_{s\mathbf{y}}\mathbf{R}_{\mathbf{y}}^{-1}\mathbf{r}_{s\mathbf{y}}^H. \tag{2.40}$$

### 2.3.2 DFE Equalizer

Within the DFE structure, in addition to the transversal filter in the feed forward path, a feedback filter is also employed in order to feedback previous decisions and utilize them to reduce ISI as shown in Fig. 2.18. The utilization of the decision device in DFE equalization provides it with nonlinear characteristic. The decision device tries to determine which symbol of a set of modulation levels was actually transmitted. After each symbol estimation, the DFE equalizer with the aid of filter structure can compute the channel effect on following symbols and compensate the input of the decision device for the next samples. This postcursor channel removal takes place by using a feedback filter structure.

By defining the returned symbols through the feedback filter as

$$\mathbf{s} = \begin{bmatrix} s(n-\Delta) \\ s(n-\Delta-1) \\ . \\ . \\ . \\ . \\ s(n-\Delta-N_b) \end{bmatrix}, \tag{2.41}$$

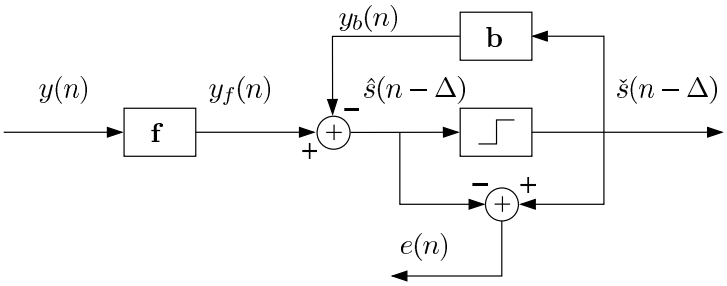


**Figure 2.18:** DFE equalizer structure.

and using the same definitions for the observed symbols, estimated symbols and filter taps given in LE section, the covariance matrix

$$\mathbf{R} \triangleq \begin{bmatrix} \mathbf{R}_s & \mathbf{R_{sy}} \\ \mathbf{R}_{\mathbf{sy}}^H & \mathbf{R_y} \end{bmatrix}, \tag{2.42}$$

is assumed to be positive-definite and invertible, where $\mathbf{R_{sy}} \in \mathbb{C}^{N_b \times N_f}$. The positive-definiteness of $\mathbf{R}$ guarantees that both $\mathbf{R_y}$ and the Schur complement of $\mathbf{R}$ are positive-definite matrices too, i.e.

$$\mathbf{R_y} > 0, \quad \mathbf{R}_\delta \triangleq \mathbf{R}_s - \mathbf{R_{sy}}\mathbf{R_y}^{-1}\mathbf{R}_{\mathbf{sy}}^H > 0,$$

where the Schur complement is denoted by $\mathbf{R}_\delta$ [25].

For the DFE structure, the error signal given in (2.25) can be rewritten as follows

$$\begin{aligned} e(n-\Delta) = s(n-\Delta) &- \sum_{l_f=0}^{N_f-1} f(l_f) y(n-l_f) \\ &+ \sum_{l_b=1}^{N_b} b(l_b) s(n-l_b). \end{aligned} \tag{2.43}$$

Moreover, the error signal can be written in vector form as

$$e(n) = \mathbf{b}^H \mathbf{s} - \mathbf{f}^H \mathbf{y}, \tag{2.44}$$

where

$$\mathbf{b}^H \triangleq [1 \quad b(1) \quad \cdots \quad b(N_b)], \tag{2.45}$$

hence, the optimization problem in (2.31) becomes

$$\Delta J = \min_{\mathbf{f},\mathbf{b}} E\left[|\mathbf{b}^H\mathbf{s} - \mathbf{f}^H\mathbf{y}|^2\right], \tag{2.46}$$

$$\begin{aligned}\Delta J =& \min_{\mathbf{f},\mathbf{b}} E\left[(\mathbf{b}^H\mathbf{s} - \mathbf{f}^H\mathbf{y})(\mathbf{b}^H\mathbf{s} - \mathbf{f}_k^H\mathbf{y})^H\right] \\ =& \min_{\mathbf{f},\mathbf{b}}(\mathbf{b}^H E[\mathbf{s}\mathbf{s}^H]\mathbf{b} - \mathbf{b}^H E[\mathbf{s}\mathbf{y}^H]\mathbf{f} - \mathbf{f}^H E[\mathbf{y}\mathbf{s}^H]\mathbf{b} + \mathbf{f}_k^H E[\mathbf{y}\mathbf{y}^H]\mathbf{f}_k).\end{aligned} \tag{2.47}$$

By substituting $\mathbf{R_{sy}}$, (2.47) can be rewritten as

$$\Delta J = \min_{\mathbf{f},\mathbf{b}}(\mathbf{b}^H\mathbf{R_s}\mathbf{b} - \mathbf{b}^H\mathbf{R_{sy}}\mathbf{f} - \mathbf{f}^H\mathbf{R_{sy}^H}\mathbf{b} + \mathbf{f}^H\mathbf{R_y}\mathbf{f}). \tag{2.48}$$

The optimal $\mathbf{f}^H$ is determined by differentiating $\Delta J$ with respect to $\mathbf{f}$, thats

$$\frac{\partial \Delta J}{\partial \mathbf{f}} = -\mathbf{b}^H\mathbf{R_{sy}} + \mathbf{f}^H\mathbf{R_y} \tag{2.49}$$

Then from (2.49) we can find $\mathbf{f}^H$ as given below

$$\mathbf{f}^H = \mathbf{b}^H\mathbf{R_{sy}}\mathbf{R_y^{-1}}. \tag{2.50}$$

Substituting this expression into (2.48), we get

$$\begin{aligned}\Delta J =& \min_{\mathbf{b}}(\mathbf{b}^H\mathbf{R_s}\mathbf{b} - \mathbf{b}^H\mathbf{R_{sy}}\mathbf{R_y^{-1}}\mathbf{R_{sy}^H}\mathbf{b} \\ &- \mathbf{b}^H\mathbf{R_{sy}}\mathbf{R_y^{-1}}\mathbf{R_{sy}^H}\mathbf{b} + \mathbf{b}^H\mathbf{R_{sy}}\mathbf{R_y^{-1}}\mathbf{R_y}\mathbf{R_y^{-1}}\mathbf{R_{sy}^H}\mathbf{b}) \\ =& \min_{\mathbf{b}}(\mathbf{b}^H\mathbf{R_s}\mathbf{b} - \mathbf{b}^H\mathbf{R_{sy}}\mathbf{R_y^{-1}}\mathbf{R_{sy}^H}\mathbf{b}) \\ =& \min_{\mathbf{b}}(\mathbf{b}^H\left(\mathbf{R_s} - \mathbf{R_{sy}}\mathbf{R_y^{-1}}\mathbf{R_{sy}^H}\right)\mathbf{b}) \\ =& \min_{\mathbf{b}}(\mathbf{b}^H\mathbf{R}_\delta\mathbf{b}).\end{aligned} \tag{2.51}$$

Recall that the leading entry of vector $\mathbf{b}$ is unity, so that (2.51) is actually a constrained problem of the form

$$\min_{\mathbf{b}} \mathbf{b}^H\mathbf{R}_\delta\mathbf{b} \quad \text{subject to} \quad \mathbf{b}^H\mathbf{e}_0 = 1 \tag{2.52}$$

where

$$\mathbf{e}_o = [1 \quad 0 \quad 0\ldots0]^T.$$

Employing the Gauss-Markov theorem [25] for constrained optimization, we can find the optimal value of $\mathbf{b}$ as

$$\mathbf{b}^H = \frac{\mathbf{e}_o^T \mathbf{R}_\delta^{-1}}{\mathbf{e}_o^T \mathbf{R}_\delta^{-1} \mathbf{e}_o}. \tag{2.53}$$

The denominator in (2.53) represents the (1,1) entry of $\mathbf{R}_\delta^{-1}$, while the numerator is the first row of $\mathbf{R}_\delta^{-1}$. By substituting the above equation of $\mathbf{b}^H$ into (2.53), we can calculate the resulting **MMSE** of the original optimization problem (2.48), that's

$$\mathbf{MMSE}_{DFE} = \frac{1}{\mathbf{e}_o^T \mathbf{R}_\delta^{-1} \mathbf{e}_o.} \tag{2.54}$$

## 2.4 Joint Equalization and Decoding in an Iterative system

In the previous sections, all blocks in the receiver system, decoding or equalization, were processing the data in a sequential fashion. The bit redundancy and the channel characteristics have been used in the decoding procedure and the equalization process to more enhancement in signal quality and data equalization, respectively. In this section, a higher efficiency approach will be introduced. The approach consists of both the equalizer and decoder procedures in a single receiver were data is processed in an iterative manner. This method was first proposed by Douillard [57], and it is called turbo equalization (TE) [58] because of its similarity with turbo coding. Douillard has shown that even for high dispersive multipath fading channels the detrimental effects of ISI can be removed with this approach. The iterative equalization and decoding processes in TE receiver [59] can obtain impressive performance for receivers that receive data from a multipath selective channels, i.e. those that suffer from ISI effects.

The original TE includes maximum likelihood (ML) equalizer and a MAP decoder as depicted in Fig.2.19. In each iteration, number of sequence operations are executed within two layers. The two layers are separated by an interleaver and a deinterleaver. The inner layer consists of the channel and ML equalizer operations, while the outer layer includes an encoder and decoder. The iterative receivers are exchanging soft information bits between the inner layer and the

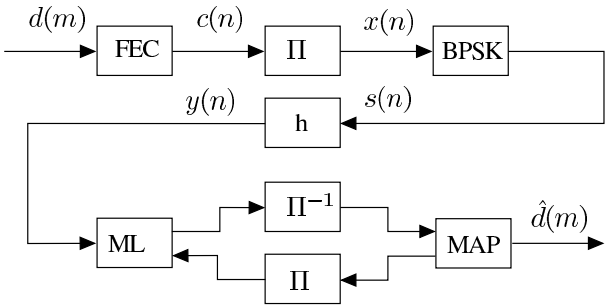


**Figure 2.19:** ML turbo equalization.

outer layer during detection process. In first iteration, there is no feedback information from the outer layer, hence the equalization is done based on the channel impulse response. While in the later iterations, the equalizer is also using the decoder feedback soft bits for improving equalization operations. As the number of iteration increases, the quality of the signal between the equalizer and the decoder is improved. This is the principle of TE system. Although, TE can provide improved BER performance, however, this iterative scheme can be sensitive to error propagation.

Usually the equalization part of the TE system is based on the Bahl Cock Jelinek Raviv (BCJR) algorithm [60]. When channel response and *a priori* information of the transmitted symbols are available in the receiver, exact APP values of the transmitted symbols can be calculated by using BCJR algorithm ( i.e. optimal equalizer ). The ideal equalization of BCJR is come in the expense of high computational complexity which increases exponentially as a function of symbol mapping type and channel response length.

The high complexity of optimal equalization of BCJR has encouraged researchers to seek and investigate numerous suboptimal solutions which provide low equalization complexity. A familiar SISO linear equalizer (SISO-LE) [61] is a notable development along this direction. The SISO-LE has been employed with MAP decoder for constructing a turbo like equalization system [62], such that the complexity was reduced from exponential to polynomial. SISO-DFE structure is another example of turbo like equalization which was proposed in [61]. In multipath fading channel transmission, DFE usually outperforms LE. However,

when hard decision bits are fed through feedback filters in iterative equalization techniques, SISO-LE can provide better performance than SISO-DFE due to error propagation [62]. For this reason, various techniques have been proposed to mitigate feedback error propagation so as to improve SISO-DFE performance [63] [64] [29]. Recently, it has been shown in [65] that the SISO-DFE can outperform SISO-LE if extrinsic information is reformulated such that it can combat error propagation more efficiently.

In turbo equalization, the output of the equalizer part, as shown in Fig. 2.20, is the LLR of $s(n)$

$$e_{eq}(s) = \ln\frac{\Pr(s(n)=+1|\mathbf{y})}{\Pr(s(n)=-1|\mathbf{y})} - \tilde{l}_{eq}(s(n)), \tag{2.55}$$

where

$$\mathbf{y} = [y(1), y(2), \ldots, y(L_t)],$$

and $L_t$ is the length of the interleaved sequence. The equalizer requires the information of the *a priori* probabilities of all input bits affecting $y(n)$ to generate the *a posterior* values. These *a priori* soft bits are provided by the decoder according to the following formula

$$\tilde{l}_{eq}(s(n)) = \ln\left(\frac{\Pr(s(n)=+1)}{\Pr(s(n)=-1)}\right). \tag{2.56}$$

In the first iteration, these *a priori* bits are not available and are all initially set to zeros, however, when the turbo iteration ensues, these soft bits are generated and passed by the outer decoder. The MAP decoder computes the *a posteriori* information of $c(n)$

$$e_{de}(c(n)) = \ln\left(\frac{\Pr(c(n)=+1/\Upsilon)}{\Pr(c(n)=-1/\Upsilon)}\right) - \ln\left(\frac{\Pr(c(n)=+1)}{\Pr(c(n)=-1)}\right), \tag{2.57}$$

where

$$\Upsilon = \left[\tilde{l}_{de}(c(1)), \tilde{l}_{de}(c(2)), \ldots, \tilde{l}_{de}(c(L_t))\right],$$

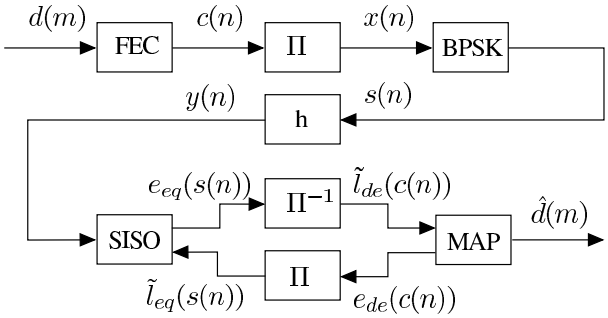


**Figure 2.20:** Iterative equalization using SISO and MAP decoder.

and the output of the equalizer is considered to be the *a priori* $\tilde{l}_{de}(c(n))$ for the decoder after deinterleaving process. The decoder also computes the data bit sequence

$$\hat{d}(m) = \text{argmax}_{\{d\in(1,0)\}}\Pr(d(m) = d|\Upsilon). \tag{2.58}$$

After initial estimation of a block of received symbols, the equalization and decoding operations are applied to the same set of the received symbols. The iterative process is then stopped by a suitable termination criterion.

The SISO block consists of two main operations. First, the received signal is processed by the equalizer filters to generate the estimate $\hat{s}(n)$ of the original transmitted signal $s(n)$. This is done by using traditional MMSE criterion with the deviation that the SISO also makes use of the prior information $\tilde{l}_{eq}(s(n))$, i.e $\text{E}(s(n))$ and $\text{Cov}(s(n), s(n))$. The MMSE computes $\hat{s}(n)$ from the received symbols $y(n)$ by minimizing the cost function $(\text{E}|s(n) - \hat{s}(n)|^2)$. The second step consists of forming the output $e_{eq}(s(n))$ based on the filtered estimate $\hat{s}(n)$, the channel impulse response and the current filter coefficient taps.

The output of the SISO is obtained by utilizing the estimate $\hat{s}(n)$ instead of $y(n)$ [66] [67], i.e.

$$\begin{aligned} e_{eq}(s(n)) &= \ln\frac{\text{P}(s(n) = +1|\hat{s}(n))}{\text{P}(s(n) = -1|\hat{s}(n))} - \ln\frac{\text{P}(s(n) = +1)}{\text{P}(s(n) = -1)} \\ &= \ln\frac{p(\hat{s}(n)|s(n) = +1)}{p(\hat{s}(n)|s(n) = -1)}, \end{aligned} \tag{2.59}$$

which requires $p(\hat{s}(n)|s(n) = s)$ of $\hat{s}(n)$ conditioned on $s(n) = s$, $s \in \{-1, 1\}$. The MMSE requires the statistics $\overline{s}(n) = \text{E}[s(n)]$ and $\overline{v}(n) = \text{Cov}[s(n), s(n)]$ of

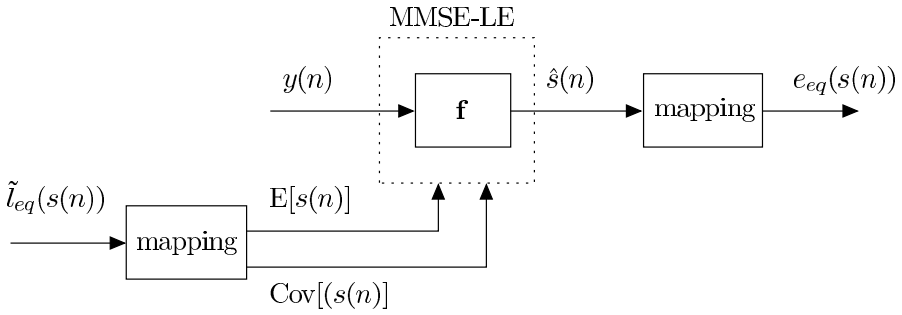


**Figure 2.21:** SISO-LE equalizer structure.

symbols $s(n)$ to produce the estimation symbols $\hat{s}(n)$. The $s(n)$ are assumed to be equiprobable and i.i.d, which corresponds to $\mathrm{E}[s(n)]$ =0 and $\mathrm{Cov}[s(n), s(n)]$ =1, $\forall n$. In general, the mean and covariance values of $s(n)$ are determined as

$$\begin{aligned}\overline{s}(n) &= \sum_{s\in\{-1,1\}} s\mathrm{P}(s(n)=s) \\ &= \mathrm{P}(s(n)=+1) - \mathrm{P}(s(n)=-1) \\ &= \frac{e^{\tilde{l}_{eq}(s(n))}}{1+e^{\tilde{l}_{eq}(s(n))}} - \frac{1}{1+e^{\tilde{l}_{eq}(s(n))}} = \tanh(\frac{\tilde{l}_{eq}(s(n))}{2})\end{aligned} \quad , \tag{2.60}$$

$$\overline{v}(n) = \sum_{s\in\{-1,1\}} |s-\mathrm{E}[s(n)]|^2 \mathrm{P}(s(n)=s) = 1-\overline{s}(n). \tag{2.61}$$

After MMSE equalization, we assume that the probability density functions (pdf) $p(\hat{s}(n)|s(n)=s)$, $s\in\{-1,1\}$, are Gaussian with parameters $\mu_s(n) = \mathrm{E}[\hat{s}(n)|s(n)=s]$ and $\sigma_s^2(n) = \mathrm{Cov}[\hat{s}(n),\hat{s}(n)|s(n)=s]$ [68]

$$p(\hat{s}(n)|s(n)=s) \approx \phi(\frac{(\hat{s}(n)-\mu_s(n))}{\sigma_s(n)})/\sigma_s(n), \tag{2.62}$$

where

$$\phi(x) = \frac{e^{\frac{-x^2}{2}}}{\sqrt{2\pi}}. \tag{2.63}$$

The above assumption enormously simplifies the computation of equalizer output $\hat{s}(n)$. Moreover, the output symbols $e_{eq}(s(n))$ should not depend on the particular *a priori* LLR $\tilde{l}_{eq}(s(n))$, hence, it is required that $\hat{s}(n)$ does not depend on $\tilde{l}_{eq}(s(n))$ which affects the MMSE derivation.

### 2.4.1 Linear MMSE Turbo-Equalization

The MMSE equalizer for this approach is SISO-LE , shown in Fig.2.21, which consists of a length $N_f$ filter with coefficient $f(l_f)$, $l_f = -N_1, 1-N_1, \ldots, 0, \ldots, N_2$, where $N_f = N_1 + N_2$, which are defined by the linear MMSE estimate $\hat{s}(n)$ of $s(n)$[69]

$$\hat{s}(n) = \mathrm{E}[s(n)] + \mathrm{Cov}[x(n), \mathbf{y}]\mathrm{Cov}[\mathbf{y}, \mathbf{y}]^{-1}\left(\mathbf{y} - \mathrm{E}[\mathbf{y}]\right), \tag{2.64}$$

given the observation

$$\mathbf{y} \triangleq [y(n - N_2, y(n - N_2 + 1), \ldots, y(n + N_1)]^H$$

For data transmission over multipath fading channels, (2.64) becomes

$$\hat{s}(n) = \overline{s}(n) + \overline{v}(n)\check{\mathbf{h}}^H(\sigma^2\mathbf{I}_N + \mathbf{HVH}^H)^{-1}\left(\mathbf{y} - \mathbf{H}\overline{\mathbf{s}}\right) \tag{2.65}$$

where $\mathbf{H}$ is the channel convolution matrix given by (2.29) and

$$\overline{\mathbf{s}} \triangleq [\overline{s}(n - L - N_2 + 1), \overline{s}(n - L - N_2 + 2, \ldots, \overline{s}(n + N_1)]^H,$$

$$\mathbf{V} \triangleq \mathrm{Diag}(v(n - L - N_2 + 1), v(n - L - N_2 + 2), \ldots, v(n + N_1)),$$

$$\check{\mathbf{h}} \triangleq \mathbf{H}[\mathbf{0}_{1\times(N_2+L-1)} \quad 1 \quad \mathbf{0}_{1\times N_1}]^H.$$

In (2.65), it is obvious that $\hat{s}(n)$ depends on $\tilde{l}_{eq}(s(n))$ via $\overline{s}(n)$ and $\overline{v}(n)$. Therefore, to make $\hat{s}(n)$ independent of $\tilde{l}_{eq}(s(n))$, we set $\tilde{l}_{eq}(s(n))$ to zeros while computing $\hat{s}(n)$, yielding $\overline{s}(n) = 0$ and $\overline{v}(n) = 1$. Hence, (2.65) can be changed as follows

$$\hat{s}(n) = \check{\mathbf{h}}^H\mathrm{Cov}[\mathbf{y}, \mathbf{y}]^{-1}(\mathbf{y} - \mathbf{H}\overline{\mathbf{s}} + (\overline{s}(n) - 0)\check{\mathbf{h}}), \tag{2.66}$$

where

$$\mathrm{Cov}[\mathbf{y}, \mathbf{y}] = \sigma^2\mathbf{I}_N + \mathbf{HVH}^H + (1 - v(n))\check{\mathbf{h}}\check{\mathbf{h}}^H.$$

The MMSE equalizer output can be written as

$$\hat{s}(n) = \sum_{l_f=-N1}^{N_2} f(l_f)(y(n - l_f) - \mathrm{E}[y(n - l_f)]), \tag{2.67}$$

where

$$E[y(n)] = \sum_{l=0}^{L-1} h(l)\overline{s}(n-l).$$

Consequently, the vector $\mathbf{f}$ is set as follows

$$\mathbf{f} \triangleq (\sigma^2\mathbf{I}_N + \mathbf{H}\mathbf{V}\mathbf{H}^H + (1-v(n))\check{\mathbf{h}}\check{\mathbf{h}}^H)^{-1}\check{\mathbf{h}}. \tag{2.68}$$

This yields the final formula

$$\hat{s}(n) = \mathbf{f}^H(\mathbf{y} - \mathbf{H}\overline{\mathbf{s}} + \overline{s}(n)\mathbf{s}\check{\mathbf{h}}), \tag{2.69}$$

from which the parameters $\mu^2(n)$ and $\sigma^2(n)$ of $\hat{s}(n)$ are determined

$$\begin{aligned} \mu(n) &= \mathbf{f}^H(\mathrm{E}(\mathbf{y}|s(n)=s) - \mathbf{H}\overline{\mathbf{s}} + \overline{s}(n)\check{\mathbf{h}}) \\ &= s\mathbf{f}^H\check{\mathbf{h}}, \end{aligned} \tag{2.70}$$

$$\begin{aligned} \sigma^2(n) &= \mathbf{f}^H\mathrm{Cov}(\mathbf{y},\mathbf{y}|s(n)=s)\mathbf{f} \\ &= \mathbf{f}^H(\sigma^2\mathbf{I}_N + \mathbf{H}\mathbf{V}\mathbf{H}^H - v(n)\check{\mathbf{h}}\check{\mathbf{h}}^H)\mathbf{f} \\ &= \mathbf{f}^H\check{\mathbf{h}}(1 - \check{\mathbf{h}}^H\mathbf{f}). \end{aligned} \tag{2.71}$$

The output $e_{eq}(s(n))$ is then follows as

$$\begin{aligned} e_{eq}(s(n)) &= \ln \frac{\phi\left(\frac{\hat{s}(n)-\mu_{(s=+1)}(n))}{\sigma_{(s=+1)}(n)}\right)/\sigma_{(s=+1)}(n)}{\phi\left(\frac{\hat{s}(n)-\mu_{(s=-1)}(n))}{\sigma_{(s=-1)}(n)}\right)/\sigma_{(s=-1)}(n)} \\ &= 2\mathbf{f}^H\frac{\left(\mathbf{y} - \mathbf{H}\overline{\mathbf{s}} + \overline{s}(n)\check{\mathbf{h}}\right)}{1 - \check{\mathbf{h}}^H\mathbf{f}}. \end{aligned} \tag{2.72}$$

In first the iteration, $\tilde{l}_{eq}(s(n)) = 0$, $\forall n$, and hence $\overline{s}(n) = 0$ and $v(n) = 1$. This leads to changing (2.68) to a usual MMSE-LE solution [1]

$$\begin{aligned} \mathbf{f}_{NA} &= (\sigma^2\mathbf{I}_N + \mathbf{H}\mathbf{V}\mathbf{H}^H + (1-v(n))\check{\mathbf{h}}\check{\mathbf{h}}^H)^{-1}\check{\mathbf{h}}|_{\tilde{l}_{eq}(s(n))=0} \\ &= (\sigma^2\mathbf{I}_N + \mathbf{H}\mathbf{V}\mathbf{H}^H)^{-1}\check{\mathbf{h}}. \end{aligned} \tag{2.73}$$

### 2.4.2 Non-Linear MMSE Turbo-Equalization

The DFE equalizer consists of a length $N_f$ feed-forward filter with coefficients $f(l_f)$, $l_f = -N_1, 1-N_1, \ldots, N_2$, and a stictly causal length $N_b$ feedback filter

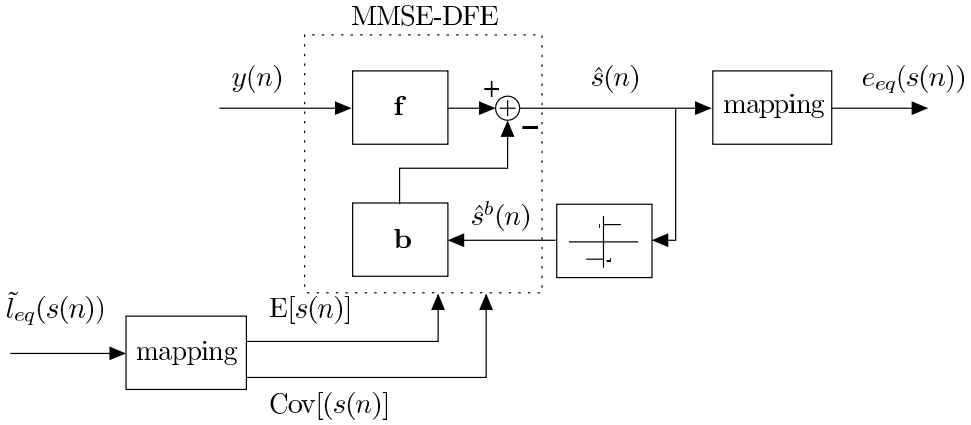


**Figure 2.22:** SISO-DFE equalizer structure.

with a coefficients $b(l_b)$, $l_b = 1, 2, \ldots, N_b$ as depicted in Fig. 2.22. A general expression for MMSE-DFE equalizer is given as follows [61]

$$\begin{aligned}\hat{s}(n) = \overline{s}(n) + \left(\sum_{l_f=-N_f}^{0} f(l_f)\left(y(n-l_f) - \mathrm{E}[y(n-l_f)]\right)\right) \\ - \left(\sum_{l_b=1}^{N_b} b(l_b)(\hat{s}^b(n-l_b) - \mathrm{E}[\hat{s}(n-l_b)])\right)\end{aligned} \tag{2.74}$$

where $\hat{s}^b(n)$ are past decided estimates of $\hat{s}(n)$ and obtained using appropriate decision function, that's

$$\hat{s}^b(n) = \begin{cases} 1 & \hat{s}(n) \geqslant 0 \\ -1 & \hat{s}(n) < 0 \end{cases}, \tag{2.75}$$

for BPSK modulation. We assume that the feedback estimated symbols $\hat{s}^b(n)$ are error-free, i.e. $\hat{s}^b(n) = s(n)$, $\forall n$. The relation between the feed forward $\mathbf{f}$ and feedback $\mathbf{b}$ coefficients [1]

$$b(l_b) = \sum_{l=0}^{N_b} h(l) f(l_b - l), \quad l_b = 1, 2, \ldots, N_b \tag{2.76}$$

can be substituted in (2.74) and the output equation becomes [59]

$$\hat{s}(n) = \overline{s}(n) + \mathbf{f}^H(\mathbf{y} - \mathbf{H}\bar{\mathbf{s}}), \tag{2.77}$$

where $\mathbf{H} \in \mathbb{C}^{N_f \times (N_b + N_f - 1)}$ is the channel convolution matrix, and

$$\overline{\mathbf{s}} \triangleq [\hat{s}^b(n-N_b+1),\ldots,\hat{s}^b(n-1),\overline{s}(n),\overline{s}(n+1),\ldots,\overline{s}(n+N_f-1)]^T,$$

$$\mathbf{y} = [y(n), y(n+1),\ldots,y(n+N_f-1)]^T.$$

In (2.64), applying

$$\mathbf{f}^H = \mathbf{Cov}[s(n),\mathbf{y}]\mathbf{Cov}[\mathbf{y},\mathbf{y}]^{-1}, \tag{2.78}$$

to (2.77), we get

$$\hat{s}(n) = \overline{s}(n) + v(n)\check{\mathbf{h}}^H\left(\sigma^2\mathbf{I}_N + \mathbf{HVH}^H\right)^{-1}(\mathbf{y}-\mathbf{H}\overline{\mathbf{s}}), \tag{2.79}$$

where

$$\mathbf{V} \triangleq \mathrm{Diag}(\mathbf{0}_{(1\times N_b)}, v(n), v(n+1),\ldots,v(n+N_f-1)),$$

$$\check{\mathbf{h}} \triangleq \mathbf{H}[\mathbf{0}_{(1\times N_b)},\mathbf{1},\mathbf{0}_{(1\times N_f-1)}]^H.$$

As in MMSE-LE, $\overline{s}(n)$ and $v(n)$ are replaced with 0 and 1, respectively, to ensure that $\hat{s}(n)$ is independent from $\overline{s}(n)$ which is computed as

$$\hat{s}(n) = 0 + \check{\mathbf{h}}^H\left(\sigma^2\mathbf{I}_N + \mathbf{HVH}^H + (1-v(n))\check{\mathbf{h}}\check{\mathbf{h}}^H\right)^{-1}(\mathbf{y}-\mathbf{H}\overline{\mathbf{s}} + (\overline{s}(n)-0)\check{\mathbf{h}}). \tag{2.80}$$

Having the final expression for feed forward filter coefficients

$$\mathbf{f} \triangleq \check{\mathbf{h}}^H\left(\sigma^2\mathbf{I}_N + \mathbf{HVH}^H + (1-v(n))\check{\mathbf{h}}\check{\mathbf{h}}^H\right)^{-1}\check{\mathbf{h}},$$

the MMSE estimate

$$\hat{s}(n) = \mathbf{f}(\mathbf{y}-\mathbf{H}\overline{\mathbf{s}} + \overline{s}(n)\check{\mathbf{h}}),$$

the statistics

$$\mu(n) = s\mathbf{f}^H\check{\mathbf{h}}, \tag{2.81}$$

$$\sigma^2(n) = \mathbf{f}^H\check{\mathbf{h}}(1-\check{\mathbf{h}}^H\mathbf{f}), \tag{2.82}$$

and the output LLR

$$e_{eq}(s(n)) = 2\mathbf{f}^H\frac{(\mathbf{y}-\mathbf{H}\overline{\mathbf{s}} + \overline{s}(n)\check{\mathbf{h}})}{1-\check{\mathbf{h}}^H\mathbf{f}}, \tag{2.83}$$

can be determined as in MMSE-LE section. During first iteration, $\tilde{l}_{eq}s(n) = 0$, hence, $\mathbf{f}$ is computed using usual MMSE-DFE solution, that's

$$\mathbf{f}_{NA} \triangleq \left(\sigma^2\mathbf{I}_N + \mathbf{H}\text{Diag}(0_{(1\times N_b)}\mathbf{1}_{1\times N_f})\mathbf{H}^H\right)^{-1}\check{\mathbf{h}}, \tag{2.84}$$

and the corresponding output is given by

$$e_{eq}(s(n)) = \frac{2\mathbf{f}_{NA}\mathbf{y}}{1-\check{\mathbf{h}}^H\mathbf{f}_{NA}}. \tag{2.85}$$

The suboptimal solution for MMSE-DFE can also be derived for efficiently computing $\mathbf{f}$, however, it exhibits inferior performance to the MMSE-LE based methods. Therefore, we omit the corresponding derivations here.

## 2.5 Chapter Summary

In this chapter, the basic concepts of communication channels characteristics, encoding, decoding and equalization techniques have been introduced. Tapped delay channel and acoustic shallow water channel characteristics have been demonstrated with details, so as to be applied on the proposed receivers in the later chapters. Channel encoding is a well-known and efficient technique to overcome channel corruptions. The concept of two types of a channel encoding have been presented in this chapter, which are convolution coding and turbo coding.

Furthermore, this chapter depicts non-iterative and iterative equalization techniques which are the key concepts employed extensively in the thesis. Within non-iterative equalization, the equalization and decoding processes are taken place separately and the equalizer depends on the channel characteristics to compute filters taps for equalizing received symbols. LE and DFE are two examples of non-iterative equalizers given in this chapter. While for iterative equalization techniques, the equalization and the decoding are processed jointly in iterative manner such that the apriori information is exchanged between the equalizer and decoder via interleaver permutation for each iteration, such that, the equalization process used also the apriori information provided by the decoder for further reduction of ISI. Linear and non-linear MMSE based equalization are two iterative equalization approaches presented in this chapter.

# 3

# Multiuser Detection Schemes

## 3.1 Introduction

Iterative detection is a strategy to use estimated data symbols in the current iteration to form an estimate of the inter-symbol interference (ISI) or multi-access interference (MAI), and then subtracting it from received signals before detection or equalization in next iteration. It has extensively been studied in direct sequence-code division multiple access (DS-CDMA)[70] [71]. Interleaved division multiple access (IDMA) [72] [73] is another multiaccess scheme which mainly depends on the iterative process for constructing the mean and variance of the total interference from the detected symbols and extracting it from the received signal in the next iteration. IDMA is another kind of the multiple access scheme in which each user is differ from the other user by using a specific interleaver pattern. IDMA can be presented as a special case of CDMA [74] and obtaining many advantages from DS-CDMA. IDMA removes MAI and ISI efficiently by employing random interleaving and chip by chip (CBC) iterative multiuser detection which can handle large numbers of users.

In this chapter, we review the widely studied multiuser detection algorithms based on DS-CDMA and IDMA detection. We briefly explain the detection algorithms used by DS-CDMA systems, and then the iterative detection algorithm of IDMA is illustrated for both frequency flat and multipath channels. To maintain simplicity, only synchronous CDMA and IDMA systems are described in this chapter.

## 3.2 DS-CDMA Detection Schemes

The utilization of DS-CDMA in most applications such as IS-95 and 3G cellular communication standards (CDMA2000, WCDMA, and TD-SCDMA) makes CDMA one of the most popular multiple access techniques in recent years [75]. Each user in DS-CDMA defers from other users by using a distinct coded waveform. Although DS-CDMA shows a higher system performance than traditional time division multiple access (TDMA) and frequency division multiple access (FDMA), its performance is limited by MAI from other users and ISI caused by multipath fading. Therefore, numerous multiuser and equalization techniques have been proposed to suppress these two types of interference. The concept of multiuser detection has been introduced in [4]. After Verdu, various multiuser detectors have been proposed for DS-CDMA systems, such as optimal multiuser detectors, linear minimum mean squared error (MMSE)-based multiuser detector and the decorrelator [76]. Applying turbo principles to multiuser detection produces a variety of iterative multiuser detection algorithms, such as serial interference cancellation (SIC) [77], parallel interference cancellation (PIC)[78][79], probabilistic data association (PDA) detector [80], turbo MMSE-based multiuser detection [81][82] and turbo maximum *a posteriori* probability (MAP)-based multiuser detection[83][75].

## 3.3 Signal Model

The uplink transmission of an uncoded $K$-user DS-CDMA system is depicted in Fig. 3.1 over a multipath fading channel. The information symbols $\{b_k\}_{n=0}^{N_s-1}$ for user $k$, where $1 \leqslant k \leqslant K$, are spread by a length $S$ spreading sequence $\mathbf{g}_k = [g_k(1), g_k(2), \ldots, g_k(S)]$ and the resulting sequence $\mathbf{s}_k$ is transmitted through a multiple access channel. To keep our description concise, the vectors $\mathbf{s}_k$, $\mathbf{g}_k$ and $\mathbf{b}_k$ are assumed to be real numbered taking values from $\{-1, 1\}$, although they are not restricted to be real.

By assuming a synchronous uplink transmission, the received signal can be

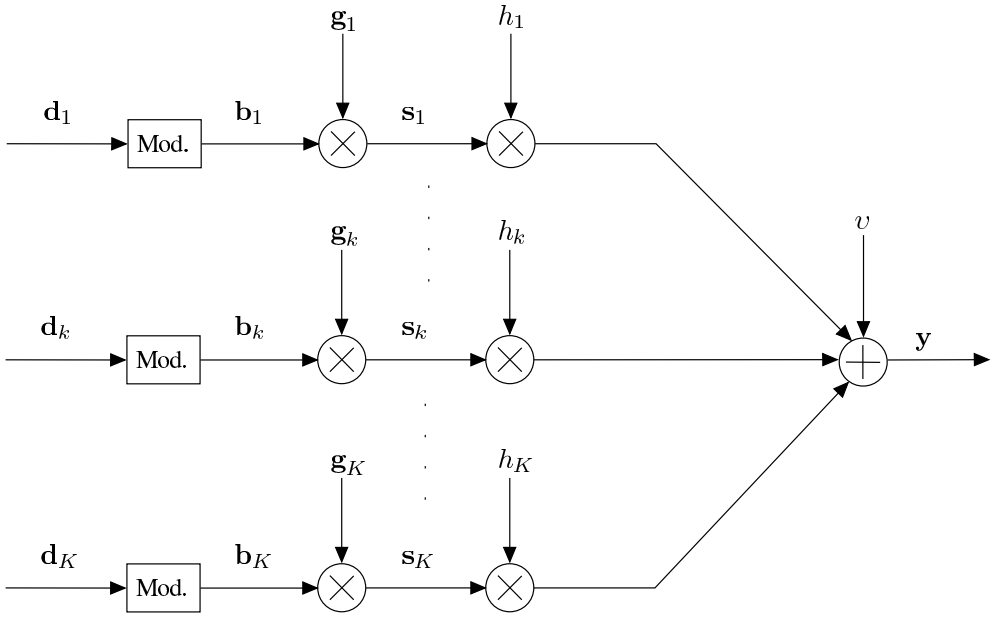


**Figure 3.1:** Diagram of an uplink DS-CDMA system with $K$ users.

expressed as follows

$$\mathbf{y}(n) = \sum_{k=1}^{K} h_k b_k(n)\mathbf{g}_k + \mathbf{v}(n), \quad n = -\infty, \ldots, \infty \tag{3.1}$$

where $h_k$ denotes the channel coefficient for user-$k$, $\mathbf{y}(n) = [y_1(n), y_2(n), \ldots, y_S(n)]$ denotes the $S$-dimensional received signal vector associated with $n$th symbol, and $\mathbf{v}(n) = [v_1(n), v_2(n), \ldots, v_S(n)]^T$ is a zero mean independent $S$-dimensional Gaussian random vector with covariance $\sigma^2\mathbf{I}_S$ ($\mathbf{I}_S$ denotes an $S \times S$ identity matrix).

For simplicity, we can ignore the index $(n)$ and write (3.1) in matrix form as follows

$$\mathbf{y} = [\mathbf{GHb} + \mathbf{v}]^T, \tag{3.2}$$

where $\mathbf{H} = \mathrm{Diag}(h_1, h_2, \ldots, h_K)$ is a diagonal matrix, $\mathbf{G} = [\mathbf{g}_1^T, \mathbf{g}_2^T, \ldots, \mathbf{g}_K^T]^T$, and $\mathbf{b} = [b_1, b_2, \ldots, b_K]^T$.

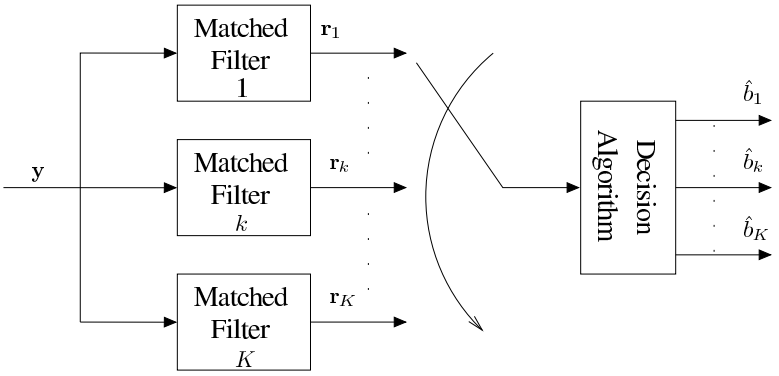


**Figure 3.2:** Optimum detector for $k$-user CDMA Gaussian channels.

## 3.4 Non-Iterative DS-CDMA Detection

### 3.4.1 Optimal Detector

The block diagram of the optimum receiver is shown in Fig. 3.2 for $K$ users. The receiver includes a bank of matched filters, where each filter is matched to a specific user's spreading signature. The received signal containing MAI is processed through the matched filters and the resulting outputs $\mathbf{r} = [r_1, r_2, \ldots, r_K]$ enter the decision algorithm that is utilized to approximate the desired decisions.

Feeding the received signal to the bank filters yields

$$\mathbf{r} = \mathbf{G}^T\mathbf{y} = \mathbf{RHb} + \mathbf{G}^T\mathbf{v}, \tag{3.3}$$

where $\mathbf{R} = \mathbf{G}^T\mathbf{G}$ is the correlation matrix between users and $\mathbf{G}^T\mathbf{v}$ is a $K$-dimensional zero mean vector with covariance $\sigma^2\mathbf{R}$.

A maximum likelihood (ML) sequence detector can be used to implement the optimal receiver algorithm at the output of the matched filter bank. The ML detector can be realized by using a dynamic programming algorithm such as the Viterbi algorithm [4].

### 3.4.2 Suboptimal Multiuser Detector

The improved system performance obtained by the optimal detection requires high computational complexity. Theoretically, the complexity of the optimum

CDMA receiver grows exponentially with the number of users. In practice, to reduce the complexity of the optimum receiver, suboptimal receivers are employed with linear complexity. However, this results in over-all performance degradation.

There are many types of suboptimal detection algorithms such as decorrelator and linear MMSE-based detector. The decorrelator introduced in [84], which uses a linear tranformation of the matched filter output to completely remove the MAI. It is asymptotically optimal as the SNR goes to infinity, i.e $\sigma^2$ goes to zero. The decorrelator has a computational complexity that increases linearly with the number of users but with suboptimal performance. The decorrelator multiplies the outputs of the matched filter bank $\mathbf{r}$ by the inverse of the crosscorrelation matrix, that is

$$\mathbf{R}^{-1}\mathbf{r} = \mathbf{H}\mathbf{b} + \mathbf{R}^{-1}\mathbf{G}^{T}\mathbf{v}. \tag{3.4}$$

For a noiseless channel, the second term on the right-hand side of (3.4) becomes zero, hence, the approximation of the transmitted sequence can be given as

$$\hat{\mathbf{b}}_k = \text{sign}(\mathbf{R}^{-1}\mathbf{r}) = \text{sign}(\mathbf{H}\mathbf{b}). \tag{3.5}$$

On other hand, the linear MMSE multiuser detection substitutes the inverse crosscorrelation matrix by the matrix $\mathbf{M}$ that minimizes the mean-square error between the actual data and the mapping of the matched filter bank. That is

$$\min_{\mathbf{M}\in\mathbf{R}^{K\times K}} \text{E}[||\mathbf{b} - \mathbf{M}\mathbf{r}||^2]. \tag{3.6}$$

The matrix $\mathbf{M}$ is given by [4]

$$\mathbf{M} = [\mathbf{R} + \sigma^2\mathbf{H}^2]^{-1}. \tag{3.7}$$

Thus, the linear MMSE outputs is given as follows

$$\hat{\mathbf{b}}_k = \text{sign}(\mathbf{M}\mathbf{r}) = \text{sign}\left([\mathbf{R} + \sigma^2\mathbf{H}^2]^{-1}\mathbf{r}\right). \tag{3.8}$$

In general, the MMSE detector achieves the best performance compared to the correlator detector, but it needs perfect channel state information (CSI). Even though the correlator detector does not need CSI, however, it suffers from a numerical problem when $\mathbf{R}$ is nearly singular. Moreover, both detectors need to know the spreading sequences of all the users. To prevent the requirement of the CSI and all users' spreading signature, adaptive MMSE, blind MMSE, and iterative detectors are proposed [82][85][86][4].

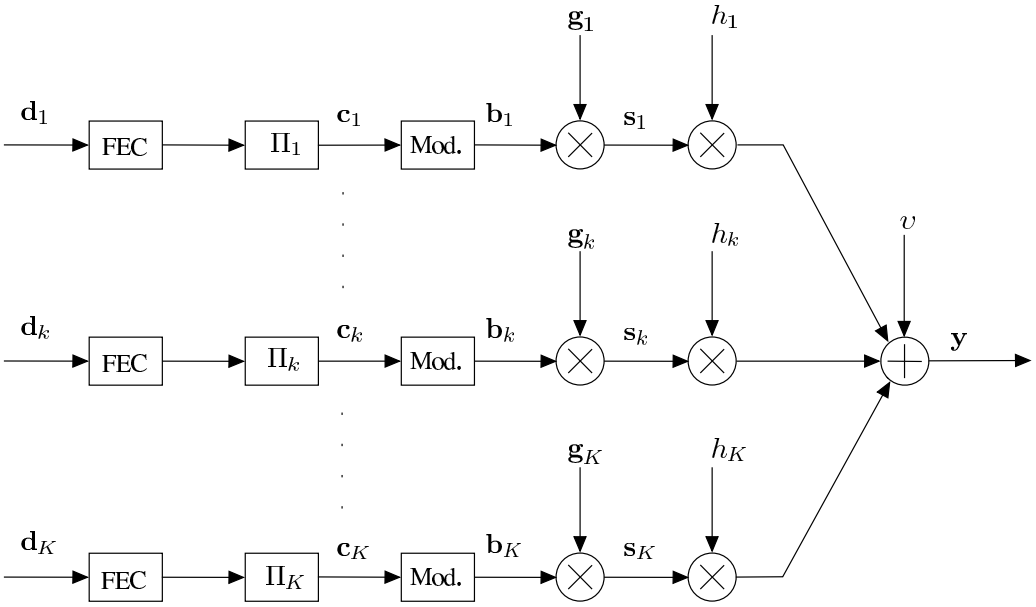


**Figure 3.3:** Transmitter structure of coded CDMA system for $K$ users.

## 3.5 Iterative CDMA Detection

The success of turbo codes as FEC codes, channel estimation and channel equalization resulted in various iterative multiuser detectors [87]-[88]. The output of the current iteration fed back to the front-end is appropriately used in the next iteration. PIC, SIC and PDA are three examples of uncoded iterative multiuser detection. However, the iterative detectors are usually designed for coded receivers. This is because coding is common for practical systems such as IS-95 and CDMA2000. At the same time, using coding to feed-back information can greatly reduce the error propagation within the feedback symbols. The coded iterative detector has a greater complexity than uncoded systems. Therefore, iterative detectors are alternative solutions.

A coded turbo CDMA system is depicted in Fig. 3.3. The information bits of each user $\mathbf{d}_k$ are coded by an FEC encoder, then interleaved and spread before being modulated and transmitted on a multiple access channel. The utilization of a different interleaver for each user makes each user's coded data independent of others, and meets the requirement of the turbo principle.

The general iterative receiver for coded CDMA system is shown in Fig. 3.4. The receiver consists of two major parts, which are the multiuser detector and the bank of $K$ single user *a posteriori* probability (APP) decoders (DEC). These two parts exchange extrinsic information via interleavers and deinterleavers. The APP performs SISO decoding where its feedback symbols $\tilde{l}_k(s(n))$ are used as a priori information in multiuser detection processes to generate $e_k(s(n))$. The multiuser detector may use the feedback information in a different manner. In optimal detection, it is taken as *a priori* probabilities of +1 or -1 for each coded bit [89][90]. While in MMSE detectors, the extrinsic information is used to estimate the mean and covariance of each coded bit [68][91].

The MMSE detection achieves good performance at relatively low complexity, hence, it becomes prominent among all multiuser detectors. The MMSE computes $e(b_k(n))$ [68] as

$$e(b_k) = \frac{2h_k\lambda_k^T(\mathbf{V}_k + \sigma^2\mathbf{R}^{-1})(\mathbf{R}^{-1}\mathbf{r} - \mathbf{H}\overline{\mathbf{b}}_k)}{1 - h_k^2\lambda_k^T(\mathbf{V}_k + \sigma^2\mathbf{R}^{-1})^{-1}\lambda_k}, \tag{3.9}$$

where

$$\overline{\mathbf{b}}_k = [\overline{b}_1, \overline{b}_2, \ldots, \overline{b}_K]^T,$$

with $\overline{b}_k = \tanh(\tilde{l}_k/2)$ denoting the mean of $b_k$,

$$\mathbf{V}_k = \mathrm{Diag}(h_1^2 v_1, \ldots, h_{k-1}^2 v_{k-1}, h_k^2, h_{k+1}^2 v_{k+1}, \ldots, h_K^2 v_k)$$

with $v_k = 1 - (\overline{b}_k)^2$ denoting the variance of $b_k$ and $\lambda_k$ is a $K$-dimensional vector of all zeros except for the $k$th element, which is 1.

## 3.6 IDMA Detection Algorithm

New studies in iterative detection techniques have showed that the complexity of MUD could be reduced to a level comparable to single user detection. IDMA is a possible scheme toward this direction. Unlike CDMA which uses spreading code to provide coding gain, IDMA employs a low coding rate which results in a notable reduction in complexity. Since IDMA is a chip by chip detector, it has the same advantages like CDMA such as asynchronous transmission, robustness against fading and cross-cell interference.

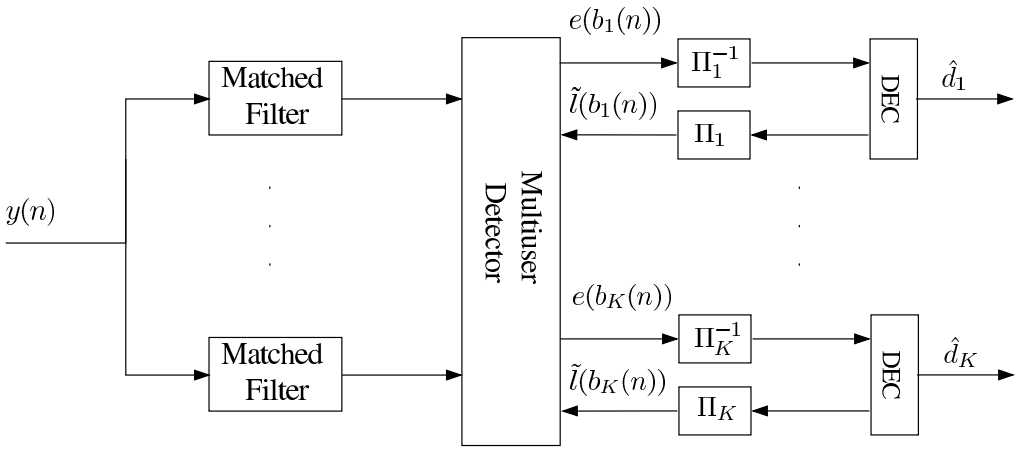


**Figure 3.4:** Structure of iterative CDMA receiver.

### 3.6.1 Signal Model

In this section, the basic principles of IDMA are introduced. Fig.3.5 depicts the uplink IDMA transmitter of the $K$users. Let $\{d_k\}$ denote the binary message sequence and $\{c_k\}_{i=0}^{N_d/R_c-1}$ denote the user's data after error control encoding with $R_c$ and $N_d$ representing the code rate and number of transmitted data bits, respectively. A specific interleaver pattern for each user ($\Pi_k$) then permutes the coded output bits. After interleaving, each group of interleaved coded bits $\{x_k\}$ are mapped to QPSK symbols $\{s_k\}_{n=0}^{N_s-1}$, where $N_s$ is the number of transmitted symbols that are taken from a $M$-ary symbol alphabet: $\chi \triangleq \{\alpha_1, ..., \alpha_M\}$ with $E\{\chi\} = 0$ and $E\{|\alpha_q|^2\} = 1$. We use superscripts I and Q or function notation Re(.) and Im(.) to indicate the real and imaginary parts, respectively. After symbol mapping, we have

$$s_k(n) = s_k^I(n) + j s_k^Q(n).$$

Interleavers are the only means in IDMA detection to separate users' signals, therefore, choosing weakly correlated different interleaver schemes is very important to obtain good IDMA performance. Li Ping [92] proposed a random interleaver generated randomly and independently. This type of interleaver can randomize the MAI at the receiver end efficiently. The power interleaver [93],

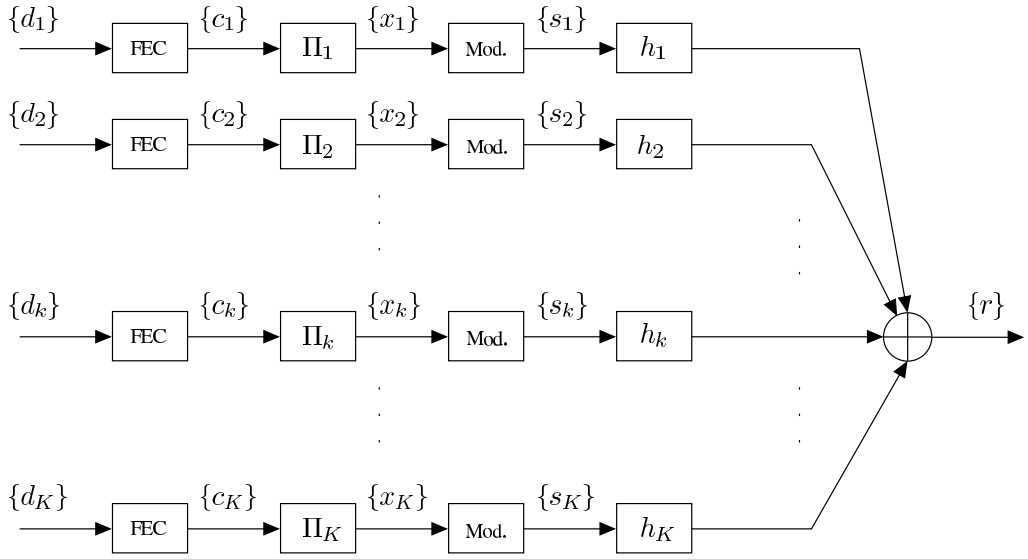


**Figure 3.5:** The transmitter components for the K users.

orthogonal interleaver, pseudo random interleaver [94] and 2-dimensional interleaver [95] are other examples of interleavers that can be used in IDMA systems for obtaining better performance. In this thesis, random interleavers have been used in the IDMA transceiver to retain the simplicity of the system.

### 3.6.2 IDMA on AWGN Channels

Our focus is the detection algorithm for IDMA on noisy channels described in [73]. For AWGN channels, the received signal can then be represented as

$$r(n) = \sum_{k} s_k(n) + \upsilon(n), \tag{3.10}$$

where $\upsilon(n)$ are samples of additive White Gaussian noise (AWGN) with variance $\sigma^2 = N_0/2$. An iterative suboptimal receiver structure has been illustrated in Fig. 3.6. The receiver structure includes an elementary signal estimator (ESE) and $K$ single-user a posteriori probability (APP) decoders (DECs) such that the multiple access and coding constraints are considered separately in the ESE and DECs. The outputs of the ESE and DECs are LLRs of $\{s_k^I(n), s_k^Q(n)\}$ defined below [6][96]

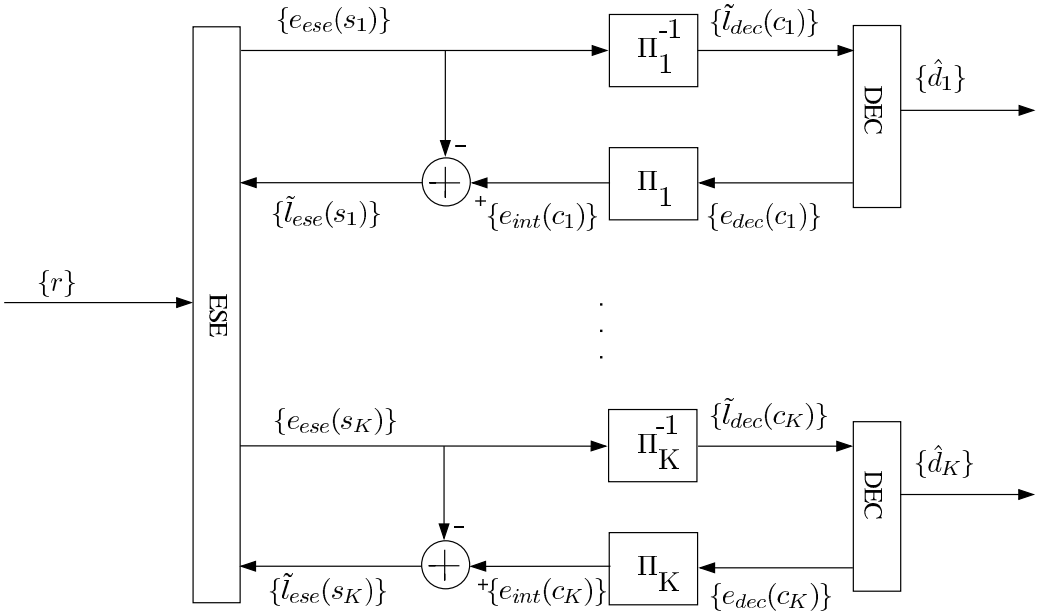


**Figure 3.6:** IDMA Reciever for AWGN channels.

$$e(s_k^I(n)) \equiv \log\left(\frac{Pr(s_k^I(n)=+1)}{Pr(s_k^I(n)=-1)}\right), \qquad \forall k,n. \tag{3.11}$$

We concentrate on detecting the real part, $s_k^I(n)$, as detection of $s_k^Q(n)$ can be handled in a similar manner.

A global turbo-type iterative process is then applied to process the LLRs generated by the ESE ($e_{ese}$) and DECs ($e_{dec}$). The ESE operation can be carried out in a chip-by-chip manner because of the random interleaver, with only one sample $r(n)$ used at a time. We can rewrite (3.10) as

$$r(n) = s_k(n) + \zeta(n), \tag{3.12}$$

where

$$\zeta(n) = r(n) - s_k(n) = \sum_{k' \neq k} s_{k'}(n) + v(n) \tag{3.13}$$

is the MAI interference plus noise distortions in $r(n)$ with respect to user $k$. $\zeta(n)$ can be approximated as a Gaussian variable according to the central limit

theorem and $r(n)$ can be characterized by a conditional Gaussian probability density function

$$p\left(r^I(n)|s_k^I(n)=\mp 1\right)=\frac{1}{\sqrt{2\pi \mathrm{Var}[\zeta(n)]}}\exp\left(-\frac{\left(r^I(n)-(\mp 1+\mathrm{E}[\zeta(n)])\right)^2}{2\mathrm{Var}[\zeta(n)]}\right) \tag{3.14}$$

where Var[.] and E[.] are the variance and mean, respectively. The chip-by-chip detection in ESE based on (3.12)-(3.14) can be given in two steps. The first step estimates the interference mean and variance as follows

$$\mathrm{E}[r^I(n)]=\sum_k \mathrm{E}[s_k^I(n)], \tag{3.15a}$$

$$\mathrm{Var}[r^I(n)]=\sum_k \mathrm{Var}[s_k^I(n)]+\sigma^2, \tag{3.15b}$$

$$\mathrm{E}[\zeta(n)^I]=\mathrm{E}[r^I(n)]-\mathrm{E}[s_k^I(n)], \tag{3.15c}$$

$$\mathrm{Var}[\zeta(n)^I]=\mathrm{Var}[r^I(n)]-\mathrm{Var}[s_k^I(n)], \tag{3.15d}$$

where (E$[r^I(n)]$, Var $[r^I(n)]$) are the real part of the total mean and the total variance of the received signal, and (E$[\zeta(n)^I]$, Var $[\zeta(n)^I]$) are the real part of the total mean and the total variance of the interference, respectively. Step two generates the LLR values as given below

$$\begin{aligned} e_{ese}(s_k^I(n)) &= \log\left(\frac{p\left(r^I(n)|s_k^I(n)=+1\right)}{p\left(r^I(n)|s_k^I(n)=-1\right)}\right) \\ &= \log\left(\frac{\exp\left(-\frac{(r^I(n)-\mathrm{E}[\zeta(n)]-1)^2}{2\mathrm{Var}[\zeta(n)]}\right)}{\exp\left(-\frac{(r^I(n)-\mathrm{E}[\zeta(n)]+1)^2}{2\mathrm{Var}[\zeta(n)]}\right)}\right) \\ &= 2\frac{r^I(n)-\mathrm{E}[\zeta^I(n)]}{\mathrm{Var}[\zeta^I(n)]}. \end{aligned} \tag{3.16}$$

The DECs employ standard APP decoding on $\tilde{l}_{\mathrm{dec}}(c_k(i)))$ to generate *a posteriori* LLRs $e_{\mathrm{dec}}(c_k(i)))$. The output of the DECs are LLRs of $(\{s_k^I(n)\},\{s_k^I(n)\})$. The real LLRs are defined as

$$\mathrm{Re}\{e_{dec}(c_k)\}=\log\left(\frac{P_r(\Gamma_k/\mathrm{Re}\{s_k\}=+1)}{P_r(\Gamma_k/\mathrm{Re}\{s_k\}=-1)}\right). \tag{3.17}$$

where $\Gamma_k$ denotes the equalized and deinterleaved version of the outputs of the ESE. The equations presented for the real part can also be adjusted accordingly to obtain the imaginary part $\mathrm{Im}\{e_{\mathrm{dec}}(c_k)\}$ of the extrinsic LLRs. The extrinsic LLRs of the DEC after interleaving are given by

$$\tilde{l}_{ese}(x_k(i)) = e_{int}(x_k(i)) - e_{ese}(x_k(i)), \tag{3.18}$$

however, for a number of users less than 16 [10], equation (3.18) can be approximated as follows:

$$\tilde{l}_{ese}(x_k(i)) = e_{int}(x_k(i)). \tag{3.19}$$

The $\tilde{l}_{pic}(x_k(i))$ soft chips are used to generate the statistics as follows

$$\mathrm{E}(s_k(n)) = \tanh(\frac{\tilde{l}_{ese}(x_k(i))}{2}) + i\ \tanh(\frac{\tilde{l}_{ese}(x_k(i+1))}{2}), \tag{3.20a}$$

$$\mathrm{Var}(s_k(n)) = \left(1 - (\tanh(\frac{\tilde{l}_{pic}(x_k(i))}{2}))^2\right) + i\left(1 - (\tanh(\frac{\tilde{l}_{pic}(x_k(i+1))}{2}))^2\right). \tag{3.20b}$$

The real and imaginary parts of $s_k(n)$ are assumed to be uncorrelated due to the interleavers. The ESE uses $E(s_k(n))$ and $\mathrm{Var}(s_k(n))$ to update the interference mean and variance in (3.15a)-(3.15d). Initially, $E(s_k(n)) = 0$ and $\mathrm{Var}(s_k(n)) = I$ for all $k, n$, implying no information is fed back from the DECs.

### 3.6.3 IDMA Over Multipath Selective Channels

In this section, the detection algorithm for IDMA scheme in complex multipath fading channels is introduced [97]. We assume a channel model with $L_k$ paths for the $k$th user, with complex-valued fading coefficients $\{h_k(l)\}_{l=0}^{L_k-1}$. Hence, the received signal is given as follows

$$r(n) = \sum_{k,l} h_k(l)s_k(n-l) + \upsilon(n). \tag{3.21}$$

We concentrate on $s_k^I(n)$ detection for the $k$th user from path $l$. Rewriting (3.21) as

$$r(n+l) = h_k(l)s_k(n) + \zeta_{k,l}(n), \tag{3.22}$$

where $\zeta_{k,l}(n)$ consists of MAI, ISI and noise dispersions and we denote $h_k^*(l)$ as complex conjugate of $h_k(l)$. The phase shift due to $h_k(l)$ is cancelled out by $h_k^*(l)r(n+l)$, which means that $\mathrm{Im}(h_k^*(l)r(n+l))$ is not a function of $\mathrm{Re}(h_k^*(l)r(n+l))$. Hence, by generating

$$\tilde{r}(n+l) = h_k^*(l)r(n+l) =\mid h_k(l) \mid^2 s_k(n) + \tilde{\zeta}_{k,l}(n), \tag{3.23}$$

the total interference $\tilde{\zeta}_{k,l}(n) = h_k^*\zeta_{k,l}(n)$ can be approximated as a Gaussian variable. This is employed to generate LLRs for $s_k(n)$ by ESE detection

$$\begin{aligned} e_{ese}(s_k^I(n))_l &= \log\left(\frac{p\left(\tilde{r}^I(n+l)|s_k^I(n)=+1\right)}{p\left(\tilde{r}^I(n+l)|s_k^I(n)=-1\right)}\right) \\ &= \log\left(\frac{\exp\left(-\frac{(\tilde{r}^I(n+l)-\mathrm{E}[\tilde{\zeta}_{k,l}(n)]-|h_k(l)|^2)^2}{2\mathrm{Var}[\tilde{\zeta}_{k,l}(n)]}\right)}{\exp\left(-\frac{(\tilde{r+l}^I(n)-\mathrm{E}[\tilde{\zeta}_{k,l}(n)]+|h_k(l)|^2)^2}{2\mathrm{Var}[\tilde{\zeta}_{k,l}(n)]}\right)}\right) \\ &= 2 \mid h_k(l) \mid^2 \frac{\tilde{r}^I(n+l) - \mathrm{E}[\tilde{\zeta}_{k,l}^I(n)]}{\mathrm{Var}[\tilde{\zeta_{k,l}}^I(n)]}, \end{aligned} \tag{3.24}$$

and

$$e_{ese}(s_k^I(n)) = \sum_{l=0}^{L_k-1} e_{ese}(s_k^I(n))_l. \tag{3.25}$$

For determining $e_{ese}(s_k^I(n))_l$ in (3.24), the calculations to find $\mathrm{E}[\tilde{\zeta_{k,l}}^I(n)]$ and $\mathrm{Var}[\tilde{\zeta_{k,l}}^I(n)]$ should be considered. Defining the covariance matrix as

$$\mathbf{Cov} = \begin{pmatrix} \mathrm{Var}[\alpha^I] & \mathrm{E}[\alpha^Q\alpha^Q] - \mathrm{E}[\alpha^I]\mathrm{E}[\alpha^Q] \\ \mathrm{E}[\alpha^Q\alpha^Q] - \mathrm{E}[\alpha^I]\mathrm{E}[\alpha^Q] & \mathrm{Var}[\alpha^Q] \end{pmatrix}, \tag{3.26}$$

then according to (3.23), we have

$$\mathrm{E}[\tilde{\zeta}_{k,l}(n)] = h_k^*(l)\tilde{\zeta}_{k,l}(n), \tag{3.27a}$$

$$\mathrm{Var}[\tilde{\zeta}_{k,l}(n)] = \mathbf{R}_k^T(l)\mathbf{Cov}(\zeta_{k,l}(n))\mathbf{R}_k(l), \tag{3.27b}$$

where

$$\mathbf{R}_k(l) = \begin{pmatrix} h_k^I(l) & -h_k^Q(l) \\ h_k^I(l) & h_k^I(l) \end{pmatrix}. \tag{3.28}$$

Then by (3.22), we obtain

$$\mathrm{E}[\zeta_{k,l}(n)] = \mathrm{E}[r(n+l)] - h_k(l)\mathrm{E}[s_k(n)], \tag{3.29a}$$

$$\mathbf{Cov}(\zeta_{k,l}(n)) = \mathbf{Cov}(r(n+l)) - \mathbf{R}_k(l)\mathbf{Cov}(s_k(n))\mathbf{R}_k^T(l). \tag{3.29b}$$

In (3.29a) and (3.29b), the mean and variance of the received signal are estimated as follows

$$\mathrm{E}(r(n)) = \sum_{k,l} \mathrm{E}[s_k(n-l)], \tag{3.30a}$$

$$\mathbf{Cov}(r(n)) = \sum_{k,l} \mathbf{R}_k(l)\mathbf{Cov}(s-k(n-l))\mathbf{R}_k^T(l) + \sigma^2\mathbf{I}, \tag{3.30b}$$

where $\mathbf{I}$ is a $2 \times 2$ identity matrix. The outputs of the ESE are used by the DECs to generate extrinsic LLRs for $s_k^I(n)$ and $s_k^Q(n)$ which in turn return back to the ESE to generate the following statistics

$$\mathrm{E}[s_k(n)] = \tanh(\frac{\tilde{l}_{ese}(x_k(i))}{2}) + i\tanh(\frac{\tilde{l}_{ese}(x_k(i+1))}{2}), \tag{3.31a}$$

$$\mathbf{Cov}(s_k(n)) = \begin{pmatrix} 1-(\tanh(\frac{\tilde{l}_{ese}(x_k(i))}{2}))^2 & 0 \\ 0 & 1-(\tanh(\frac{\tilde{l}_{ese}(x_k(i+1))}{2}))^2 \end{pmatrix}. \tag{3.31b}$$

### 3.6.4 Chapter Summary

This chapter focuses on CDMA and IDMA transmission systems. The optimal and sub-optimal multiuser detection for CDMA system based on MMSE criteria have been explained with mathematical equations. Moreover, the general components of iterative CDMA receiver and the fundamental concepts of iterative chip-by-chip IDMA detection are demonstrated for sake of comparing their performances in multipath fading channels when the proposed multidimensional equalization systems are applied on them in later chapters.

# 4

# Optimization and Analysis of Centralized Multi-dimensional Equalizers

## 4.1 Introduction

Employing interleaving schemes in a rake IDMA receiver and special spreading sequences in CDMA detection are examples of traditional multiuser detection schemes for selective channels. Alternatively, utilizing MDE with MUD is another method for combating channel effects and successful symbol detection. The structure of MDE and MUD schemes depends on the transmission scenario. For a downlink scenario, since all users are transmitting signal over same channel characteristics, one equalizer could be used with IDMA detection [31][98]. The situation is further worsened for uplink transmission. In spite of MAI in the received signal, different ISI disruption occurs in each user signal due to different channel effects. Therefore, using MDE with MUD for uplink requires a special design to combine symbol equalization and detection techniques. In this chapter, we introduce MDE for mitigating MAI and ISI on multipath selective channels.

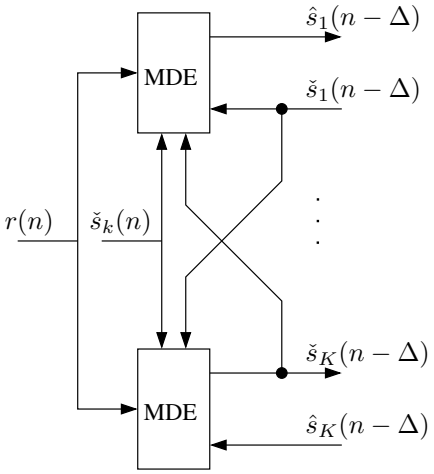


**Figure 4.1:** Centralized MDE structure.

## 4.2 Optimal Centralized MDE-IDMA Receiver

Fig 4.1 depicts the centralized MDE receiver structure. The sequence $\{s_k\}_{n=0}^{N_s-1}$ is the $k$th user transmitted symbols, where $N_s$ is the number of the transmitted symbols, which are taken from a $M$-ary symbol alphabet: $\chi \triangleq \{\alpha_1, ..., \alpha_M\}$ with $E\{\chi\} = 0$ and $E\{|\alpha_q|^2\} = 1$. We assume a channel model with $L_k$ paths for the $k$th user, with complex-valued fading coefficients $\{h_k(l)\}_{l=0}^{L_k-1}$. The received signal can then be represented as

$$r(n) = \sum_{k,l} h_k(l) s_k(n-l) + \upsilon(n), \tag{4.1}$$

where $\upsilon(n)$ are complex-valued samples of zero-mean AWGN with variance $\sigma_v^2 = N_0/2$.

The MDEs are responsible for jointly removing MAI and ISI effects. For each iteration the extrinsic LLRs, for some integer delay $\Delta \geqslant 0$, are exchanged between the MDE and the decoders. The MDE equalizer can be designed as MLE or MDFE. Assuming that the feedback symbols from the DECs are free of errors, *i.e* the $\check{s}_k(n-\Delta)$ can be replaced with $s_k(n-\Delta)$, and the criterion for designing the MDE equalizer coefficients is obtained by minimizing the variance of the error signal, which can be given as

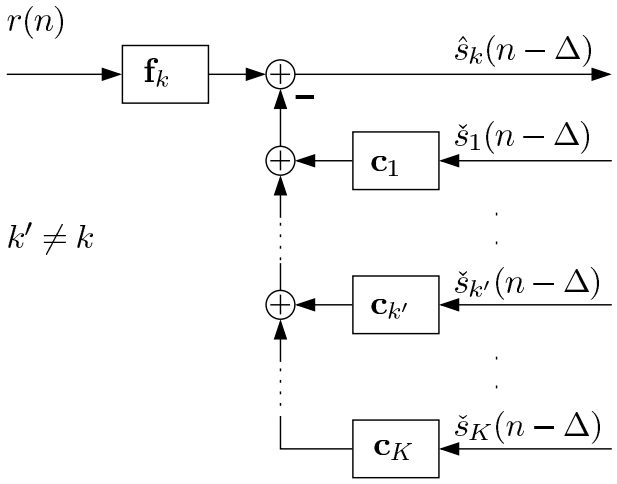


**Figure 4.2:** MLE structure.

$$e_k(n-\Delta) = s_k(n-\Delta) - \hat{s}_k(n-\Delta). \tag{4.2}$$

### 4.2.1 Multi-dimensional LE (MLE)

The MLE structure is shown in Fig.4.2. The received data symbols $r(n)$ in (4.1) can be rewritten as follows:

$$\begin{aligned} r(n) = h_k(0)s_k(n) + \underbrace{\sum_{l=1}^{l=L_k-1} h_k(l)s_k(n-l)}_{ISI} \\ + \underbrace{\sum_{k',l=0}^{l=L_k-1} h_{k'}(l)s_{k'}(n-l)}_{MAI} + \upsilon(n), \quad \forall j \in [0, N_s) \end{aligned} \tag{4.3}$$

where $1 \leqslant k' \leqslant K$ and $k' \neq k$.

By expressing the received observed symbols and the returned feedback sym-

$$\boldsymbol{\Xi}_k \triangleq \mathrm{E}\begin{bmatrix} s_k(n-\Delta) \\ s_1(n-\Delta) \\ \vdots \\ s_{k'}(n-\Delta) \\ \vdots \\ s_K(n-\Delta) \\ \mathbf{y} \end{bmatrix}\begin{bmatrix} \mathbf{s}_k \\ \mathbf{s}_1 \\ \vdots \\ \mathbf{s}_{k'} \\ \vdots \\ \mathbf{s}_K \\ \mathbf{y} \end{bmatrix}^H \triangleq \begin{bmatrix} \lambda_k & \mathbf{r}_{s_k\mathbf{s}_1} & \cdots & \mathbf{r}_{s_k\mathbf{s}_{k'}} & \cdots & \mathbf{r}_{s_k\mathbf{s}_K} & \mathbf{r}_{s_k\mathbf{y}} \\ \mathbf{r}_{s_1\mathbf{s}_k} & \lambda_1 & \cdots & \mathbf{r}_{s_1\mathbf{s}_{k'}} & \cdots & \mathbf{r}_{s_1\mathbf{s}_K} & \mathbf{r}_{s_1\mathbf{y}} \\ \vdots & \vdots & \ddots & \vdots & \ddots & \vdots & \vdots \\ \mathbf{r}_{s_{k'}\mathbf{s}_k} & \mathbf{r}_{s_{k'}\mathbf{s}_1} & \cdots & \lambda_{k'} & \cdots & \mathbf{r}_{s_{k'}\mathbf{s}_K} & \mathbf{r}_{s_{k'}\mathbf{y}} \\ \vdots & \vdots & \ddots & \vdots & \ddots & \vdots & \vdots \\ \mathbf{r}_{s_K\mathbf{s}_k} & \mathbf{r}_{s_K\mathbf{s}_1} & \cdots & \mathbf{r}_{s_K\mathbf{s}_{k'}} & \cdots & \lambda_K & \mathbf{r}_{s_K\mathbf{y}} \\ \mathbf{R}_{\mathbf{y}\mathbf{s}_k} & \mathbf{R}_{\mathbf{y}\mathbf{s}_1} & \cdots & \mathbf{R}_{\mathbf{y}\mathbf{s}_{k'}} & \cdots & \mathbf{R}_{\mathbf{y}\mathbf{s}_K} & \mathbf{R}_{\mathbf{y}} \end{bmatrix} \tag{4.5}$$

bols in column form as

$$\mathbf{y} = \begin{bmatrix} r(n) \\ r(n-1) \\ r(n-2) \\ . \\ . \\ . \\ . \\ r(n-N_f+1) \end{bmatrix}, \quad \mathbf{s}_{k'} = \begin{bmatrix} s_{k'}(n-\Delta) \\ s_{k'}(n-\Delta-1) \\ s_{k'}(n-\Delta-2) \\ . \\ . \\ . \\ . \\ s_{k'}(n-\Delta-N_c+1) \end{bmatrix}, \tag{4.4}$$

where $N_f$ and $N_c$ are the lengths of feed forward filter and cross-over filter taps, respectively, the covariances and cross-covariances of $\mathbf{y}$ and $\mathbf{s}_{k'}$ ($\boldsymbol{\Xi}_k$) can be obtained as given in (4.5), where

$$\lambda_k = [\underbrace{0 \quad 0 \quad \ldots}_{\Delta} 1 \quad \ldots \quad 0 \quad 0],$$

is a vector of length $N_c$, and $(.)^H$ denotes the conjugate transpose operation.

By assuming low correlation between users' data sequence, the cross-covariance values can be assumed to be zero, that is

$$\boldsymbol{\Xi}_k \triangleq \begin{bmatrix} \lambda_k & 0 & \cdots & 0 & \cdots & 0 & \mathbf{r}_{s_k\mathbf{y}} \\ 0 & \lambda_1 & \cdots & 0 & \cdots & 0 & \mathbf{r}_{s_1\mathbf{y}} \\ \vdots & \vdots & \ddots & \vdots & \ddots & \vdots & \vdots \\ 0 & 0 & \cdots & \lambda_{k'} & \cdots & 0 & \mathbf{r}_{s_{k'}\mathbf{y}} \\ \vdots & \vdots & \ddots & \vdots & \ddots & \vdots & \vdots \\ 0 & 0 & \cdots & 0 & \cdots & \lambda_K & \mathbf{r}_{s_K\mathbf{y}} \\ \mathbf{R}_{\mathbf{y}\mathbf{s}_k} & \mathbf{R}_{\mathbf{y}\mathbf{s}_1} & \cdots & \mathbf{R}_{\mathbf{y}\mathbf{s}_{k'}} & \cdots & \mathbf{R}_{\mathbf{y}\mathbf{s}_K} & \mathbf{R}_{\mathbf{y}} \end{bmatrix} \tag{4.6}$$

hence,

$$\mathbf{\Xi}_k = \begin{bmatrix} \mathbf{\Xi}_\sigma & \mathbf{\Xi}_{s_k\mathbf{y}} \\ \mathbf{\Xi}_{\mathbf{y}s_k} & \mathbf{R}_\mathbf{y} \end{bmatrix}, \tag{4.7}$$

where $\mathbf{\Xi}_{s_k\mathbf{y}} \in \mathbb{C}^{K\times N_f}$ and $\mathbf{\Xi}_{\mathbf{y}s_k} \in \mathbb{C}^{N_f\times N_cK}$ denotes the last column and last row of the matrix $\mathbf{\Xi}_k$, respectively, $\mathbf{\Xi}_\sigma \in \mathbb{C}^{K\times N_cK}$ is the remaining elements of matrix $\mathbf{\Xi}_k$, and $(.^H)$ denotes the conjugate transpose.

Moreover, the processes $s_k(n-\Delta)$ and $\mathbf{s}_{k'}$ are jointly wide-sense stationary with $\mathbf{y}$ so the the quantities

$$\mathbf{R}_\mathbf{y} = \mathrm{E}\left[\mathbf{y}\mathbf{y}^H\right] = \textstyle\sum_k \mathbf{H}_{d_k}\mathbf{R}_{\mathbf{s}_k}\mathbf{H}_{d_k}^H + \mathbf{R}_v,$$

$$\mathbf{r}_{s_k\mathbf{y}} = \mathrm{E}\left[s_k(n-\Delta)\mathbf{y}^H\right] = \Lambda_{s_k}\mathbf{H}_{d_k}^H,$$

$$\mathbf{r}_{\mathbf{s}_{k'}\mathbf{y}} = \mathrm{E}\left[\mathbf{s}_{k'}\mathbf{y}^H\right] = \textstyle\sum_{k'} \mathbf{R}_{\mathbf{c}_{k'}}\mathbf{H}_{d_k'}^H,$$

are independent of $n$, where

$$\Lambda_{s_k} = [\underbrace{0 \quad 0 \quad \dots}_{\Delta} 1 \quad \dots \quad 0 \quad 0],$$

$\mathbf{H}_{d_k}$ is the channel matrix of size $(N_f \times L_k + N_f - 1)$ which is constructed from the estimated channel taps during training mode

$$\mathbf{H}_{d_k} = \begin{bmatrix} h_k(0) & \dots & h_k(L_k-1) & 0 & \dots & 0 \\ \vdots & \ddots & \ddots & \ddots & \ddots & \vdots \\ 0 & \dots & 0 & h_k(0) & \dots & h_k(L_k-1) \end{bmatrix}, \tag{4.8}$$

and $\mathbf{R}_{s_k}$ and $\mathbf{R}_{\mathbf{c}_{k'}}$ are the covariance matrices of the $k$th user and interfered users' data symbols of sizes $(N_f + L_k - 1 \times N_f + L_k - 1)$ and $(N_c \times N_f + L_k - 1)$, respectively.

The covariance matrix for each user

$$\mathbf{R}_k \triangleq \begin{bmatrix} \sigma_k & \mathbf{r}_{s_k\mathbf{y}} \\ \mathbf{r}_{s_k\mathbf{y}}^H & \mathbf{R}_\mathbf{y} \end{bmatrix}, \tag{4.9}$$

is assumed to be positive definite and invertible. This assumption also makes $\mathbf{R}_\mathbf{y}$ positive-definite and invertible. The positive-definiteness of $\mathbf{R}_\mathbf{y}$ guarantees that both $\mathbf{R}_{\mathbf{y}_k}$ and the Schur complement of $\mathbf{R}_k$ with respect to $\mathbf{R}_\mathbf{y}$ are positive-definite matrices too, i.e

$$\mathbf{R}_{\mathbf{y}} > 0, \quad \mathbf{\Xi}_{\delta_k} \triangleq \mathbf{\Xi}_{\sigma} - \mathbf{\Xi}_{s\mathbf{y}}\mathbf{R}_{\mathbf{y}}^{-1}\mathbf{\Xi}_{\mathbf{ys}} > 0,$$

where the Schur complement is denoted by $\mathbf{\Xi}_{\delta_k}$ [25].

The optimal filter taps for the $k$th user can be determined by solving

$$\Delta J = \min_{\mathbf{f}_k, \mathbf{c}_{k'}} E|e_k(n-\Delta)|^2. \tag{4.10}$$

where $\mathbf{f}_k$ and $\mathbf{c}_{k'}$ are the $k$th user feed-forward and crossover filters, respectively. Moreover, (4.2) can be rewritten as

$$e_k(n-\Delta) = s_k(n-\Delta) - \sum_{k,l_f=0}^{l_f=N_f-1} f_k^*(l_f) r(n-l_f) + \sum_{k',l_c=0}^{l_c=N_c-1} c_{k'}^*(l_c) s_{k'}(n-\Delta-l_c). \tag{4.11}$$

By collecting the coefficients of $f_k^*(l_f)$ and $c_{k'}^*(l_c)$ in row form

$$\mathbf{f}_k^H \triangleq [f_k^*(0) \quad f_k^*(1) \quad \cdots \quad f_k^*(N_f-1)],$$

$$\mathbf{c}_{k'}^H \triangleq [c_{k'}^*(0) \quad c_{k'}^*(1) \quad \cdots \quad c_{k'}^*(N_c-1)],$$

the expression in (4.11) can be rewritten in vector form as follows

$$e_k(n-\Delta) = s_k(n-\Delta) - \mathbf{f}_k^H \mathbf{y} + \sum_{k'} \mathbf{c}_{k'}^H \mathbf{s}_{k'}. \tag{4.12}$$

By substituting (4.12) in (4.10), the optimization problem can be rewritten as follows

$$\Delta J = \min_{\mathbf{f}_k, \mathbf{c}_{k'}} \mathrm{E}[|s_k(n-\Delta) - \mathbf{f}_k^H \mathbf{y} + \sum_{k'} \mathbf{c}_{k'}^H \mathbf{s}_{k'}|^2]. \tag{4.13}$$

Furthermore, (4.13) can be rewritten as follows

$$
\begin{aligned}
\Delta J &= \min_{\mathbf{f}_k,\mathbf{c}_{k'}} \mathrm{E}\left[\left(s_k(n-\Delta) - \mathbf{f}_k^H\mathbf{y} + \sum_{k'}\mathbf{c}_{k'}^H\mathbf{s}_{k'}\right)\left(s_k(n-\Delta) - \mathbf{f}_k^H\mathbf{y} + \sum_{k'}\mathbf{c}_{k'}^H\mathbf{s}_{k'}\right)^H\right] \\
&= \min_{\mathbf{f}_k,\mathbf{c}_{k'}} \mathrm{E}\left[\left(s_k(n-\Delta) - \mathbf{f}_k^H\mathbf{y} + \sum_{k'}\mathbf{c}_{k'}^H\mathbf{s}_{k'}\right)\left(s_k(n-\Delta)^H - \mathbf{y}^H\mathbf{f}_k + \sum_{k'}\mathbf{s}_{k'}^H\mathbf{c}_{k'}\right)\right] \\
&= \min_{\mathbf{f}_k,\mathbf{c}_{k'}} \mathrm{E}[s_k(n-\Delta)s_k(n-\Delta)^H - s_k(n-\Delta)\mathbf{y}^H\mathbf{f}_k + s_k(n-\Delta)\sum_{k'}\mathbf{s}_{k'}^H\mathbf{c}_{k'} \\
&- \mathbf{f}_k^H\mathbf{y}s_k(n-\Delta)^H + \mathbf{f}_k^H\mathbf{y}\mathbf{y}^H\mathbf{f}_k - \mathbf{f}_k^H\mathbf{y}\sum_{k'}\mathbf{s}_{k'}^H\mathbf{c}_{k'} \\
&+ \sum_{k'}\mathbf{c}_{k'}^H\mathbf{s}_{k'}s_k(n-\Delta)^H - \sum_{k'}\mathbf{c}_{k'}^H\mathbf{s}_{k'}\mathbf{y}^H\mathbf{f}_k + \sum_{k'}\mathbf{c}_{k'}^H\mathbf{s}_{k'}\mathbf{s}_{k'}^H\mathbf{c}_{k'}].
\end{aligned}
\tag{4.14}
$$

With the aforementioned definitions (4.14), becomes

$$
\begin{aligned}
\Delta J &= \min_{\mathbf{f}_k,\mathbf{c}_{k'}} \mathrm{E}[1 - \mathbf{r}_{s_k\mathbf{y}}\mathbf{f}_k + 0 \\
&- \mathbf{f}_k^H\mathbf{r}_{\mathbf{y}s_k} - \mathbf{f}_k^H\mathbf{R}_\mathbf{y}\mathbf{f}_k + \mathbf{f}_k^H\sum_{k'}\boldsymbol{\Xi}_{\mathbf{s}_{k'}\mathbf{y}}^H\mathbf{c}_{k'} \\
&+ 0 - \sum_{k'}\mathbf{c}_{k'}^H\boldsymbol{\Xi}_{\mathbf{s}_{k'}\mathbf{y}}\mathbf{f}_k + \sum_{k'}\mathbf{c}_{k'}^H\boldsymbol{\Xi}_\sigma\mathbf{c}_{k'}] \\
&= \min_{\mathbf{f}_k,\mathbf{c}_{k'}}\{1 - \mathbf{r}_{s_k\mathbf{y}}\mathbf{f}_k - \mathbf{f}_k^H\mathbf{r}_{\mathbf{y}s_k}^H + \mathbf{f}_k^H\mathbf{R}_\mathbf{y}\mathbf{f}_k - \mathbf{f}_k^H\boldsymbol{\Xi}_{\mathbf{s}_{k'}\mathbf{y}}^H\mathbf{c} - \mathbf{c}^H\boldsymbol{\Xi}_{\mathbf{s}_{k'}\mathbf{y}}\mathbf{f}_k + \mathbf{c}^H\mathbf{I}\mathbf{c}\}
\end{aligned}
\tag{4.15}
$$

where

$$
\mathbf{c} = [\mathbf{c}_1^H \quad \ldots \quad \mathbf{c}_{k'}^H \quad \ldots \quad \mathbf{c}_K^H]^H,
$$

and

$$
\boldsymbol{\Xi}_{\mathbf{s}_{k'}\mathbf{y}}^H = \left[\mathbf{R}_{\mathbf{y}\mathbf{s}_1} \ldots \mathbf{R}_{\mathbf{y}\mathbf{s}_{k'}} \ldots \mathbf{R}_{\mathbf{y}\mathbf{s}_K}\right].
$$

of sizes $(K-1)N_c \times 1$ and $N_f \times (K-1)N_c$, respectively.

The optimal $\mathbf{f}_k^H$ is determined by differentiating $\Delta J$ with respect to $\mathbf{f}_k$ and setting it equal to zero.

$$
\frac{\partial \Delta J}{\partial \mathbf{f}_k} = -\mathbf{r}_{s_k\mathbf{y}} + \mathbf{f}_k^H\mathbf{R}_\mathbf{y} - \mathbf{c}^H\boldsymbol{\Xi}_{\mathbf{s}_{k'}\mathbf{y}}, \tag{4.16}
$$

hence,

$$\mathbf{f}_k^H = \left(\mathbf{r}_{s_k\mathbf{y}} + \mathbf{c}^H \boldsymbol{\Xi}_{\mathbf{s}_{k'}\mathbf{y}}\right) \mathbf{R}_{\mathbf{y}}^{-1}. \tag{4.17}$$

On the other hand, the optimal $\mathbf{c}^H$ is also determined by differentiating $\Delta J$ with respect to $\mathbf{c}_k$.

$$\frac{\partial \Delta J}{\partial \mathbf{c}_k} = -\mathbf{f}_k^H \boldsymbol{\Xi}_{\mathbf{s}_{k'}\mathbf{y}}^H + \mathbf{c}^H \mathbf{I}, \tag{4.18}$$

and by substituting (4.17) in (4.18), we have

$$\begin{aligned} \frac{\partial \Delta J}{\partial \mathbf{c}_k} &= -\left(\mathbf{r}_{s_k\mathbf{y}} + \mathbf{c}^H \boldsymbol{\Xi}_{\mathbf{s}_{k'}\mathbf{y}}\right) \mathbf{R}_{\mathbf{y}}^{-1} \boldsymbol{\Xi}_{\mathbf{s}_{k'}\mathbf{y}}^H + \mathbf{c}^H \mathbf{I} \\ &= -\mathbf{r}_{s_k\mathbf{y}} \mathbf{R}_{\mathbf{y}}^{-1} \boldsymbol{\Xi}_{\mathbf{s}_{k'}\mathbf{y}}^H + \mathbf{c}^H \left(\mathbf{I} - \boldsymbol{\Xi}_{\mathbf{s}_{k'}\mathbf{y}} \mathbf{R}_{\mathbf{y}}^{-1} \boldsymbol{\Xi}_{\mathbf{s}_{k'}\mathbf{y}}^H\right). \end{aligned} \tag{4.19}$$

Then the optimal $\mathbf{c}$ filter taps can be calculated by setting (4.19) to be equal to zero.

$$\begin{aligned} \mathbf{c}^H &= \mathbf{r}_{s_k\mathbf{y}} \mathbf{R}_{\mathbf{y}}^{-1} \boldsymbol{\Xi}_{\mathbf{s}_{k'}\mathbf{y}}^H (\mathbf{I} - \boldsymbol{\Xi}_{\mathbf{s}_{k'}\mathbf{y}} \mathbf{R}_{\mathbf{y}}^{-1} \boldsymbol{\Xi}_{\mathbf{s}_{k'}\mathbf{y}}^H)^{-1} \\ &= \mathbf{r}_{s_k\mathbf{y}} \mathbf{R}_{\mathbf{y}}^{-1} \boldsymbol{\Xi}_{\mathbf{s}_{k'}\mathbf{y}}^H \mathbf{R}_{\delta_{k'}}^{-1}, \end{aligned} \tag{4.20}$$

where

$$\mathbf{R}_{\delta_{k'}} \triangleq \mathbf{I} - \boldsymbol{\Xi}_{\mathbf{s}_{k'}\mathbf{y}} \mathbf{R}_{\mathbf{y}}^{-1} \boldsymbol{\Xi}_{\mathbf{s}_{k'}\mathbf{y}}^H > 0. \tag{4.21}$$

At the first iteration, $\check{s}_{k'}(n-\Delta) = 0$ for all $k', n$, implying no information is fed back from the other users. For the next iteration, each user returns the soft encoded bits from the DECs to remove MAI effects. The error propagation in the feedback bits is reduced as the number of iterations is increased. On the other hand, an increase in the number of users leads to a reduction in the correlation property between the users' data symbols and hence results in lower system performance.

### 4.2.2 Multi-dimensional DFE (MDFE)

Within the MDFE structure, each user utilizes its own estimated symbols to feed the CMD equalizer, $\mathbf{b}_k$, consisting of $N_b$ taps as shown in Fig. 4.3. Using the same definitions for the observed symbols, estimated symbols and filter taps, the covariances and cross-covariances for the CDFE can be obtained as given

$$\boldsymbol{\Xi}_k \triangleq E\begin{bmatrix}\mathbf{s}_k\\ \mathbf{s}_1\\ \vdots\\ \mathbf{s}_{k'}\\ \vdots\\ \mathbf{s}_K\\ \mathbf{y}\end{bmatrix}\begin{bmatrix}\mathbf{s}_k\\ \mathbf{s}_1\\ \vdots\\ \mathbf{s}_{k'}\\ \vdots\\ \mathbf{s}_K\\ \mathbf{y}\end{bmatrix}^H \triangleq \begin{bmatrix}\mathbf{R}_{\mathbf{s}_k} & \mathbf{R}_{\mathbf{s}_k\mathbf{s}_1} & \cdots & \mathbf{R}_{\mathbf{s}_k\mathbf{s}_{k'}} & \cdots & \mathbf{R}_{\mathbf{s}_k\mathbf{s}_K} & \mathbf{R}_{\mathbf{s}_k\mathbf{y}}\\ \mathbf{R}_{\mathbf{s}_1\mathbf{s}_k} & \mathbf{R}_{\mathbf{s}_1} & \cdots & \mathbf{R}_{\mathbf{s}_1\mathbf{s}_{k'}} & \cdots & \mathbf{R}_{\mathbf{s}_1\mathbf{s}_K} & \mathbf{R}_{\mathbf{s}_1\mathbf{y}}\\ \vdots & \vdots & \ddots & \vdots & \ddots & \vdots & \vdots\\ \mathbf{R}_{\mathbf{s}_{k'}\mathbf{s}_k} & \mathbf{R}_{\mathbf{s}_{k'}\mathbf{s}_1} & \cdots & \mathbf{R}_{\mathbf{s}_{k'}} & \cdots & \mathbf{R}_{\mathbf{s}_{k'}\mathbf{s}_K} & \mathbf{R}_{\mathbf{s}_{k'}\mathbf{y}}\\ \vdots & \vdots & \ddots & \vdots & \ddots & \vdots & \vdots\\ \mathbf{R}_{\mathbf{s}_K\mathbf{s}_k} & \mathbf{R}_{\mathbf{s}_K\mathbf{s}_1} & \cdots & \mathbf{R}_{\mathbf{s}_K\mathbf{s}_{k'}} & \cdots & \mathbf{R}_{\mathbf{s}_K} & \mathbf{R}_{\mathbf{s}_K\mathbf{y}}\\ \mathbf{R}_{\mathbf{y}\mathbf{s}_k} & \mathbf{R}_{\mathbf{y}\mathbf{s}_1} & \cdots & \mathbf{R}_{\mathbf{y}\mathbf{s}_{k'}} & \cdots & \mathbf{R}_{\mathbf{y}\mathbf{s}_K} & \mathbf{R}_{\mathbf{y}}\end{bmatrix}. \tag{4.22}$$

The assumption of low correlation between users' signals simplifies (4.22) to

$$\boldsymbol{\Xi}_k \triangleq \begin{bmatrix}\mathbf{R}_{\mathbf{s}_k} & 0 & \cdots & 0 & \cdots & 0 & \mathbf{R}_{\mathbf{s}_k\mathbf{y}}\\ 0 & \mathbf{R}_{\mathbf{s}_1} & \cdots & 0 & \cdots & 0 & \mathbf{R}_{\mathbf{s}_1\mathbf{y}}\\ \vdots & \vdots & \ddots & \vdots & \ddots & \vdots & \vdots\\ 0 & 0 & \cdots & \mathbf{R}_{\mathbf{s}_{k'}} & \cdots & 0 & \mathbf{R}_{\mathbf{s}_{k'}\mathbf{y}}\\ \vdots & \vdots & \ddots & \vdots & \ddots & \vdots & \vdots\\ 0 & 0 & \cdots & 0 & \cdots & \mathbf{R}_{\mathbf{s}_K} & \mathbf{R}_{\mathbf{s}_K\mathbf{y}}\\ \mathbf{R}_{\mathbf{y}\mathbf{s}_k} & \mathbf{R}_{\mathbf{y}\mathbf{s}_1} & \cdots & \mathbf{R}_{\mathbf{y}\mathbf{s}_{k'}} & \cdots & \mathbf{R}_{\mathbf{y}\mathbf{s}_K} & \mathbf{R}_{\mathbf{y}}\end{bmatrix} \tag{4.23}$$

As in the linear case, the utilization of distinct interleavers for each user results in

$$\boldsymbol{\Xi}_k = \begin{bmatrix}\boldsymbol{\Xi}_\sigma & \boldsymbol{\Xi}_{\mathbf{s}_k\mathbf{y}}\\ \boldsymbol{\Xi}_{\mathbf{y}\mathbf{s}_k} & \mathbf{R}_{\mathbf{y}}\end{bmatrix}, \tag{4.24}$$

where $\boldsymbol{\Xi}_\sigma \in \mathbb{C}^{(N_b+1)K\times N_cK}$ , $\boldsymbol{\Xi}_{\mathbf{s}_k\mathbf{y}} \in \mathbb{C}^{(N_b+1)K\times N_f}$ and $\boldsymbol{\Xi}_{\mathbf{y}\mathbf{s}_k} \in \mathbb{C}^{N_f\times(N_b+1)K}$ are matrices constructed from $\boldsymbol{\Xi}_k$ by taking its diagonal, last column and last row elements, respectively.

The error signal given in (4.2) can be rewritten as follows

$$\begin{aligned} e_k(n-\Delta) &= s(n-\Delta) - \hat{s}_k(n-\Delta)\\ &= \mathbf{b}_k^H\mathbf{s}_k + \sum_{k'\neq k}\mathbf{c}_{k'}^H\mathbf{s}_{k'} - \mathbf{f}_k^H\mathbf{y}, \end{aligned} \tag{4.25}$$

where

$$\hat{s}_k(n-\Delta) = \sum_{k,l_f=0}^{N_f-1} f_k^*(l_f)y(n-l_f) - \sum_{k,l_b=1}^{N_b} b_k^*(l_b)s_k(n-l_b) - \sum_{k',l_c=0}^{N_c-1} c_{k'}^*(l_c)s_{k'}(n-l_c), \tag{4.26}$$

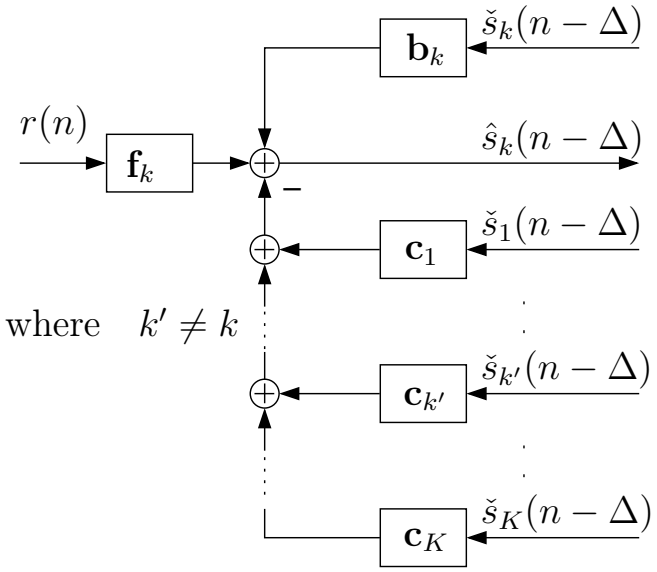


**Figure 4.3:** MDFE Structure.

$$\mathbf{s}_k = \begin{bmatrix} s_k(n-\Delta) \\ s_k(n-\Delta-1) \\ s_k(n-\Delta-2) \\ \vdots \\ s_k(n-\Delta-N_b) \end{bmatrix},$$

and

$$\mathbf{b}_k^H \triangleq [1 \quad b_k^*(1) \quad \cdots \quad b_k^*(N_b)],$$

hence, the optimization problem in (4.10) becomes

$$\Delta J = \min_{\mathbf{f}_k, \mathbf{b}_k, \mathbf{c}_{k'}} \mathrm{E}\left[ |\mathbf{b}_k^H \mathbf{s}_k + \sum_{k'} \mathbf{c}_{k'}^H \mathbf{s}_{k'} - \mathbf{f}_k^H \mathbf{y}|^2 \right], \tag{4.27}$$

$$\begin{aligned}\Delta J &= \min_{\mathbf{f}_k,\mathbf{b}_k,\mathbf{c}_{k'}} \mathrm{E}\left[(\mathbf{b}_k^H\mathbf{s}_k + \sum_{k'}\mathbf{c}_{k'}^H\mathbf{s}_{k'} - \mathbf{f}_k^H\mathbf{y})(\mathbf{b}_k^H\mathbf{s}_k + \sum_{k'}\mathbf{c}_{k'}^H\mathbf{s}_{k'} - \mathbf{f}_k^H\mathbf{y})^H\right] \\ &= \min_{\mathbf{f}_k,\mathbf{b}_k,\mathbf{c}_{k'}} [\mathbf{b}_k^H\mathrm{E}[\mathbf{s}_k\mathbf{s}_k^H]\mathbf{b}_k + \mathbf{b}_k^H\sum_{k'}\mathrm{E}[\mathbf{s}_k\mathbf{s}_{k'}^H]\mathbf{c}_{k'} - \mathbf{b}_k^H\mathrm{E}[\mathbf{s}_k\mathbf{y}^H]\mathbf{f}_k \\ &+ \sum_{k'}\mathbf{c}_{k'}^H\mathrm{E}[\mathbf{s}_{k'}\mathbf{s}_k^H]\mathbf{b}_k + \sum_{k'}\mathbf{c}_{k'}^H\mathrm{E}[\mathbf{s}_{k'}\mathbf{s}_{k'}^H]\mathbf{c}_{k'} - \sum_{k'}\mathbf{c}_{k'}^H\mathrm{E}[\mathbf{s}_{k'}\mathbf{y}^H]\mathbf{f}_k \\ &- \mathbf{f}_k^H\mathrm{E}[\mathbf{y}\mathbf{s}_k^H]\mathbf{b}_k - \mathbf{f}_k^H\sum_{k'}\mathrm{E}[\mathbf{y}\mathbf{s}_{k'}^H]\mathbf{c}_{k'} + \mathbf{f}_k^H\mathrm{E}[\mathbf{y}\mathbf{y}^H]\mathbf{f}_k).\end{aligned} \tag{4.28}$$

Using the definition of $\mathbf{c}$ and $\mathbf{R}_{\mathbf{y}\mathbf{s}_{k'}}$, (4.28) can be rewritten as

$$\begin{aligned}\Delta J = \min_{\mathbf{f}_k,\mathbf{b}_k,\mathbf{c}_{k'}} &\mathbf{b}_k^H\mathbf{R}_{\mathbf{s}_k}\mathbf{b}_k + \mathbf{b}_k^H\mathbf{R}_{\mathbf{s}_k\mathbf{s}_{k'}}\mathbf{c} - \mathbf{b}_k^H\mathbf{R}_{\mathbf{s}_k\mathbf{y}}\mathbf{f}_k + \mathbf{c}^H\mathbf{R}_{\mathbf{s}_{k'}\mathbf{s}_k}\mathbf{b}_k + \mathbf{c}^H\mathbf{\Xi}_{\mathbf{s}_{k'}}\mathbf{c} - \mathbf{c}^H\mathbf{\Xi}_{\mathbf{s}_{k'}\mathbf{y}}\mathbf{f}_k \\ &- \mathbf{f}_k^H\mathbf{R}_{\mathbf{s}_k\mathbf{y}}^H\mathbf{b}_k - \mathbf{f}_k^H\mathbf{\Xi}_{\mathbf{y}\mathbf{s}_{k'}}\mathbf{c} + \mathbf{f}_k^H\mathbf{R}_{\mathbf{y}}\mathbf{f}_k.\end{aligned} \tag{4.29}$$

The low correlation between users' data sequences provided by different random interleaver sequences produces zero values of cross-covariance matrices between $k$th user and $k'$ users, therefore, (4.29) become as follows

$$\begin{aligned}\Delta J = \min_{\mathbf{f}_k,\mathbf{b}_k,\mathbf{c}_{k'}} &(\mathbf{b}_k^H\mathbf{R}_{\mathbf{s}_k}\mathbf{b}_k - \mathbf{b}_k^H\mathbf{R}_{\mathbf{s}_k\mathbf{y}}\mathbf{f}_k + \mathbf{c}^H\mathbf{\Xi}_{\mathbf{s}_{k'}}\mathbf{c} - \mathbf{c}^H\mathbf{\Xi}_{\mathbf{s}_{k'}\mathbf{y}}\mathbf{f}_k - \mathbf{f}_k^H\mathbf{R}_{\mathbf{s}_k\mathbf{y}}^H\mathbf{b}_k \\ &- \mathbf{f}_k^H\mathbf{\Xi}_{\mathbf{y}\mathbf{s}_{k'}}\mathbf{c} + \mathbf{f}_k^H\mathbf{R}_{\mathbf{y}}\mathbf{f}_k).\end{aligned} \tag{4.30}$$

Next, the optimal $\mathbf{f}_k^H$ is determined by differentiating $\Delta J$ with respect to $\mathbf{f}_k$ and equalling it to zero,

$$\frac{\partial\Delta J}{\partial\mathbf{f}} = -\mathbf{b}_k^H\mathbf{R}_{\mathbf{s}_k\mathbf{y}} - \mathbf{c}^H\mathbf{\Xi}_{\mathbf{s}_{k'}\mathbf{y}} + \mathbf{f}_k^H\mathbf{R}_{\mathbf{y}} \tag{4.31}$$

then from (4.31) we can find $\mathbf{f}_k^H$ as given bellow

$$\mathbf{f}_k^H = \left(\mathbf{b}_k^H\mathbf{R}_{\mathbf{s}_k\mathbf{y}} + \mathbf{c}^H\mathbf{\Xi}_{\mathbf{s}_{k'}\mathbf{y}}\right)\mathbf{R}_{\mathbf{y}}^{-1}. \tag{4.32}$$

By substituting $\mathbf{f}_k^H$ into (4.30), we get

$$
\begin{aligned}
\Delta J = \min_{\mathbf{b}_k,\mathbf{c}_{k'}} (&\mathbf{b}_k^H \mathbf{R}_{\mathbf{s}_k} \mathbf{b}_k - \mathbf{b}_k^H \mathbf{R}_{\mathbf{s}_k\mathbf{y}} \mathbf{R}_{\mathbf{y}}^{-1} \mathbf{R}_{\mathbf{y}\mathbf{s}_k} \mathbf{b}_k - \mathbf{b}_k^H \mathbf{R}_{\mathbf{s}_k\mathbf{y}} \mathbf{R}_{\mathbf{y}}^{-1} \boldsymbol{\Xi}_{\mathbf{y}\mathbf{s}_{k'}} \mathbf{c} + \mathbf{c}_{k'}^H \boldsymbol{\Xi}_{\mathbf{s}_{k'}} \mathbf{c} \\
&+ \mathbf{c}^H \boldsymbol{\Xi}_{\mathbf{s}_{k'}\mathbf{y}} \mathbf{R}_{\mathbf{y}}^{-1} \mathbf{R}_{\mathbf{y}\mathbf{s}_k} \mathbf{b}_k - \mathbf{c}^H \boldsymbol{\Xi}_{\mathbf{s}_{k'}\mathbf{y}} \mathbf{R}_{\mathbf{y}}^{-1} \boldsymbol{\Xi}_{\mathbf{y}\mathbf{s}_{k'}} \mathbf{c} - \mathbf{b}_k^H \mathbf{R}_{\mathbf{s}_k\mathbf{y}} \mathbf{R}_{\mathbf{y}}^{-1} \mathbf{R}_{\mathbf{y}\mathbf{s}_k} \mathbf{b}_k \\
&- \mathbf{c}^H \boldsymbol{\Xi}_{\mathbf{s}_{k'}\mathbf{y}} \mathbf{R}_{\mathbf{y}}^{-1} \mathbf{R}_{\mathbf{y}\mathbf{s}_k} \mathbf{b}_k - \mathbf{b}_k^H \mathbf{R}_{\mathbf{s}_k\mathbf{y}} \mathbf{R}_{\mathbf{y}}^{-1} \boldsymbol{\Xi}_{\mathbf{y}\mathbf{s}_{k'}} \mathbf{c} - \mathbf{c}^H \boldsymbol{\Xi}_{\mathbf{s}_{k'}\mathbf{y}} \mathbf{R}_{\mathbf{y}}^{-1} \boldsymbol{\Xi}_{\mathbf{y}\mathbf{s}_{k'}} \mathbf{c} \\
&+ \left(\mathbf{b}_k^H \mathbf{R}_{\mathbf{s}_k\mathbf{y}} + \mathbf{c}^H \boldsymbol{\Xi}_{\mathbf{s}_{k'}\mathbf{y}}\right) \mathbf{R}_{\mathbf{y}}^{-1} \mathbf{R}_{\mathbf{y}} \mathbf{R}_{\mathbf{y}}^{-1} \left(\mathbf{R}_{\mathbf{y}\mathbf{s}_k} \mathbf{b}_k + \boldsymbol{\Xi}_{\mathbf{y}\mathbf{s}_{k'}} \mathbf{c}\right)) \\
\Delta J = \min_{\mathbf{b}_k,\mathbf{c}_{k'}} (&\mathbf{b}_k^H \mathbf{R}_{\mathbf{s}_k} \mathbf{b}_k - \mathbf{b}_k^H \mathbf{R}_{\mathbf{s}_k\mathbf{y}} \mathbf{R}_{\mathbf{y}}^{-1} \mathbf{R}_{\mathbf{y}\mathbf{s}_k} \mathbf{b}_k - \mathbf{b}_k^H \mathbf{R}_{\mathbf{s}_k\mathbf{y}} \mathbf{R}_{\mathbf{y}}^{-1} \boldsymbol{\Xi}_{\mathbf{y}\mathbf{s}_{k'}} \mathbf{c} + \mathbf{c}_{k'}^H \boldsymbol{\Xi}_{\mathbf{s}_{k'}} \mathbf{c} \\
&+ \mathbf{c}^H \boldsymbol{\Xi}_{\mathbf{s}_{k'}\mathbf{y}} \mathbf{R}_{\mathbf{y}}^{-1} \mathbf{R}_{\mathbf{y}\mathbf{s}_k} \mathbf{b}_k - \mathbf{c}^H \boldsymbol{\Xi}_{\mathbf{s}_{k'}\mathbf{y}} \mathbf{R}_{\mathbf{y}}^{-1} \boldsymbol{\Xi}_{\mathbf{y}\mathbf{s}_{k'}} \mathbf{c} - \left[\left(\mathbf{b}_k^H \mathbf{R}_{\mathbf{s}_k\mathbf{y}} + \mathbf{c}^H \boldsymbol{\Xi}_{\mathbf{s}_{k'}\mathbf{y}}\right) \mathbf{R}_{\mathbf{y}}^{-1} \left(\mathbf{R}_{\mathbf{y}\mathbf{s}_k} \mathbf{b}_k + \boldsymbol{\Xi}_{\mathbf{y}\mathbf{s}_{k'}} \mathbf{c}\right)\right] \\
&+ \left[\left(\mathbf{b}_k^H \mathbf{R}_{\mathbf{s}_k\mathbf{y}} + \mathbf{c}^H \boldsymbol{\Xi}_{\mathbf{s}_{k'}\mathbf{y}}\right) \mathbf{R}_{\mathbf{y}}^{-1} \left(\mathbf{R}_{\mathbf{y}\mathbf{s}_k} \mathbf{b}_k + \boldsymbol{\Xi}_{\mathbf{y}\mathbf{s}_{k'}} \mathbf{c}\right)\right] \\
\Delta J = \min_{\mathbf{b}_k,\mathbf{c}_{k'}} (&\mathbf{b}_k^H \mathbf{R}_{\mathbf{s}_k} \mathbf{b}_k - \mathbf{b}_k^H \mathbf{R}_{\mathbf{s}_k\mathbf{y}} \mathbf{R}_{\mathbf{y}}^{-1} \mathbf{R}_{\mathbf{y}\mathbf{s}_k} \mathbf{b}_k - \mathbf{b}_k^H \mathbf{R}_{\mathbf{s}_k\mathbf{y}} \mathbf{R}_{\mathbf{y}}^{-1} \boldsymbol{\Xi}_{\mathbf{y}\mathbf{s}_{k'}} \mathbf{c} \\
&+ \mathbf{c}_{k'}^H \boldsymbol{\Xi}_{\mathbf{s}_{k'}} \mathbf{c} + \mathbf{c}^H \boldsymbol{\Xi}_{\mathbf{s}_{k'}\mathbf{y}} \mathbf{R}_{\mathbf{y}}^{-1} \mathbf{R}_{\mathbf{y}\mathbf{s}_k} \mathbf{b}_k - \mathbf{c}^H \boldsymbol{\Xi}_{\mathbf{s}_{k'}\mathbf{y}} \mathbf{R}_{\mathbf{y}}^{-1} \boldsymbol{\Xi}_{\mathbf{y}\mathbf{s}_{k'}} \mathbf{c}).
\end{aligned}
\tag{4.33}
$$

Moreover, (4.33) can be rewritten in terms of Schur complements as follows

$$
\Delta J = \min_{\mathbf{b}_k,\mathbf{c}_{k'}} (\mathbf{b}_k^H \mathbf{R}_{\delta_k} \mathbf{b}_k + \mathbf{c}_{k'}^H \boldsymbol{\Xi}_{\delta_{k'}} \mathbf{c} - \mathbf{b}_k^H \mathbf{R}_{\mathbf{s}_k\mathbf{y}} \mathbf{R}_{\mathbf{y}}^{-1} \boldsymbol{\Xi}_{\mathbf{s}_{k'}\mathbf{y}}^H \mathbf{c} - \mathbf{c}^H \boldsymbol{\Xi}_{\mathbf{s}_{k'}\mathbf{y}} \mathbf{R}_{\mathbf{y}}^{-1} \mathbf{R}_{\mathbf{s}_k\mathbf{y}}^H \mathbf{b}_k),
\tag{4.34}
$$

where, $\mathbf{R}_{\delta_{k'}} \triangleq \mathbf{R}_{\mathbf{s}_{k'}} - \mathbf{R}_{\mathbf{s}_{k'}\mathbf{y}} \mathbf{R}_{\mathbf{y}}^{-1} \mathbf{R}_{\mathbf{s}_{k'}\mathbf{y}}^H$ and $\boldsymbol{\Xi}_{\delta_{k'}} \triangleq \boldsymbol{\Xi}_{\sigma} - \boldsymbol{\Xi}_{\mathbf{s}_{k'}\mathbf{y}} \mathbf{R}_{\mathbf{y}}^{-1} \boldsymbol{\Xi}_{\mathbf{s}_{k'}\mathbf{y}}^H$. The cost function in (4.34) can also be expressed in matrix form, that is

$$
\Delta J = \min_{\mathbf{b}_k,\mathbf{c}_{k'}} \begin{bmatrix} \mathbf{b}_k^H & \mathbf{c}^H \end{bmatrix} \mathbf{M}_k \begin{bmatrix} \mathbf{b}_k \\ \mathbf{c} \end{bmatrix},
\tag{4.35}
$$

with a Hermitian center matrix $\mathbf{M}_k$ defined as

$$
\mathbf{M}_k = \begin{bmatrix} \mathbf{R}_{\delta_k} & -\mathbf{R}_{\mathbf{s}_k\mathbf{y}} \mathbf{R}_{\mathbf{y}}^{-1} \boldsymbol{\Xi}_{\mathbf{s}_{k'}\mathbf{y}}^H \\ -\boldsymbol{\Xi}_{\mathbf{s}_{k'}\mathbf{y}} \mathbf{R}_{\mathbf{y}}^{-1} \mathbf{R}_{\mathbf{s}_k\mathbf{y}}^H & \boldsymbol{\Xi}_{\sigma} \end{bmatrix}
\tag{4.36}
$$

and with unknown vectors $\mathbf{b}_k$ and $\mathbf{c}$. Now given any Hermitian matrix of the form

$$
\mathbf{M} = \begin{bmatrix} A & B \\ B^H & C \end{bmatrix},
\tag{4.37}
$$

with $A = A^H$, $C = C^H$, and $C$ invertible, it can be verified by direct calculation that $\mathbf{M}_k$ is positive-definite and invertible too. Furthermore, the cost function can be further simplified as follows

$$
\Delta J = \min_{\mathbf{p}_k} \mathbf{p}_k^H \mathbf{M}_k \mathbf{p}_k,
\tag{4.38}
$$

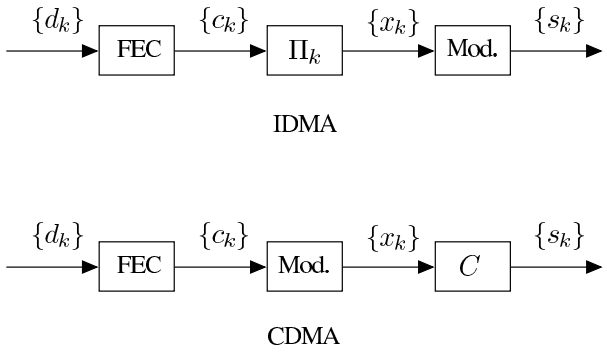


**Figure 4.4:** The IDMA and CDMA transmitter components of the $k$th user.

where $\mathbf{p}_k^H = [\mathbf{b}_k^H \quad \mathbf{c}^H]$. We recall that the leading entry of $\mathbf{p}_k$ is unity, so that (4.38) is a constrained problem of the form

$$\min_{\mathbf{p}_k} \mathbf{p}_k^H \mathbf{M}_k \mathbf{p}_k, \quad \text{subject to} \quad \mathbf{p}_k \mathbf{e}_o = 1, \tag{4.39}$$

where $\mathbf{e}_o \in \mathbb{C}^{(N_b+(K-1)N_c)\times 1}$ is the first basis vector given as

$$\mathbf{e}_o \triangleq \texttt{col}\{1, 0, 0, \ldots, 0\}. \tag{4.40}$$

Using Gauss-Markov theorem for constrained optimization, the optimal value for $\mathbf{p}_k^H$ and minimum mean square error (mmse) are given by

$$\mathbf{p}_k^H = \frac{\mathbf{e}_o^T \mathbf{M}_k^{-1}}{\mathbf{e}_o^T \mathbf{M}_k^{-1} \mathbf{e}_o}, \tag{4.41}$$

$$\mathbf{mmse} = \frac{1}{\mathbf{e}_o^T \mathbf{M}_k^{-1} \mathbf{e}_o}. \tag{4.42}$$

## 4.3 MDE and Multiuser detection

As mentioned in previous sections, the MDE depends on the low correlation property between the users' data signals for obtaining efficient equalization. This property can be achieved by using unique code signatures in CDMA, while for IDMA the interleavers are used for distinguishing users' symbols and providing low signal correlation.

Fig. 4.4 depicts transmitter structures of the $k$th user for IDMA and CDMA systems. Let $\{d_k\}$ denote the binary message sequence and $\{c_k\}_{i=0}^{N_d R_c - 1}$ denote

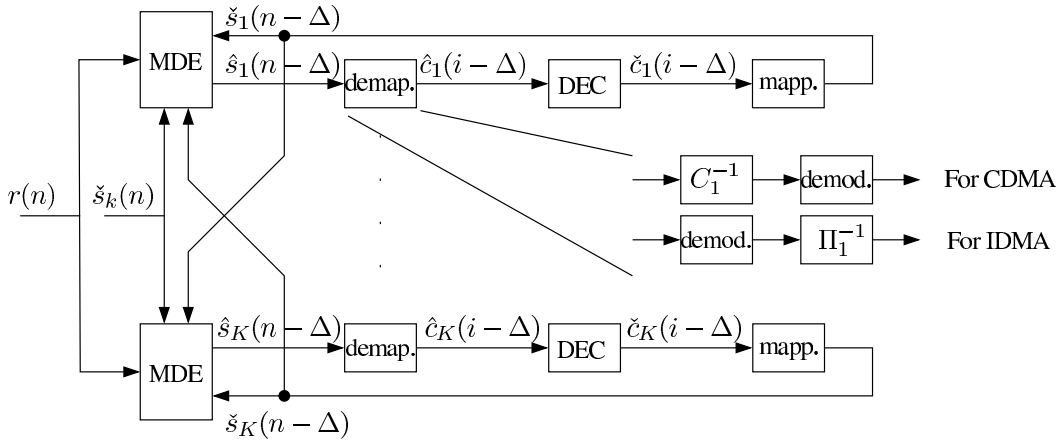


**Figure 4.5:** The general multiuser MDE structure.

the user's data after error control encoding with $R_c$ and $N_d$ representing the code rate and number of transmitted data bits, respectively. For IDMA, a specific interleaver pattern for each user ($\Pi_k$) then permutes the coded output bits. These interleavers are generated pseudo-randomly and independently. After interleaving, each group of interleaved coded bits $\{x_k\}$ are mapped to symbols $\{s_k\}_{n=0}^{N_s-1}$. While in CDMA, the coded bits are mapped and then the generated symbols are spread ($C$) using a unique spreading code for each user.

The general centralized mutliuser MDE receiver is shown in Fig. 4.5. In this figure, the equalized symbols $\hat{s}_k(n-\Delta)$ and the estimated symbols $\check{s}_k(n-\Delta)$ are exchanged between the MDE and the DEC for each user through mapping and demapping operations. The function of the mapper and the demapper is to decide whether the detection is based on IDMA or CDMA as shown in the figure. Furthermore, it can be noted that the MDE efficiency directly depends on the error propagation in the estimated feedback symbols $\check{s}_k$. Hence, the type and the code rate of the DECs have a considerable effect on the equalization process.

## 4.4 Iterative Channel Estimation for Optimal MDE-MUD Receivers

The optimal MDE receiver depends on the estimated channel taps that are utilized in the MAI elimination processes. The accuracy of the estimated channel impacts significantly the receiver performance. Therefore, an iterative channel estimator has been designed to estimate channel taps during training mode prior to the start of the decision-directed mode. The estimated channel taps are used for constructing the covariance and cross-covariance quantities in the MDE-MUD receivers and hence, they determine the feed-forward, feedback and crossover filter taps. Furthermore, they are used to compute the covariance and cross-covariance matrices in MDE-IDMA and MDE-CDMA detections to obtain the filter taps for each of the MDE equalizers.

The iterative channel estimator is depicted in Fig. 4.6. Given the error signal in (4.2), the solution of the optimization problem is obtained by substituting (4.2) in the (4.10) which results in producing a least square (LS) equation [25]. Hence, the $k$th user channel taps could be estimated as follows

$$\hat{\mathbf{h}}_k = \left(\mathbf{H}_{t_k}^H \mathbf{H}_{t_k}\right)^{-1} \mathbf{H}_{t_k}^H \mathbf{r}_{p_k}, \tag{4.43}$$

where $\mathbf{H}_{t_k}$ is the rectangular Toeplitz data matrix of size $(L_k \times N_t + 1)$ and given as follows

$$\mathbf{H}_{t_k} = \underbrace{\left.\begin{bmatrix} p_k(0) & 0 & 0 & \dots \\ p_k(1) & p_k(0) & 0 & \dots \\ p_k(2) & p_k(1) & 0 & \dots \\ \vdots & \vdots & \vdots & \ddots \\ p_k(N_t) & p_k(N_t-1) & p_k(N_t-2) & \dots \end{bmatrix}\right\} N_t+1}_{L_k} \tag{4.44}$$

and

$$\mathbf{r}_{p_k} = \left[r_{p_k}(q)\, r_{p_k}(q-1)\, \dots r_{p_k}(q-N_f+1)\right]^T,$$

is the observed training symbols, where

$$r_{p_k}(q) = r_t(q) - \sum_{k' \neq k} \hat{h}_{k'}(l_b) p_{k'}(q-l_b). \tag{4.45}$$

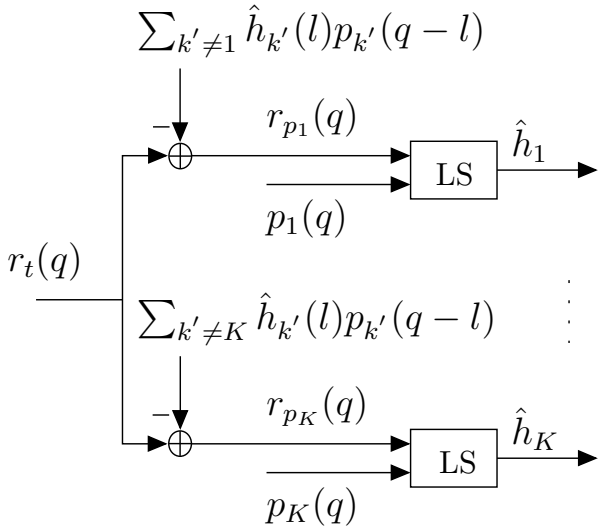


**Figure 4.6:** The iterative channel estimator structure.

Initially, the values of $\hat{h}_k$ are set to zeros. Therefore, $r_{p_k}(q)$ contains both MAI and ISI in the first iteration for the first user, while for the second user the amount of MAI is decreased and for the last user the lowest MAI is obtained. However, for the second iteration the performance of channel estimation is noticeably improved since all users have obtained initial channel taps in the first iteration. Increasing the number of iterations results in improved channel estimation performance. It is worth mentioning that the channel estimation iterations need not be the same as the number of iterations. In practice, only a few iterations are necessary to obtain accurate channel information provided the training symbols of the users are uncorrelated.

## 4.5 Simulation Results and Performance Comparisons

In this section, the performance of MDE is examined and compared for both CDMA and IDMA multiuser detection. $E_b/N_0$ is the SNR per bit, which is equal for all users. The users are transmitting QPSK symbols through frequency selective channels. For wireless transmission, 6-tap channel coefficients are utilized

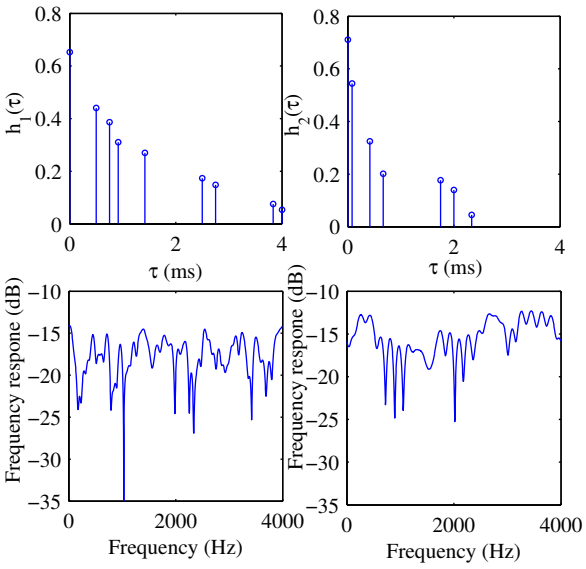


**Figure 4.7:** Impulse and frequency response of the channels used in the simulations.

based on the ITU-B channel standard. A length of 10 taps is chosen for feed-forward, feed-backward and crossover filters and 12 iterations have been used for iterative detection. On other hand, for underwater shallow channels, two different multipath channels have been used which are experimentally obtained by seatrials conducted by Newcastle University in the North Sea. Channel 1 and channel 2 have 29 and 49 taps, respectively, as shown in Fig. 4.7. Hence, the filter taps are chosen to be 40 for efficient equalization. The signature sequences in CDMA are generated using the Walsh algorithm such that they have low auto-correlation properties, which helps provide an efficient symbol equalization, while for IDMA the interleaver patterns are generated randomly and independently.

While there is no closed form expression for finding $\Delta$ in this thesis, a solution is presented that yields an algebraic interpretation of $\Delta$. The impact of $\Delta$ on equalization performance is shown in Fig. 4.8 for both MLE-IDMA and MDFE-IDMA detectors. $\Delta$ corresponds to the channel time delay, and MLE has given 1dB of SNR higher than CDFE for . A closer look at Fig. 4.8 reveals that the minimum BER is achieved for a $\Delta$ value between 5 and 19, hence, $\Delta = 12$ has

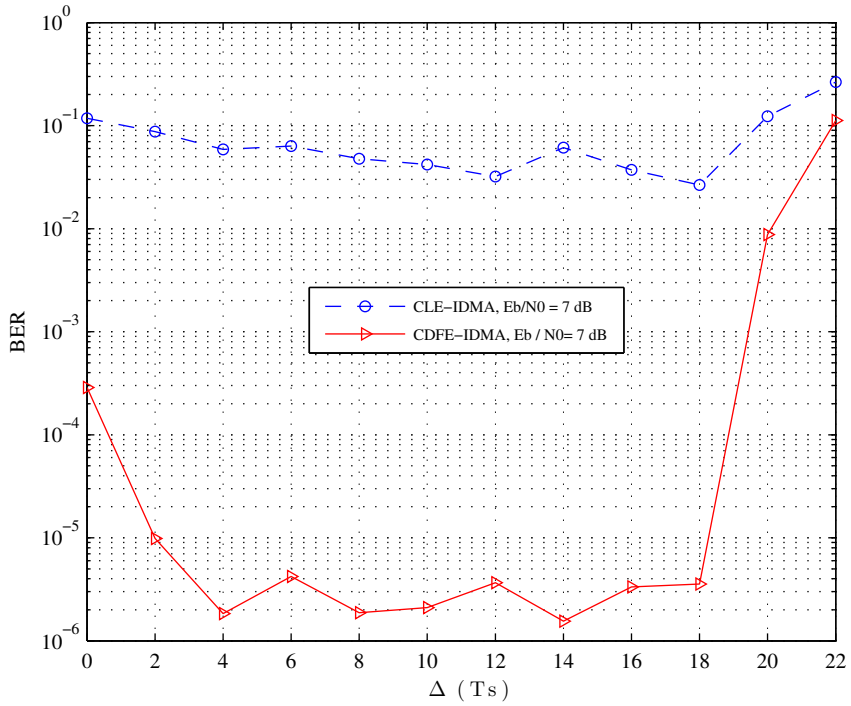


**Figure 4.8:** Optimal MLE-IDMA and MDFE-IDMA performances for various $\Delta$ values, where each 1 delay of $\Delta$ equals one symbol duration (Ts).

been used in the simulations.

## 4.5.1 Selective Fading Wireless Channels

### 4.5.1.1 MLE-MUD

It is obvious from Fig. 4.5 that utilizing lower code rates give better performance due to decreasing bit error propagation through feedback filters, and hence, obtaining higher equalization performance. The simulation examples shown in Fig. 4.9 are plotted using FEC encoder with a 1/64 code rate for both MLE and MDFE equalization employing 8 and 16 users. For a fair comparison between CDMA and IDMA detectors, we used 1/8 convolution coding employing octal generators $(275, 275, 253, 371, 331, 235, 313, 357)_8$ and 1/8 repetition coding for IDMA, while for CDMA rate 1/2 convolution and rate 1/32 spreading have

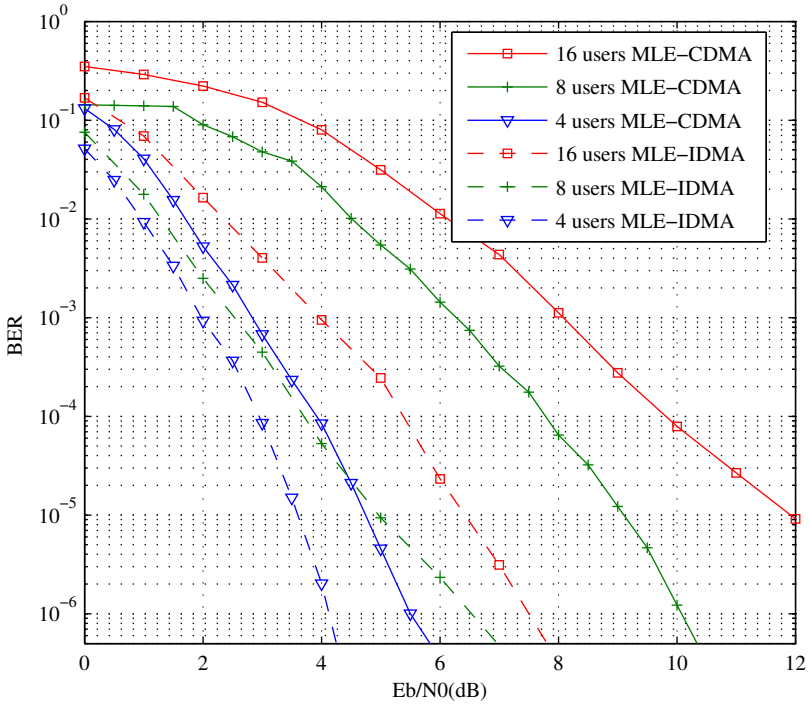


**Figure 4.9:** Performance of MLE-MUD receiver for different number of users in frequency selective channels.

been used. The reason behind using higher spreading coding than convolution coding in CDMA is to provide as low as possible correlation between users signal.

In general, it can be noted from Fig. 4.9 that the performance of MLE-IDMA is higher than MLE-CDMA. This is because the high coding rate is not only increasing the efficiency of the decoder, it also provides longer interleaver schemes which generates a very low correlation property between users data compared to the correlation obtained with the 32 spreading chips in CDMA.

The influence of ISI on the MLE performance for four users is small enough so that it can be resolved by the linear filter and hence obtains a high error correction within the DECs. However, the ISI effect is more aggressive when higher number of users are employed. The unresolved ISI in each user produces high BER after decoding. Propagating these bit errors iteratively from a specific user to the other users' MLE equalizers through cross-over filters results in more

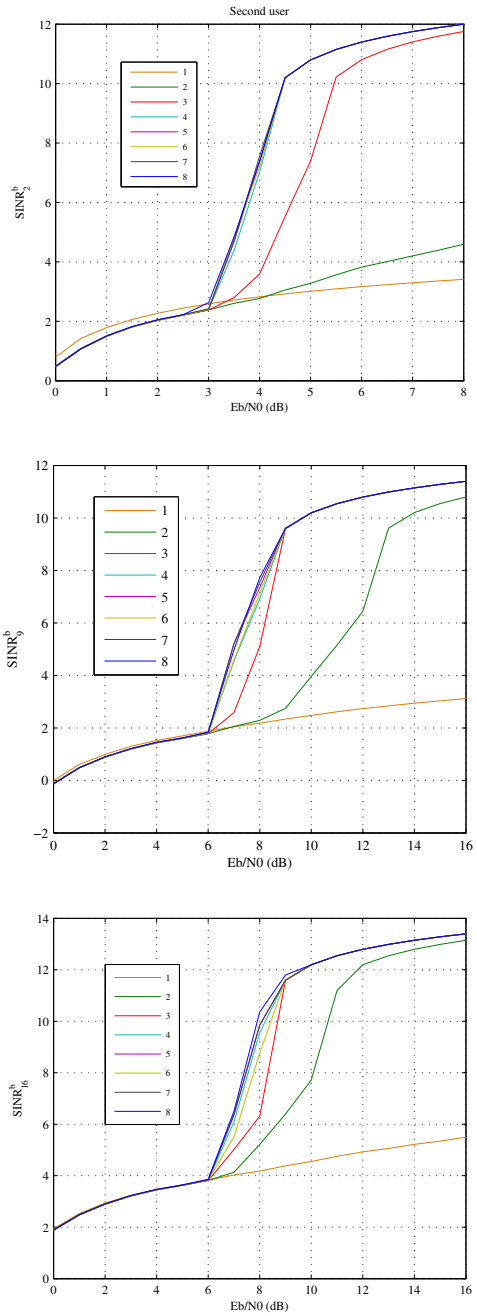


**Figure 4.10:** The improvement of SINR in crossover feedback filters within MLE-IDMA iterations.

equalization and detection errors.

The amount of average signal to interference and noise ratio (SINRB) that exists in the feedback crossover filters has an extensive effect on the MLE equalizer performance. Within each iteration, the error propagation through the crossover filters is decreased as SINR improves. The crossover SINR for user $k$ can be calculated as follows

$$\mathrm{SINR}_k^b = \frac{1}{K-1}\sum_{k'=1}^{K}\frac{\check{\mathbf{s}}_{k'}\check{\mathbf{s}}_{k'}^H}{\mathrm{E}[e_k(n)]}. \tag{4.46}$$

In contrast to the higher performance of MLE-IDMA, the improvement of SINRB during IDMA iterations is illustrated in Fig. 4.10 for 16 users. It is obvious from the figure that the second user suffers from MAI effects more than other users as at the beginning of each iteration, the second user equalization takes place when other users' feedback symbols have not been updated yet except user 1. In contrast, the $16^{th}$ user utilizes the full updated feedback symbols and thus experiences reduced error propagation. In turn, the SINRB value achieved by the $16^{th}$ user is greater than the other users. It is worth mentioning that the receiver algorithm starts by processing the users sequentially and arbitrarily from user 1 to 16.

#### 4.5.1.2 MDFE-MUD

Utilizing the same transmitter and receiver parameters employed for evaluating MLE performance, Fig. 4.11 depicts the performance of MDFE-IDMA for different user numbers and at the same time it is compared to MDFE-CDMA performances on selective fading channels. It can be seen that both systems are slightly different in performance when two users are used. This is because of utilizing an efficient decoding that almost eliminates the difference in performance that comes from the amount of ISI suppression by using feedback filters in the MDFE. Moreover, the MDFE-IDMA appears more robust to channel interference than MLE-IDMA due to the feedback filters that significantly improve symbol equalization by subtracting ISI from the received signal and hence decreasing the error rate of the symbols propagating via cross-over filters as shown in Fig. 4.12.

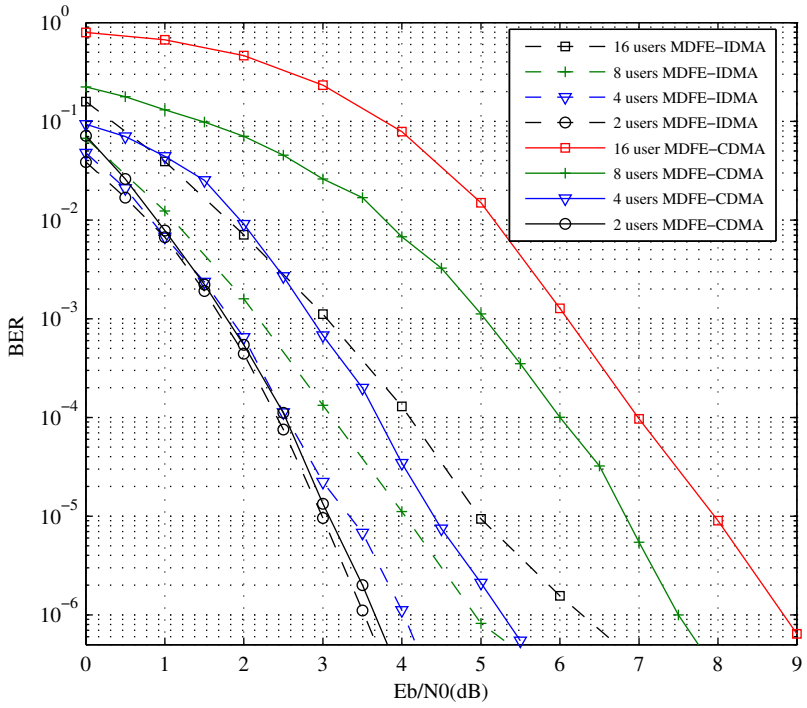


**Figure 4.11:** Performance of MDFE-MUD receiver for different number of users in frequency selective channels.

#### 4.5.1.3 Impact of Encoder Type

The elimination of error propagation is the main challenge in designing DFE equalizers. In practice, error correction in communication systems is an important operation to achieve reliable coverage. The employment of delay free hard decision for removing ISI and MAI in MDE generates error that are bursty in nature. The production of bursty errors in MDE receivers is the major obstruction regarding to improvement of system performance and limits the coding gain. In turn, the reduction of the coding gain creates more error propagation in feedback symbols from the decoder outputs such that higher degradation in equalization performance is obtained. In order to remedy this problem and improve overall iterative detection, more efficient decoding has to be employed.

Fig. 4.13 shows the performance of the MDFE equalizer for 16 users when the

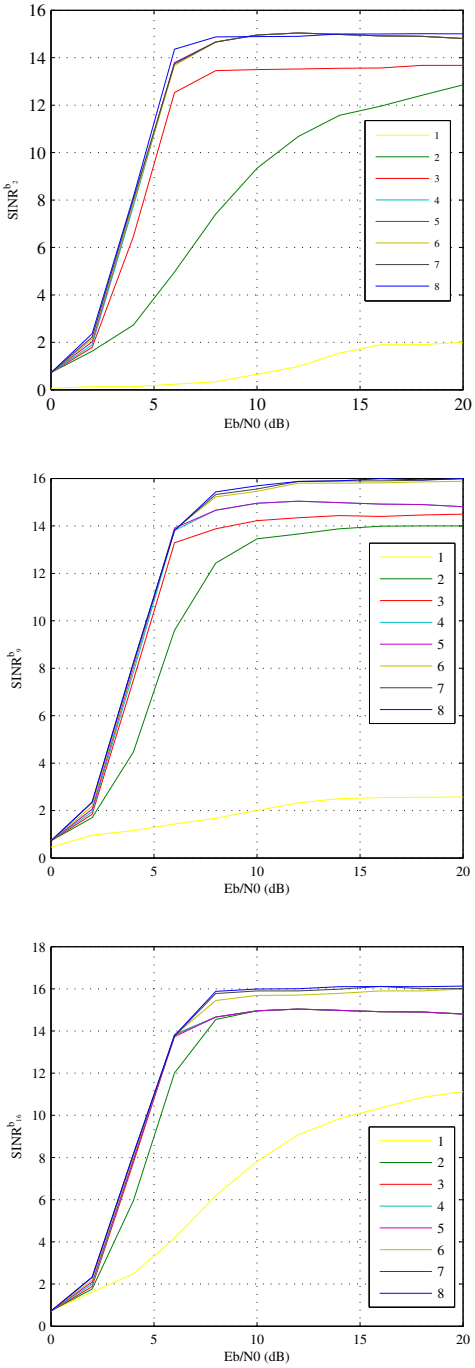


**Figure 4.12:** The improvement of SINR in crossover feedback filters within centralized MDFE-IDMA iterations.

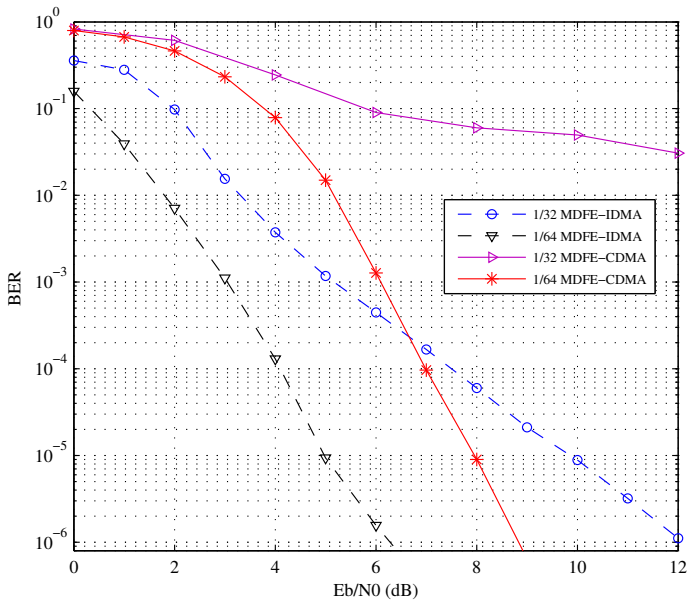


**Figure 4.13:** Effect of lower coding rate on MDFE performance.

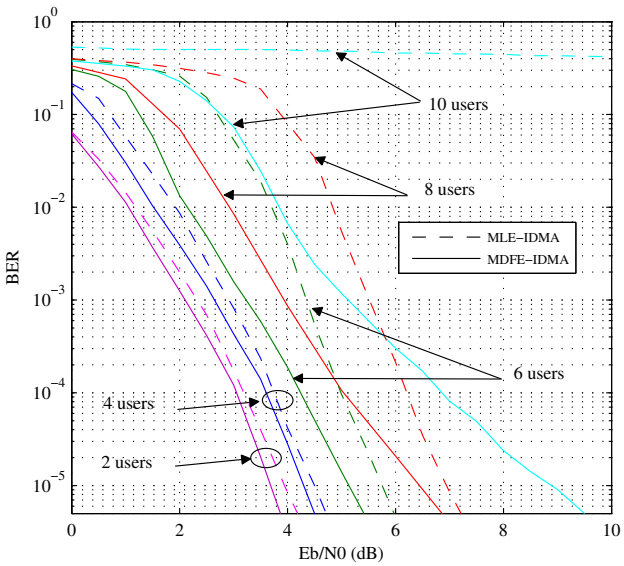


**Figure 4.14:** Performance comparison between optimal MLE-IDMA and MDFE-IDMA receivers employing 1/8 convolution coding.

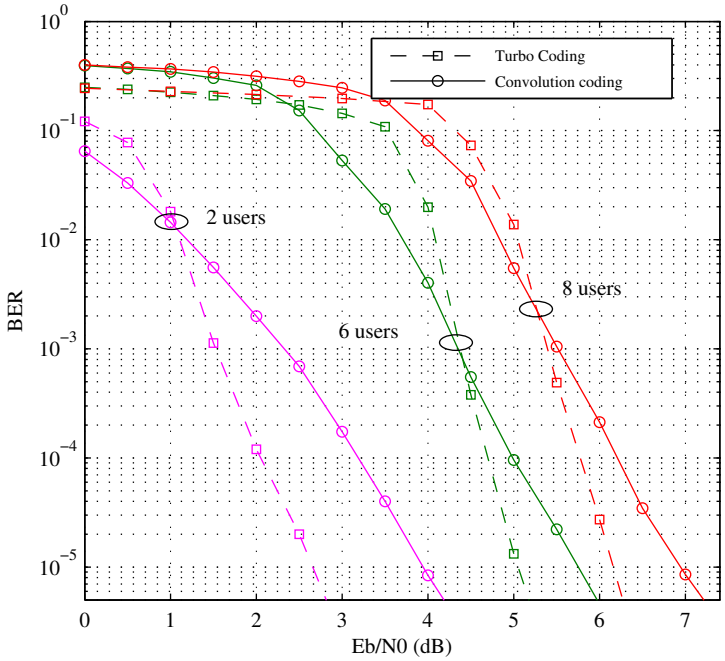


**Figure 4.15:** Impact of FEC on MLE-IDMA systems performances.

rate of repetition coding in IDMA and the spreading code in CDMA is increased to 1/4 and 1/16, respectively. As shown in the figure, both MDFE-IDMA and MDFE-CDMA performances are affected by the higher coding rate which results in higher feedback error propagation and increased correlation between users' data in IDMA and CDMA, respectively.

In contrast to the higher performance of IDMA over CDMA, and for the sake of simplicity, the performance of MLE-IDMA and MDFE-IDMA systems are compares utilizing rate 1/8 convolution coding as depicted Fig. 4.14. The interference suppression for MDFE-IDMA is significantly higher than MLE-IDMA at low coding rates, such that the high residual interference in the crossover filters of the MLE results in collapsing MLE-IDMA performance when the number of users exceeds 10 users.

Turbo codes have been shown to provide a powerful error detection and correction properity on both AWGN channel [56] [99] and Rayleigh fading channels [100]. In Fig. 4.15 the performance of MLE-IDMA system is compared when

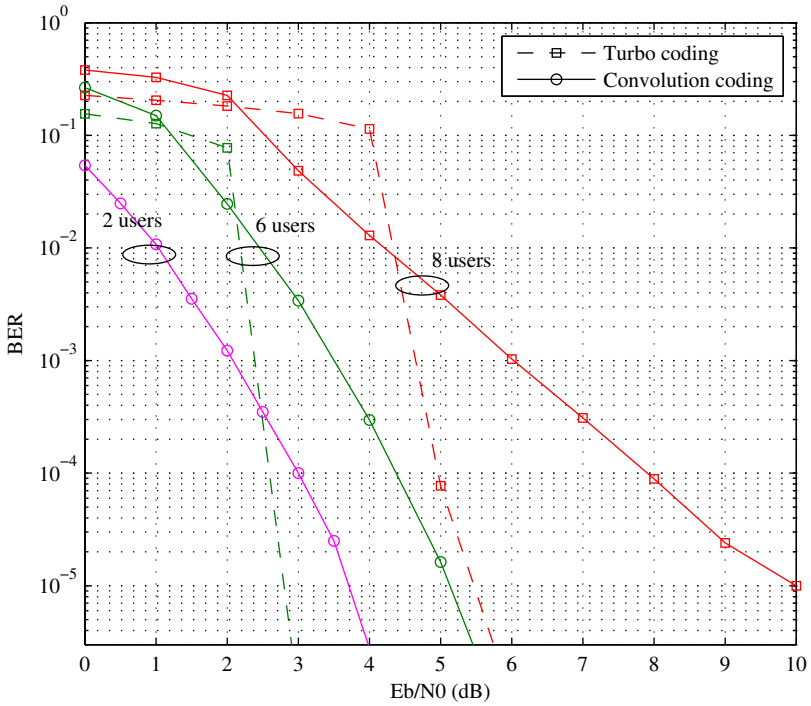


**Figure 4.16:** Impact of FEC on MDFE-IDMA systems performances.

convolution and turbo coding are used for 2, 6 and 8 users. For all cases, It could be noted that, for low SNR, convolution coding performs higher than turbo codes and the amount of this outperformance becomes larger as number of users increased. This is because, in first iteration, the turbo code performance is more affected by a poor equalization process of MLE than convolution coding, which results in producing higher error propagation symbols through crossover filters for remaining iterations. However, for higher SNR, turbo code show a significant improvement in performance compared to convolution code when it resolved the problem of feedback error propagation.

On other hand, the turbo decoder still outperforms the convolutional coding in the MDFE-IDMA system when user numbers are increased as illustrated in Fig. 4.16. Employing feedback filters in MDFE equalizers removes the ISI related to user $k$ and MAI related to the other users. The amount of ISI and MAI reduction at the MDFE equalizers outputs leads to significant reduction in error

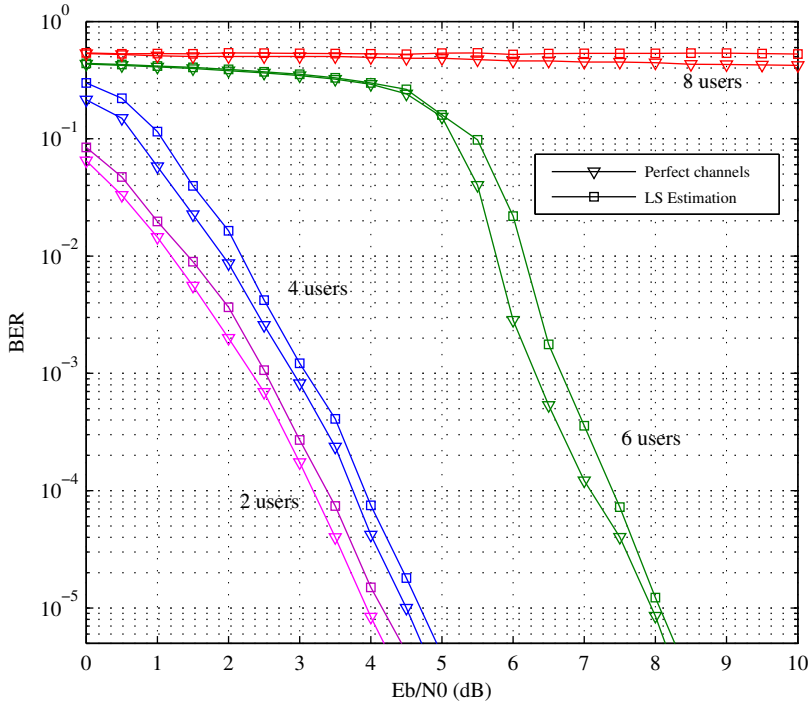


**Figure 4.17:** CLE-IDMA performance for perfect channel assumption and LS channel estimations.

propagation of the decoder inputs, and hence, maintaining the advantage of turbo codes over convolutional coding.

#### 4.5.1.4 Impact of Channel Estimation

Reducing error propagation from a specific user to the other users is very important for obtaining better performance, hence, utilizing more powerful encoder can improve the system performance. However, this is not the only factor that affects the MD equalizers. The accuracy of channel estimation is also another reason behind system performance degradation.

In order to illustrate the effect of channel estimation on MLE-IDMA and MDFE-IDMA system performances, iterative LS channel estimation is applied to 511 training symbols and the system performance is compared with perfect

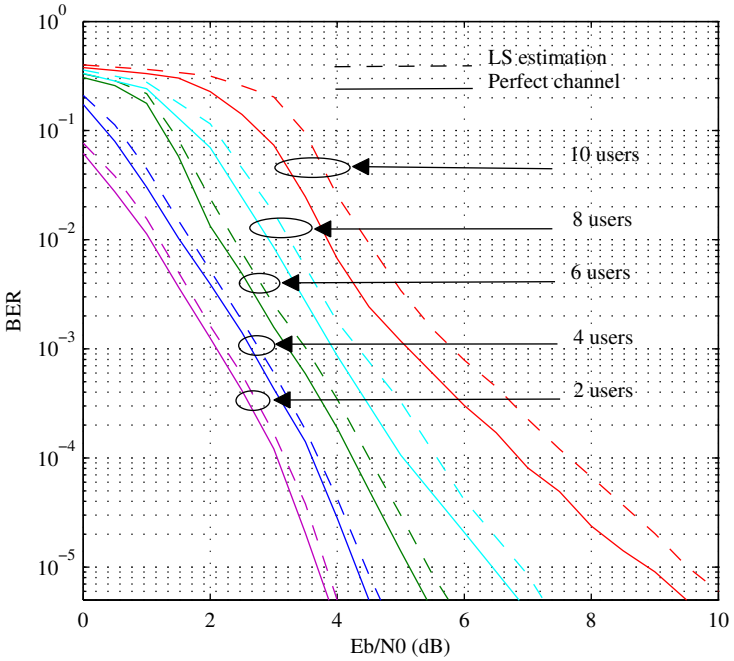


**Figure 4.18:** MDFE-IDMA performance for perfect channel assumption and LS channel estimations.

channel estimation. The training symbols are generated with an m-sequence generator which provides low autocorrelation properties that enable efficient channel estimation. Fige. 4.17 and Fig. 4.18 show the effect of estimated channel taps on the MLE-IDMA and MDFE-IDMA performances, respectively. The imperfection of the estimated channel taps increases the probability of symbol errors, and hence produces higher BER. The imperfect channel estimation effect on the system performance is more perceptible as the number of users is gradually increased for both systems.

### 4.5.2 Performance Comparison in Underwater Shallow Channels

The two-user uplink transmission shallow water acoustic scenario is shown in Fig. 4.19. Both users transmit data packets to the receiver over two distinct

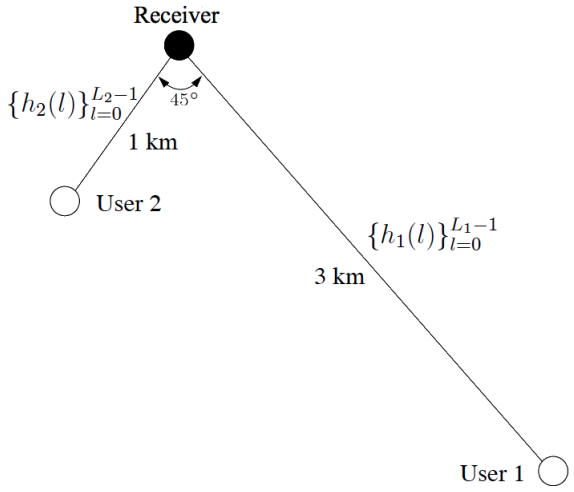


**Figure 4.19:** Underwater shallow water transmission scenario.

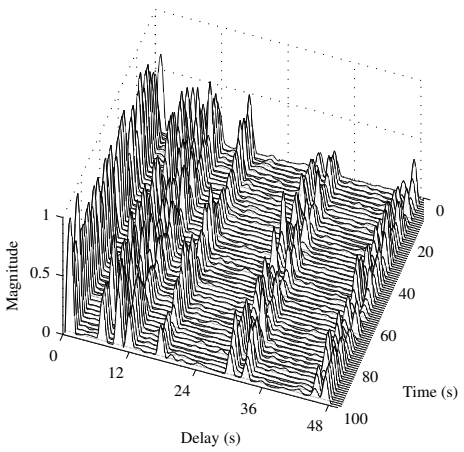


**Figure 4.20:** Normalized channel impulse response for user one.

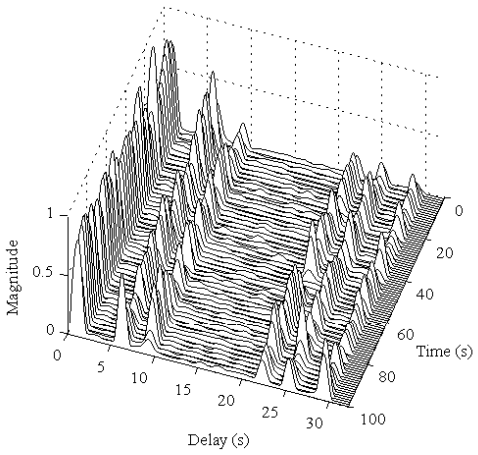


**Figure 4.21:** Normalized channel impulse response for user two.

multipath fading channels simultaneously. User 1 and user 2 are positioned at a distance of 1 km and 3 km from the receiver respectively, so that their arriving signals form an angle of 45° between them at the receiver. Two different multipath fading channels have been used in the simulations experimentally obtained by seatrials conducted by Newcastle University in the North Sea. The normalized impulse response channels for channel 1 and channel 2 are given in Fig. 4.20

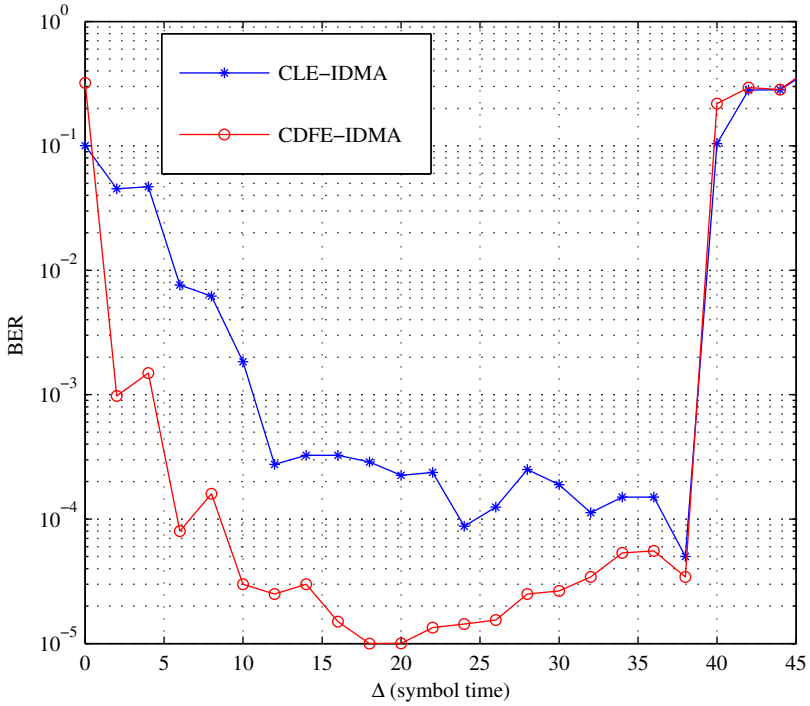


**Figure 4.22:** Impact of feedback delay $\Delta$ on MLE-IDMA and MDFE-IDMA performances.

and Fig.4.21, respectively. The multipath delay spread of channel 1(49 taps) is longer than that of channel 2 (29 taps). Accordingly, channel one is more time selective compared to channel 2. The length of the filter taps has a significant effect on removing ISI and MAI impairments. Therefore, to produce an efficient MD equalizer, all filters have 40 taps.

As mentioned before, underwater channels exhibit time selective fading, hence, the performance generally is worse than wireless channels. Fig. 4.22 shows BER versus decision delay, for values of $\Delta$ in the interval [0,45]. The optimal decision delay is 20 for both CLE-IDMA and CDFE-IDMA, but a nonoptimal choice of feedback delay can lead to a significant performance loss. Fig. 4.23 shows the performance comparison between CLE-IDMA and CDFE-IDMA for both convolution and turbo coding using QPSK mapping. As expected, CDFE-IDMA with turbo decoding can significantly remove MAI and ISI effects due to the

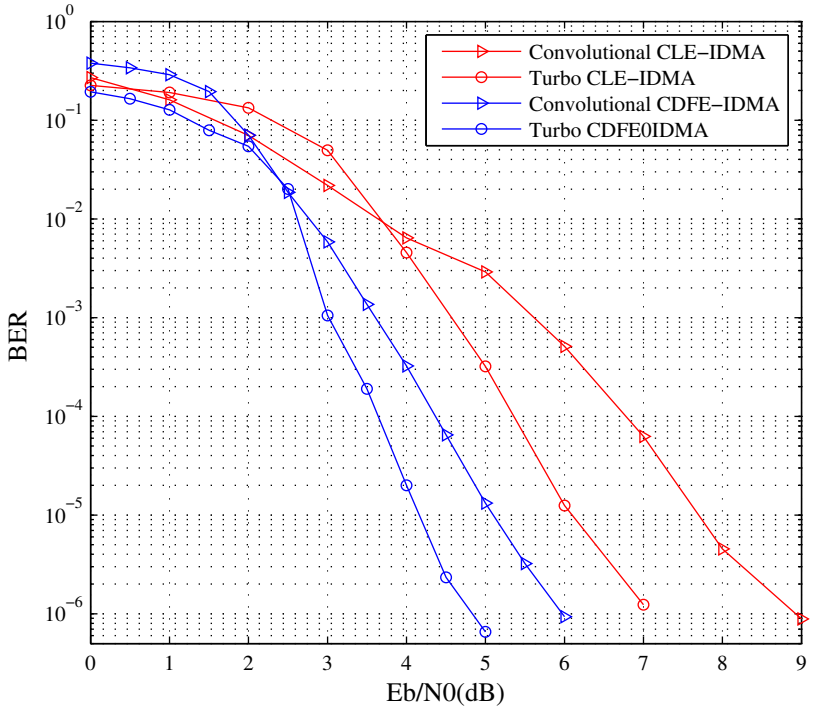


**Figure 4.23:** Impact of FEC on MLE-IDMA and MDFE-IDMA performances.

power of turbo coding in detecting and correcting bit errors, which results in less error propagation in feedback data symbols through feedback and crossover filters.

## 4.6 Chapter Summary

In this chapter, new equations are derived for determining the optimal filter coefficients for both CLE-IDMA and CDFE-IDMA equalizers. The absence of feedback filters in CLE leads to a degraded performance, while CDFE-IDMA shows higher efficiency in separating and detecting users due to jointly removing MAI and ISI impairments. Using numerical results, it has been shown that CDFE-IDMA can significantly outperform CLE-IDMA when the number of users increased. The type of encoder can increase system performance due to decreasing

error propagating in feedback symbols. The delay in feedback symbols $\Delta$ and the channel estimation effects on system performance are also given for CLE-IDMA and CDFE-IDMA systems. The same performance analysis has been carried out on the proposed systems over underwater shallow water channels.

# 5

# Decentralized Multi-Dimensional Equalization

## 5.1 Introdution

In the previous chapter, centralized MDE has been presented for multiuser detection. In centralized schemes, crossover and feedback filters are used for jointly eliminating MAI and ISI effects. The low correlation between users' data improve the equalization performance, can be obtained by employing unique codes and different interleaver schemes in CDMA and IDMA systems, respectively. The absence of crossover filters in MDE results in producing decentralized MDE (DMDE). Therefore, the process of mitigating MAI in DMDE depends on MUD characteristics.

Parallel processing of multiuser interference simultaneously removes from each user the interference produced by the remaining users accessing the channel [101]. Employing parallel interference cancellation (PIC) with DMDE creates a new structure of decentralized receiver, which can provide higher performance compared to DMDE and MDE performances. In this chapter, we proposed a new receiver that depends on both PIC and DDFE for joint MAI and ISI mitigation and it is called PIC-DDFE-IDMA. The proposed detector relies on iterative manner for estimating transmitted symbols. Next DMDE is introduced, afterwards, the components of PIC-DDFE-IDMA receiver are demonstrated. Finally, both

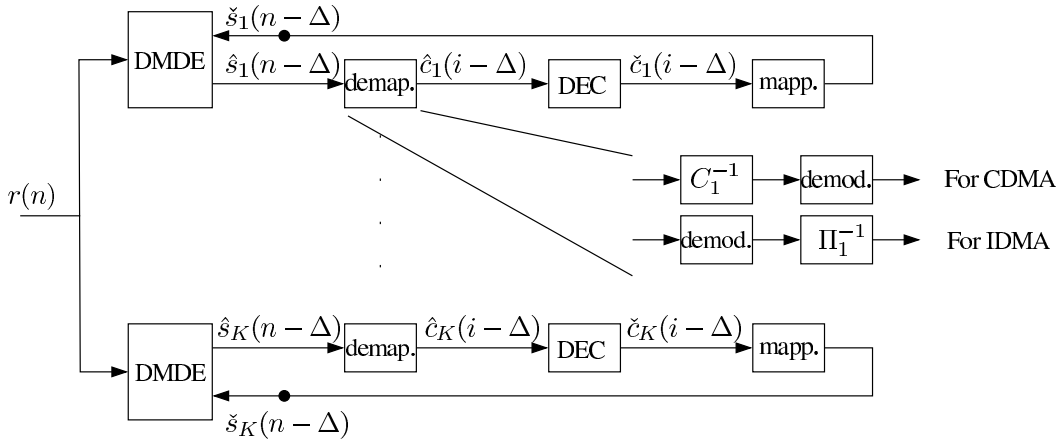


**Figure 5.1:** The general multiuser DMDE structure.

systems' performances are compared to centralized MDE system for both wireless and underwater shallow channels.

## 5.2 Iterative DDFE-MUD System

The objective of this section is to illustrate the performance of DMDE-MUD and comparing it with centralized MDE-MUD system for the multipath selective channels. The structure of DMDE is shown in Fig. 5.1. The DMDE can be constructed by using linear (DMLE) or DFE (DDFE) equalizers. In contrast of higher performance of DFE over LE, DFE has been chosen to be applied to DMDE schemes for demonstration purpose. Although, DDFE-MUD provides lower complexity than MDFE-MUD, however, this comes at the expense of lower performance as in Fig. 5.2. In addition to this, it is clear from the figure that DDFE performance significantly decreases when number of users increases from 8 to 16 users. This is due to the higher unresolved MAI in the equalizer outputs which results in more error propagation through feedback symbols. Also, Fig. 5.2 shows that DDFE-IDMA is less affected by the MAI than DDFE-CDMA when it compared to MDFE-IDMA and MDFE-CDMA, respectively. It can be deduced that the IDMA is more resistible than CDMA against MAI effects due to providing lower correlation between users' signals.

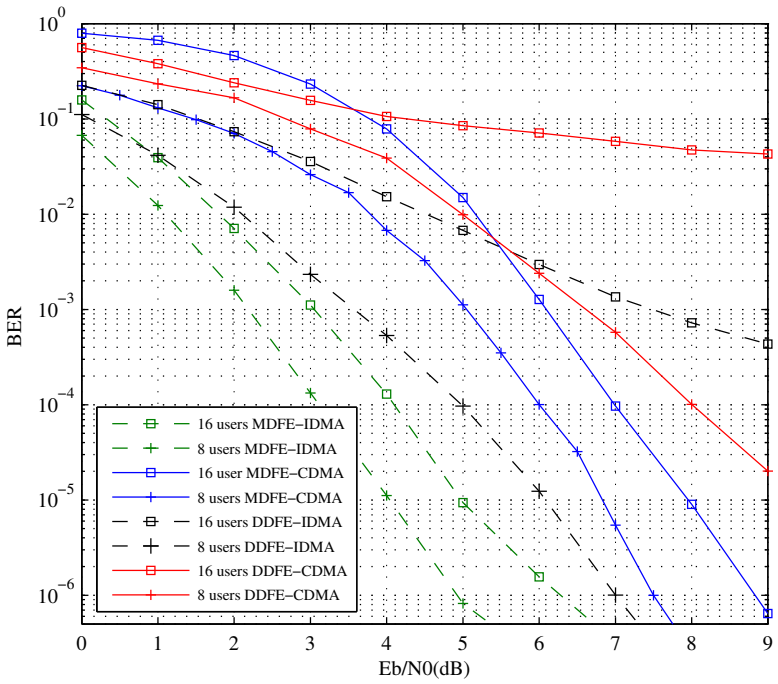


**Figure 5.2:** BER vs. Eb/N0 performance of optimal DDFE-MUD system for 8 and 16 users in frequency selective channels.

As mentioned before, the existence of unresolved MAI in DDFE structure leads to an inefficient equalizer operations. Therefore, we designed a new DDFE equalization for IDMA detection employing PIC operation such that the PIC removes MAI effects before equalizer takes place. The structure of PIC-DDFE-IDMA is presented in next section.

## 5.3 Iterative PIC-DDFE-IDMA Detection

The MDFE-IDMA structure depends on crossover filters to mitigate the MAI effects. Hence, these filters are not able to accomplish this task until their taps are fully converged. The delay in convergence of filter taps results in inefficient IDMA receiver which leads to poor performance during low SNR values. Therefore, the PIC-DDFE-IDMA receiver has been designed to minimize this error as

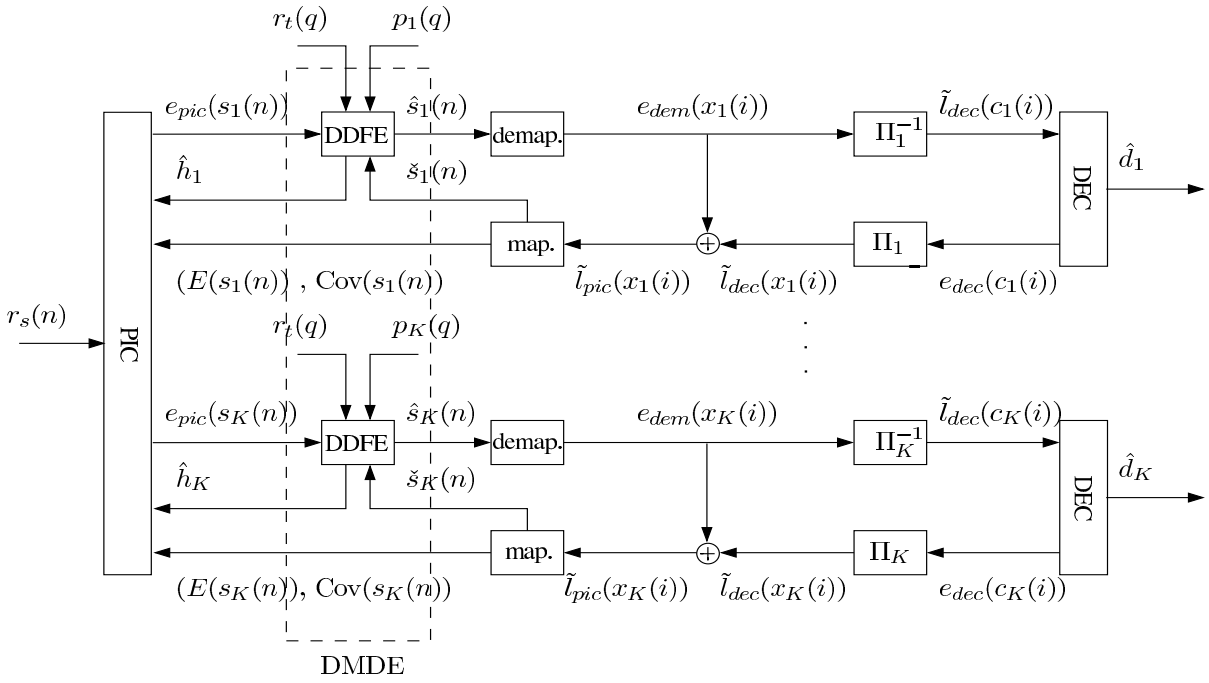


**Figure 5.3:** The proposed iterative PIC-DDFE-IDMA receiver structure.

shown in Fig. 5.3. It consists of PIC to remove MAI instead of crossover filters. Within PIC-DDFE-IDMA iterative process, PIC and DECs exchange extrinsic information, thus, the multiple access and coding constraints are considered separately. PIC-DDFE-IDMA receiver provides a suboptimal detection. During each iteration, the MAI impairments removed in PIC then the ISI removal occurred in DDFE equalizers for each user.

In the rake IDMA receiver, the received signal is first multiplied by the conjugate of the channel taps to cancel the phase shift produced by the channel between the real and imaginary part of the received symbols [10] . However, PIC-DDFE-IDMA compensates the channel dispersion by using embedded DFE inside IDMA iteration loop for each user. Generally, the PIC-DDFE-IDMA receiver consists of the following components:

### 5.3.1 PIC

The main function of PIC is to remove the MAI effects on the received signal according to a specific user. The detection of the $s_k$ symbols from $y(n)$ in (2.23) can be rewritten as

$$y(n+l) = h_k(l)s_k(n) + \eta_{k,l}(n), \tag{5.1}$$

where

$$\eta_{k.l}(n) = \sum_{k' \neq k,l} h_{k'}(l)s_{k'}(n) + \upsilon(n), \tag{5.2}$$

represents the distortion, including residual MAI and ISI plus AWGN. The output of the PIC for the $k$th user ($s_k(n)$) is given by

$$e_{pic}(s_k(n)) = \frac{y(n) - E\{\eta_k(n)\}}{\mathrm{Var}\{\eta_k(n)\}}, \tag{5.3}$$

where $E\{\eta_k(n)\}$ and $\mathrm{Var}\{\eta_k(n)\}$ are the total mean and total variance of the interference, respectively.

The complex values of the total mean and total variance of $\eta_k$ can be determined as

$$E\{\eta_k(n)\} = E(y(n+l)) - \hat{h}_k(l)E(s_k(n)), \tag{5.4}$$

$$\mathrm{Var}\{\eta_k(n)\} = \mathbf{Cov}(y(n+l)) - R_k(l)\mathbf{Cov}(s_k(n))R_k^T(l), \tag{5.5}$$

where $\hat{h}_k$ is the estimated channel taps provided by the channel estimation process taken place during training mode period, $\mathbf{Cov}(s_k(n))$ is given in (5.8), and also

$$R_k(l) = \begin{pmatrix} \mathrm{Re}\{\hat{h}_k(l)\} & -\mathrm{Im}\{\hat{h}_k(l)\} \\ \mathrm{Im}\{\hat{h}_k(l)\} & \mathrm{Re}\{\hat{h}_k(l)\} \end{pmatrix}. \tag{5.6}$$

where, Re{.} and Im{.} denote the real and imaginary parts. In (5.4) and (5.5), mean and variance can be estimated [6] [102] as follows:

$$E(r(n)) = \sum_{k,l} \hat{h}_k(l)E(s(n-l)), \tag{5.7a}$$

$$\mathbf{Cov}(r(n)) = \sum_{k,l} R_k(l)\mathbf{Cov}(s_k(n-l))R_k^T(l) + \sigma^2\mathbf{I}, \tag{5.7b}$$

where $\mathbf{I}$ is the identity matrix. The extrinsic LLRs from the PIC, $e_{\mathrm{pic}}(s_k(n))$, are then fed to the DFEs.

$$\mathbf{Cov}(s_k(n)) = \begin{pmatrix} Var(s_k^I(n) & E(s_k^Q(n)s_k^Q(n)) - E(s_k^I(n))E(s_k^Q(n)) \\ E(s_k^Q(n)s_k^Q(n)) - E(s_k^I(n))E(s_k^Q(n)) & Var(s_k^Q(n)) \end{pmatrix} \tag{5.8}$$

### 5.3.2 APP-DEC

The DECs employ standard APP decoding on $\tilde{l}_{\text{dec}}(c_k(n))$ to generate *a posteriori* LLRs $e_{\text{dec}}(c_k(n))$. The output of the DECs are the log likelihood ratios (LLR)s of $\{s_k^I(j), s_k^Q(j)\}$. The real LLRs are defined as

$$e_{dec}(s_k^I(j)) = \log\left(\frac{P_r(\mathbf{y}/s_k^I(j) = +1)}{P_r(\mathbf{y}/s_k^I(j) = -1)}\right). \tag{5.9}$$

where $\mathbf{y}$ denotes the equalized and deinterleaved version of the outputs of the PIC. The equations presented for the real part can also be adjusted accordingly to obtain the imaginary part $e_{\text{dec}}(s_k^Q(j))$ of the extrinsic LLRs. The extrinsic LLRs of the APP-DEC after upsampling and interleaving are given by

$$\tilde{l}_{\text{pic}}(x_k(n)) = \tilde{l}_{\text{dec}}(x_k(n)) - e_{\text{dem}}(x_k(n)), \tag{5.10}$$

however, for a number of users less than 16 [10], equation (5.10) can be approximated as follows:

$$\tilde{l}_{\text{pic}}(x_k(n)) = \tilde{l}_{\text{dec}}(x_k(n)). \tag{5.11}$$

The $\tilde{l}_{\text{pic}}(x_k(n))$ soft chips are used to generate the statistics given in (5.7a) and (5.7b). The hard symbols of $E(s_k(j))$ are also fed to the feedback filters of the DFE equalizers to minimize the error signal in the next IDMA iteration.

The real and imaginary parts of $s_k(j)$ are assumed to be uncorrelated due to the interleavers, and thus the off-diagonal entries of $\mathbf{Cov}(s_k(j))$ are zeros. The PIC uses $E(s_k(j))$ and $\mathbf{Cov}(s_k(j))$ to update the interference mean and variance with the aid of the channel estimated DFE filter taps, which are used in the next iteration. Initially, $E(s_k(j)) = 0$ and $\mathbf{Cov}(s_k(j)) = I$ for all $k, j$, implying no information is fed back from the DECs.

### 5.3.3 Optimal DFE Equalizer

The function of DFE equalizer is mainly to estimate the channel impulse response by using received symbols and known training symbols during the training mode

and equalizing the PIC output symbols during decision mode. The optimal filter taps for the $k$th user can be determined by solving

$$\Delta J = \min_{f_k, b_k} E|e_k|^2, \tag{5.12}$$

for both modes.

In decision mode, by assuming $s_k(n)$ and $\hat{s}_k(n)$ are jointly wide sense stationary with $e_{pic}(s_k(n))$ so that the covariance quantities

$$R_{\mathbf{y}} = E\left[\mathbf{e}_{pic}\mathbf{e}_{pic}^*\right] = H_{d_k} R_{\mathbf{s}_k} H_{d_k}^* + R_v,$$

and

$$R_{\mathbf{s}_k \mathbf{y}_{pic}} = E\left[\mathbf{s}_k \mathbf{y}_{pic}^*\right] = R_{\mathbf{s}_k} H_{d_k}^*,$$

are independent of $n$, where

$$\mathbf{e}_{pic} = [e_{pic}(0), e_{pic}(1), \ldots e_{pic}(N_f - 1)]^T,$$

$$\mathbf{s}_k = \left[\hat{s}_k(n)\hat{s}_k(n-1)\ldots\hat{s}_k(n-N_b)\right]^T,$$

and $H_{d_k}$ is a data matrix of size $(N_f \times L_b + N_f - 1)$ given in (3.17), the optimal filter taps are determined by substituting (4.2) in (5.12) and solving the optimization problem [25], that is

$$\mathbf{f}_{opt}^* = \mathbf{f}_{opt}^* R_{\mathbf{s}_k \mathbf{y}_{pic}} R_{\mathbf{y}}^{-1}, \tag{5.13}$$

and

$$\mathbf{b}_{opt}^* = \frac{e_0^T R_{\delta_k}^{-1}}{e_0^T R_{\delta_k}^{-1} e_0^T}, \tag{5.14}$$

where $R_{\delta_k}$ is the Schur complement of covariance matrix for $k$th user and it gived as follows

$$R_{\delta_k} \triangleq R_{\mathbf{s}_k} - R_{\mathbf{s}_k \mathbf{y}_{pic}} R_{\mathbf{y}} R_{\mathbf{y}_{pic} \mathbf{s}_k} > 0. \tag{5.15}$$

The BER performance of optimal PIC-DDFE-IDMA detector is depicted in Fig. 5.4 for different numbers of users employing 1/8 convolution code, 8-IDMA iterations and assuming perfect channel estimation. The performance of the

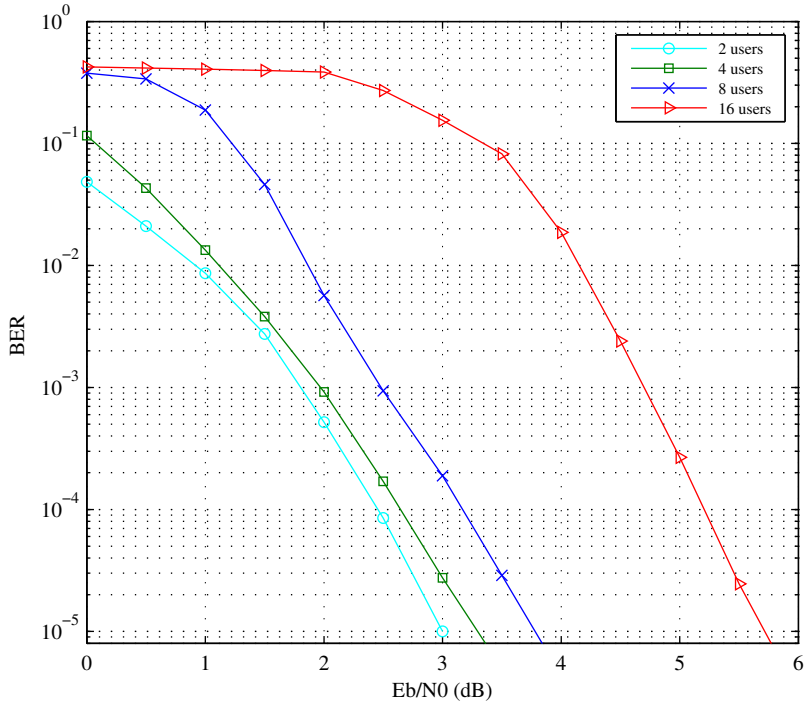


**Figure 5.4:** BER vs. Eb/N0 performance of optimal PIC-DDFE-IDMA system for different number of users in frequency selective channels.

PIC-DDFE-IDMA system is slightly decreased as the number of users is gradually increased from 2 to 8. However, when 16 users are transmitting simultaneously, higher reduction in the decentralized receiver performance is obtained. The sudden reduction in performance with 16 users is due to, firstly, the absence of feedback symbols from DECs to both PIC and DFEs. Secondly, the absence of MAI removal in the PIC in the first iteration. In turn, lower DFE efficiency leads to extensive error propagation in the feedback symbols during the second iteration. Therefore, in this case, the PIC-DDFE-IDMA needs higher SNR to completely remove MAI and ISI during detection iterations.

The effect of user population on the PIC-DDFE-IDMA performance is also investigated, where the theoretical MMSE curve is compared with the estimated MMSE as shown in Fig. 5.5. The estimated and theorietical MMSE can be calculated as

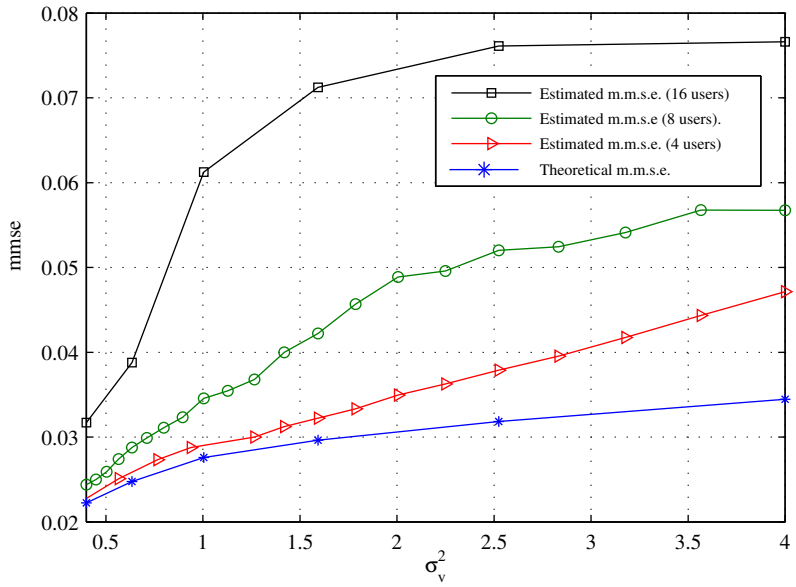


**Figure 5.5:** MMSE curve for PIC-DDFE-IDMA for different number of users.

$$\mathbf{mmse} = \frac{1}{N_s}(\hat{s}_k - s_k)(\hat{s}_k - s_k)^H, \tag{5.16}$$

$$\mathbf{mmse} = \frac{1}{e_0^T R_{\delta_k}^{-1} e_0^T}. \tag{5.17}$$

It can be seen from Fig. 5.5 that increasing of the users' number results in more deviation of theoretical and estimated curves due to effects of higher MAI and ISI interference on the performance of both PIC and DDFE equalizer.

On other hand, by obtaining the $\text{SINR}_k^b$ performance for PIC-DDFE structure as shown in Fig. 5.6, the improvement of the system performance during IDMA iteration is quite obvious when it compared to the $\text{SINR}_k^b$ performance for MDFE as given in Fig. 4.12. This means that the ability of removing MAI of the proposed decentralized system is gradually increased as the number of iterations increased, while in centralized receiver the MAI removal basically depends on the filters taps' convergence during IDMA iterations which results in a sudden enhancement of the system performance once the filter taps are completely converged.

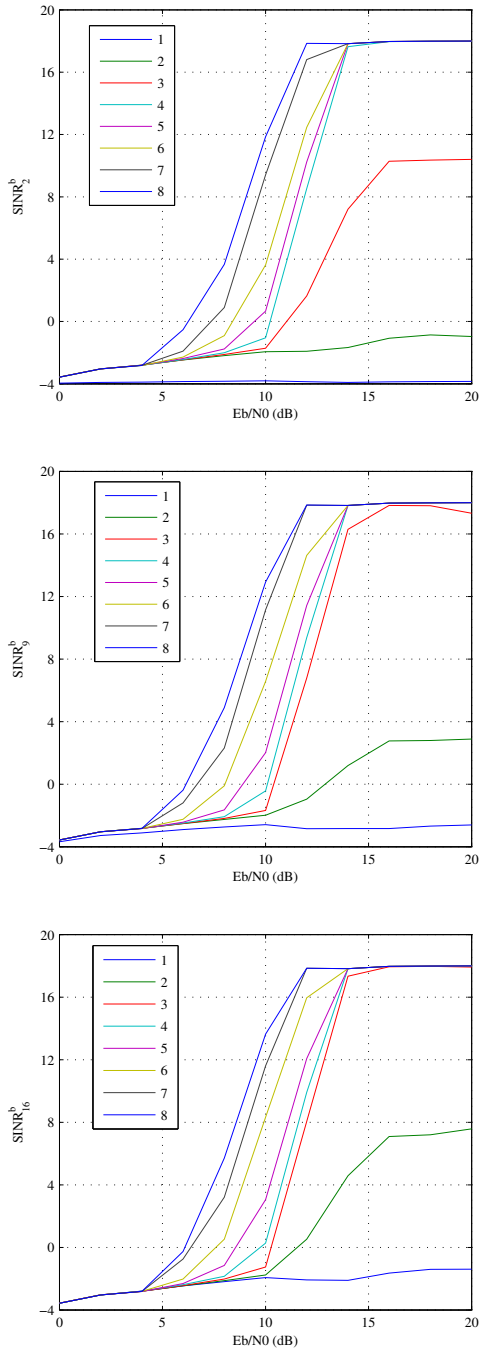


**Figure 5.6:** The improvement of SINR in crossover feedback filters within centralized PIC-DDFE-IDMA iterations.

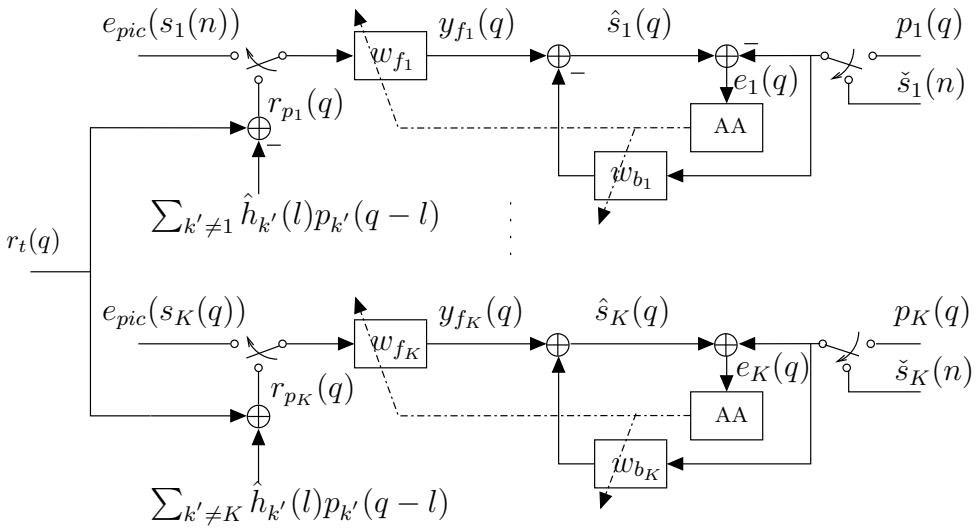


**Figure 5.7:** The iterative channel estimator structure.

## 5.4 Iterative Channel Estimation

The proposed decentralized IDMA receiver depends on the estimated channel taps for MAI eliminations processes. Hence, the accuracy of the estimated channel values has superior effect on the receiver performance. Therefore, an iterative channel estimator has been designed to estimate channels taps during training mode before IDMA detection starts at the decision mode. The estimated channel taps are used for determining the covariance and cross-covariance matrices, hence obtaining the feed-forward and feed-backward filter taps for each DFE equalizer. At the same time, the estimated channel taps are utilized by PIC processes for MAI suppression aim.

The iterative channel estimator is depicted in Fig. 5.7. Given the error signal

$$e_k(n-\Delta) = s_k(n-\Delta) - p_k(n-\Delta). \quad \text{training mode} \tag{5.18}$$

where $\mathbf{p}_k$ is the $k$th block of training symbols, the solution of the optimization problem is obtained by substituting (5.18) in (5.12) which results in producing a least square (LS) equation [25]. Hence, the $k$th user channel taps could be estimated as

$$\hat{h}_k = \left(H_{t_k}^* H_{t_k}\right)^{-1} H_{t_k}^* \mathbf{r}_{p_k}, \tag{5.19}$$

where $H_{t_k}$ is the rectangular Toeplitz data matrix of size $(L_k \times N_t + 1)$ and given as follows

$$H_{t_k} = \underbrace{\left.\begin{bmatrix} p_k(0) & 0 & 0 & \dots \\ p_k(1) & p_k(0) & 0 & \dots \\ p_k(2) & p_k(1) & 0 & \dots \\ \vdots & \vdots & \vdots & \ddots \\ p_k(N_t) & p_k(N_t-1) & p_k(N_t-2) & \dots \end{bmatrix}\right\} N_t+1}_{L_k} \tag{5.20}$$

and

$$\mathbf{r}_{p_k} = \left[r_{p_k}(q)\, r_{p_k}(q-1)\, \dots r_{p_k}(q-N_f+1)\right]^T,$$

is the observed training symbols, where

$$r_{p_k}(q) = r_t(q) - \sum_{k' \neq k} \hat{h}_{k'}(l_b) p_{k'}(q-l_b). \tag{5.21}$$

Initially, the $\hat{h}_k$ is set to zero. Therefore, $r_{p_k}(q)$ contains both MAI and ISI in the first iteration for the first user, while for the second user the amount of MAI is decreased and for final user the lower MAI is obtained. However, for the second iteration the performance of the channel estimation is noticeably improved, since all users have obtained initial channel taps in the first iteration. As long as the number of iteration increased, better channel estimation performance is obtained. It's worth mention that the channel estimation iteration not necessarily to be equal to the IDMA iteration. Few iterations enough to get accurate channel taps when the training symbols of the users have low auto-correlation property.

As in MDFE-IDMA, the iterative LS channel estimation is applied to 511 training symbols and the PIC-DDFE-IDMA system performance is compared with perfect channel estimation assumption. The training symbols are generated with m-sequence generator which provides a good correlation property that supports efficient channel estimation process. Fig. 5.8 shows the effect of estimated channel taps on the PIC-DDFE IDMA performance. The imperfection of the estimated channel taps increases the probability of symbol errors, hence produces higher BER. The channel estimation imperfection effect on the system performance is more perceptible as the number of users is gradually increased. It is

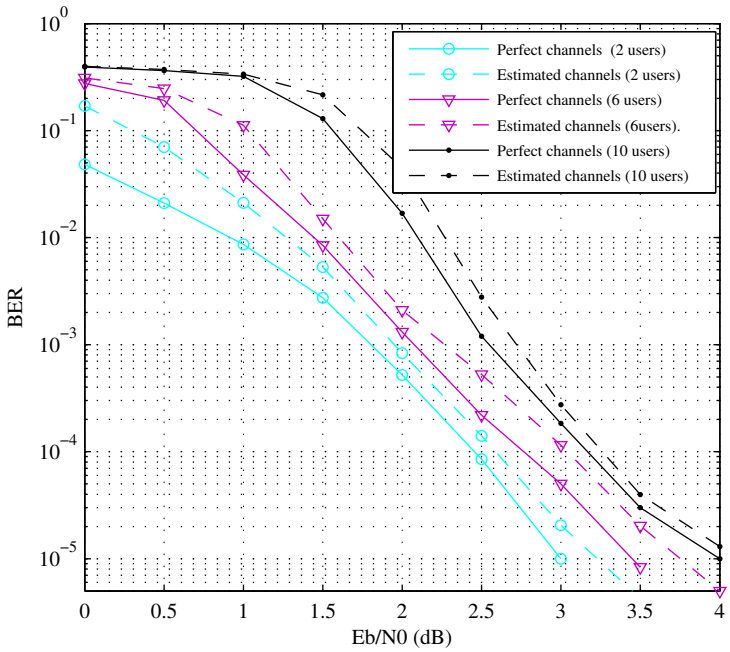


**Figure 5.8:** BER vs. Eb/N0 optimal PIC-DDFE-IDMA performance for LS and perfect channel estimations.

clear in the above figure that, decentralized equalization is less affected by MAI interference than centralized equalization for IDMA while increasing the number of users.

## 5.5 Performance of PIC-DDFE-IDMA and Comparison with MDFE-IDMA

In this section, the performance of PIC-DDFE-IDMA is presented for different rates of encoding by using convolutional and repetition codes for selective fading channels. The performance of the proposed system is also compared to MDFE-IDMA performance, which stated in the previous chapter. The same channel characteristics used in chapter four are employed in the simulation for this section. The symbols are modulated with QPSK mapping before transmitting through multipath channels.

The PIC-DDFE-IDMA performance generally depends on the equalizer performance and the decoding efficiency. The amount of feedback errors which returned back to the PIC have a significant effect on equalization process. Hence, the type and the rate of the decoder are two important factors that have to be properly chose to obtain higher system performance.

The improvement of PIC-DDFE-IDMA's performance is illustrated in Fig. 5.9 by employing higher coding rate. It can be noticed from the figure that the 1/16 rate, using 1/8 convolution and 1/2 repetition coding, is almost better than only using 1/8 convolution. The amount of improvement comes from the higher error correction and also from the higher correlation provided by 1/2 repetition code. Moreover, utilizing 1/8 convolutional coding produces approximately the same performance as 1/16 rate using 1/2 convolution and 1/8 repetition code. This is because the efficiency of error correction obtained by 1/8 convolution coding is higher than 1/2 convolution coding, which in turn compensate the higher correlation provided by 1/8 repetition coding.

The differences between MDFE and PIC-DDFE equalizers are given in Fig. 5.10 when 1/8 convolutional code is applied to the transmitted bits and IDMA principles are used for providing low correlation property between users' signals. Although they have some superficial similarities with two users, however, the DDFE still outperforms the MDFE when large numbers of users. This is because the difference between PIC and crossover filters comes to light when high amount of intereference exists in the received signal. In addition, the higher MAI suppression in DDFE can be more obvious by comparing the mmse curves as shown in Fig. 5.11.

Furthermore, the effects of shallow water selective fading channels on both PIC-DDFE-IDMA and MDFE-IDMA perfromances are shown in Fig. 5.12. As it was expected, both systems show higher performance for 1/8 convolution coding due to higher error correction among feedback chips provided by 1/8 convoltional coding.

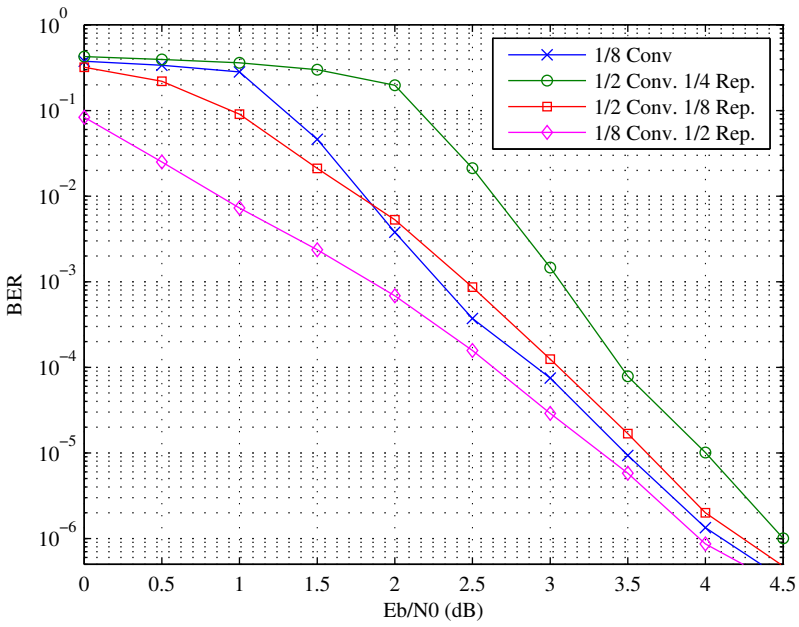


**Figure 5.9:** Effect of coding rate on PIC-DDFE-IDMA receiver for 8 users.

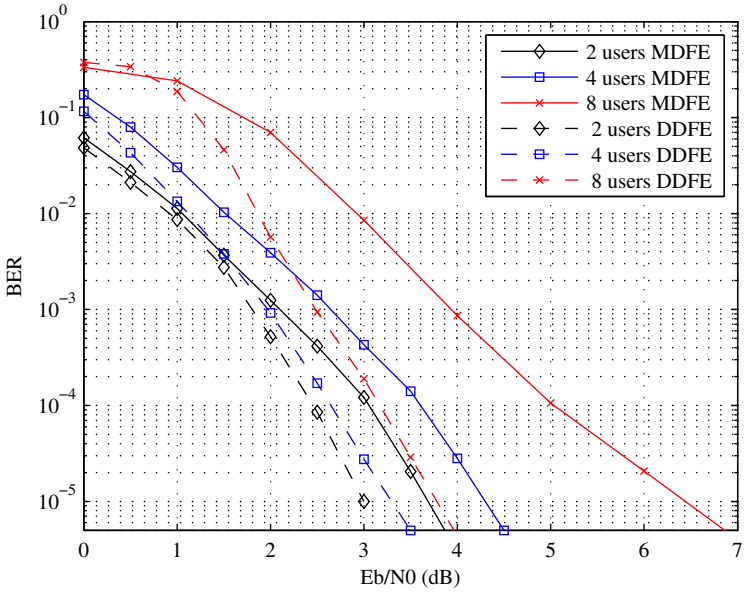


**Figure 5.10:** Performance comparison between centralized and decentralized IDMA receivers for 1/8 convolution code.

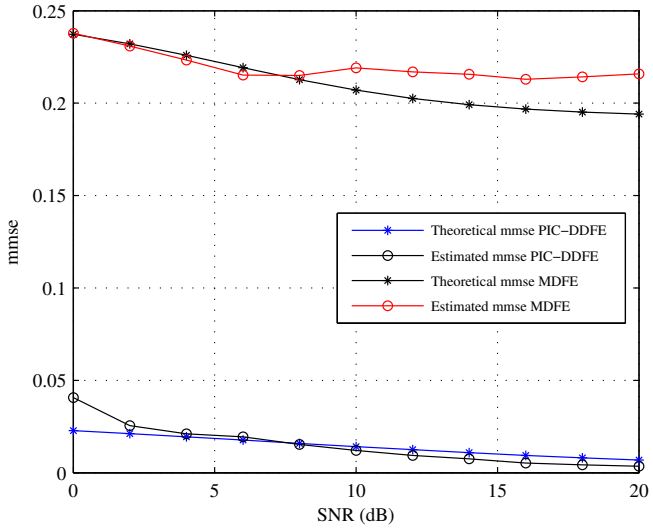


**Figure 5.11:** mmse vs SNR Performance comparison between centralized and decentralized IDMA receivers for 1/32 convolution code, 8 users.

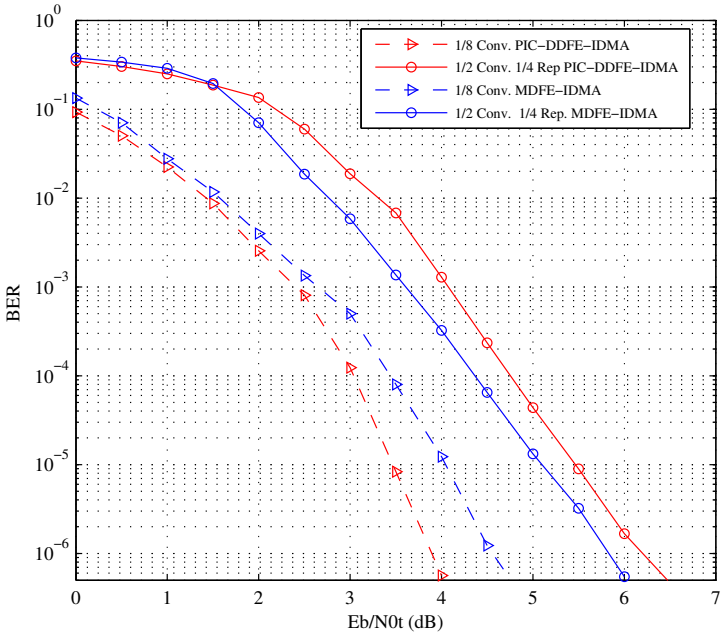


**Figure 5.12:** Performance comparison different coding types for PIC-DFE-IDMA in shallow water channels.

## 5.6 Chapter Summary

This chapter presents a new model of decentralized multidimentional equalization for IDMA system by utilizing both PIC and DFE equalizer based on MMSE approach. The PIC-DDFE equalization taken place by exchanging a proiri data symbols between the MAP decoder and the decentralized equalizer through interleavers permutation such that the ISI and MAI are removed by DDFE and PIC operations, respectively. The delay in convergence, which crossover filters in MDFE equalization were suffering from, has been removed by using MAI. The absence of crossover filters in PIC-DDFE equalization lead to a rapid convergence of the DFE equalizers filters' taps which in turn resulted in reducing the feedback error propagation. Consequently, for both wireless channels and shallow water acoustic channels, PIC-DDFE-IDMA showed higher performance than MDFE-IDMA.

# 6

# Complexity and Performance analysis of Adaptive Multi-dimensional Equalizers

Adaptive equalization is an effective process that mitigates the received signal dispersion caused by signal propagation in multipath channels. As it was mentioned in Chapter one, there is no unique adaptive algorithms. However, based on the problem requirements, various algorithms have been proposed such as LMS and RLS algorithms.

Statistical formulation can be used to progress the stochastic gradient adaptive filters. The main objective of LMS adaptive filters is to provide a solution for the MMSE estimation problem by employing an approximate gradient search. The statistics of input signals are the main factor for the adaptation process of these filters, thus they limited to be used in some applications. This problem encouraged the researchers to design a new adaptive algorithm that can replace LMS adaptation such as RLS filters. RLS filters are proposed to obtain higher adaptation efficiency than LMS by utilizing a weighted sum of the squared estimation error in a recursive manner. One of the important feature of RLS filters is that they can obtain the exact solutions to the optimization problems within iterations which provides better performance than LMS filters.

Both centralized and decentralized multidimensional equalizers, which are proposed in previous chapters, are designed by using optimal filters. However, the

optimal solutions are not practical due to the high complexity required for inverse matrix computation. Therefore; in this chapter, the optimal values for filter taps are implemented by utilizing adaptive algorithms. Both LMS and RLS algorithms have been applied to the proposed systems for comparison purpose in terms of system performance and complexity.

## 6.1 Adaptive Centralized Mulit-Dimensional Equalizer

The LMS algorithm provides slow convergence and poor tracking properties. This often makes the algorithm to be unstable. The normalized least mean square (NLMS) algorithm is a variant of LMS that solves this problem by normalizing with the power of the input data. The NLMS algorithm can be summarized by modifying 1.2 as

$$\mathbf{w}(k+1) = \mathbf{w}(k) + \frac{2\eta e(k)\mathbf{s}(k)}{\mathbf{s}(k)^H \mathbf{s}(k)}. \tag{6.1}$$

The performance of adaptive equalizer depends on the employed adaptive algorithm. Therefore, it is worth to utilize both NLMS and RLS algorithms for illustrating adaptive MDFE-IDMA performance. Fig. 6.1, Fig. 6.2 and Fig. 6.3 show the performance of MDFE-IDMA for 2, 4 and 8 users, respectively, using 1/8 convolution and 1/4 repetition coding in wireless channels. As it was expected, each of these figures shows the obvious out-performance of RLS over NLMS. It can be noticed that when the number of users is increased, RLS performance remains stable and close to the optimal performance, while NLMS tends to diverge from the optimal performance. This is because the filter taps can not be fully converged due to the higher effects of MAI dispersion, which in turn, results in a lower trucking behavior.

For the sake of more illustration about the efficiency of adaptive algorithms in the multidimensional equalizers, the ability of adaptive filters in jointly removing ISI and MAI dispersion can also be presented by plotting MMSE curves. Fig. 6.4, Fig. 6.5 and Fig. 6.6 reports the MMSE curves versus noise variance for two, four and eight users, respectively. From the figures, the optimal solution

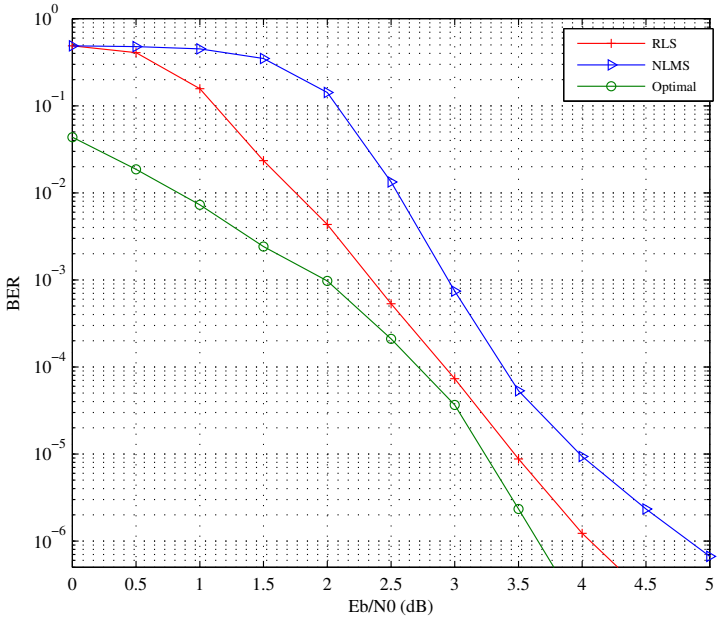


**Figure 6.1:** Adaptive MDFE-IDMA performances for two users.

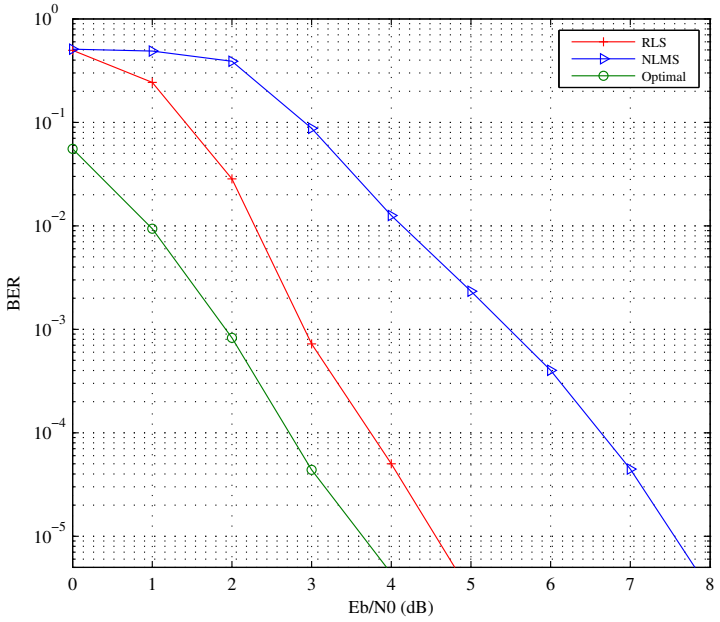


**Figure 6.2:** Adaptive MDFE-IDMA performances for four users.

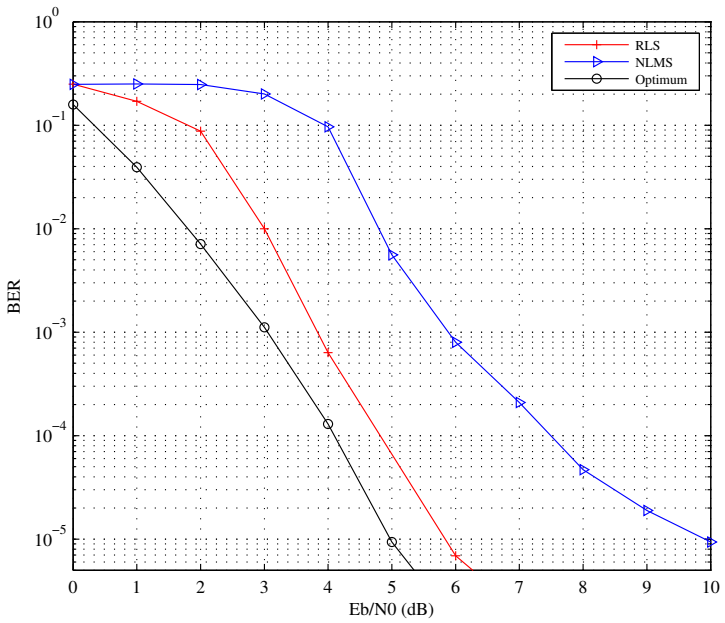


**Figure 6.3:** Adaptive MDFE-IDMA performances for eight users.

almost coincides with theoretical MMSE. NLMS performance is remained stable alongside RLS and optimal performances for two and four users. However for eight users, NLMS efficiency in calculating accurate filter coefficients is reduced due to the higher interference effects on the received signal, which makes system performance almost unstable. The NLMS algorithm is expected to lose more stability when more users are employed. Although RLS tends to give insufficient performance when there is high noise variance for 8 users, however, it is approximately providing the same performance as optimal solution, which in turn, unlike NLMS, can give a stable performance while increasing the number of users.

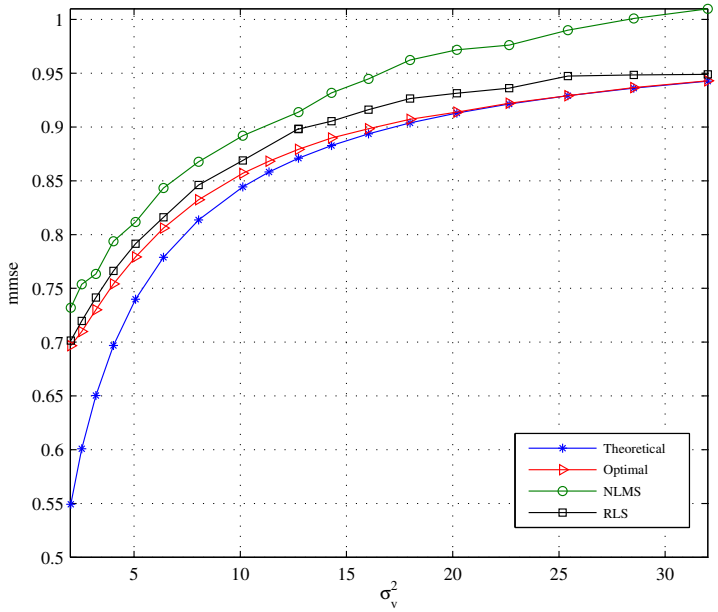


**Figure 6.4:** MMSE performance of adaptive MDFE-IDMA for two users.

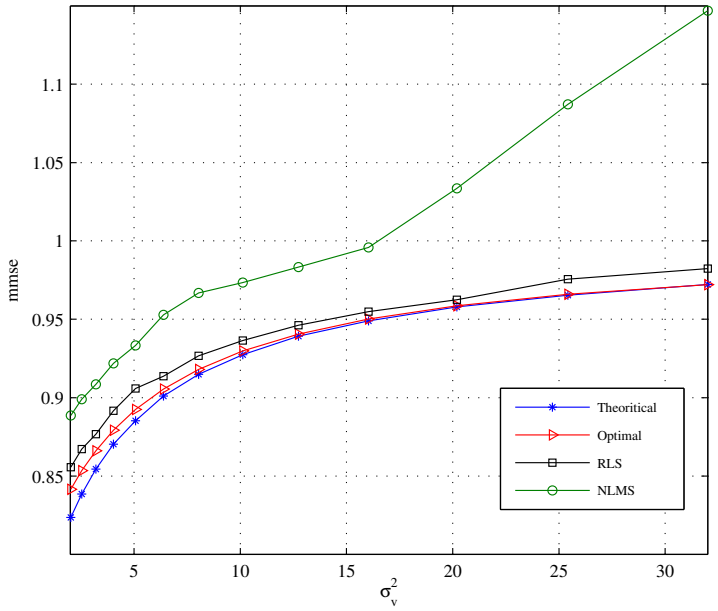


**Figure 6.5:** MMSE performance of adaptive MDFE-IDMA for four users.

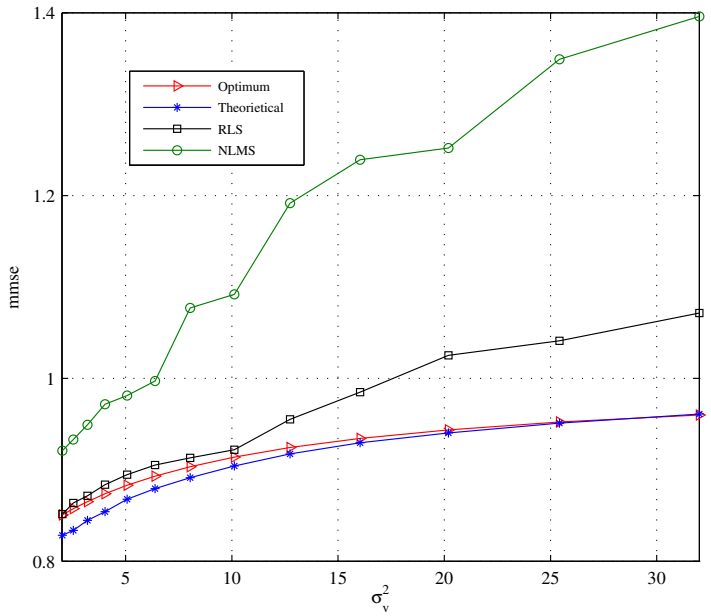


**Figure 6.6:** MMSE performance of adaptive MDFE-IDMA for eight users.

For shallow water acoustic channels, user 1 and user 2 are positioned at a distance of 1 km and 3 km from the relay, respectively, so that their arriving signals forming an angle of 45° between them at the relay as depicted in Fig. 6.7 and thier impulse responses are given in Fig. 4.7. The performance of the uplink IDMA system is evaluated using DLE, DDFE and MDFE equalizers, where DLE stands for using just forward filters and DDFE stands for the absence of the crossover filters. In contrast of higher performance of RLS over NLMS, RLS has been used as an adaptive algorithm to determine the optimal filter taps during iterative detection. The performance of the aforementioned three schemes according to their bit error rates vs. the $E_b/N_0$ in dB are given in Fig. 6.8. All filters have the same length, which is 40 taps, to enable the equalizers to overcome the ISI and MAI completely during the iterative process. The use of the previous estimated symbols for next symbol detection in DFE leads to the elimination of the ISI effects. Therefore, it was expected that DDFE will have better resistivity against channel impairments than DLE as shown in Fig. 6.8.

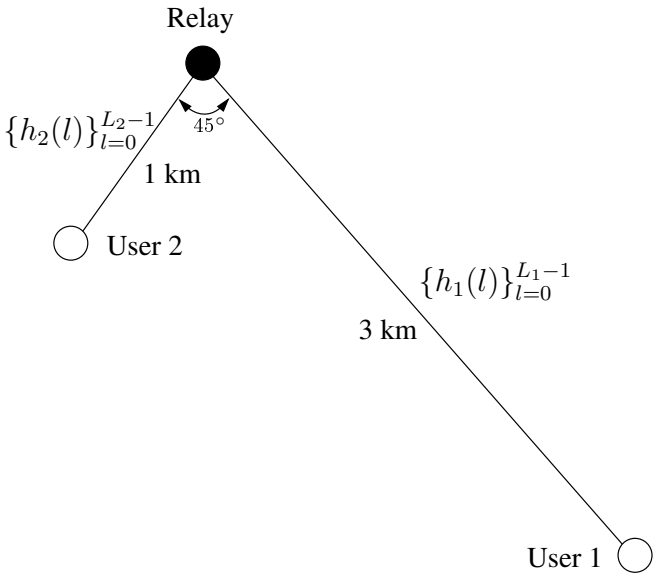


**Figure 6.7:** Two-user uplink transmission scenario.

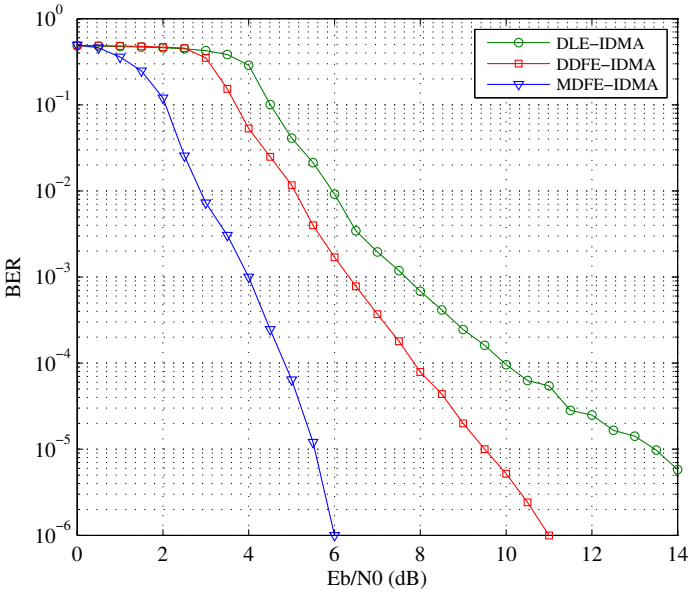


**Figure 6.8:** BER vs. $E_b/N_0$ performance for DLE, DDFE, and MDFE in multi-path fading channels.

Nevertheless, the convergence of the MSE error for both systems has a trivial difference as depicted in Fig. 6.9. This is because, the existence of the MAI generates wrong decisions at the output of the equalizers. However, in spite of both equalizers approximately have similar MSE error, the approximate 4 dB gain in $Eb/N0$ at BER=$10^{-5}$ of DDFE results from the absence of the ISI which provides more support to the IDMA detection performance.

The 3.5 dB of the difference in $Eb/N0$ performance between DDFE and MDFE in Fig. 6.8 emphasizes the extensive reduction of the effect of MAI on the received signal due to using cross feedback filters. At the same time, the convergence and tracking properties of the MDFE equalizer exhibits lower squared error at decision mode as shown in Fig. 6.9. The dramatic drop in average square error of MDFE interprets the amount of MAI suppression at the output of the equalizer. The scatter plots for both users in Fig. 6.10 demonstrates the amount of the residual interference of the equalized symbols. In spite of the higher frequency selectivity of channel 2, the corruptions of the constellation points of both users are approximately identical due to the proper equalization of adaptive MDFE to cope the MAI and ISI impairments.

## 6.2 Adaptive PIC-DDFE-IDMA

In this section, the performance of adaptive PIC-DDFE-IDMA is examined in frequency selective multipath fading channels, and at the same time, its performance is compared to MDFE-IDMA performance. The simulation examples are implemented using 1/8 convolutional coding. A length of 10 taps is chosen for feed-forward, feed-backward, and crossover filters and 12 iterations have been taken for IDMA detection.

Fig.6.11 depicts the PIC-DDFE-IDMA performance for 4 users and its performance compared to the MDFE-IDMA detector. It shows that PIC-DDFE-IDMA still outperforms MDFE-IDMA for both RLS and NLMS adaptations. On other hand, Fig. 6.12 depicts the performance of two users PIC-DDFE-IDMA system in shallow water acoustic channels for optimal, NLMS and RLS adaptation, at the same time its performance compared with MDFE-IDMA performance when RLS is used for adapting filter coefficients. Also, It could be noticed that PIC-DDFE

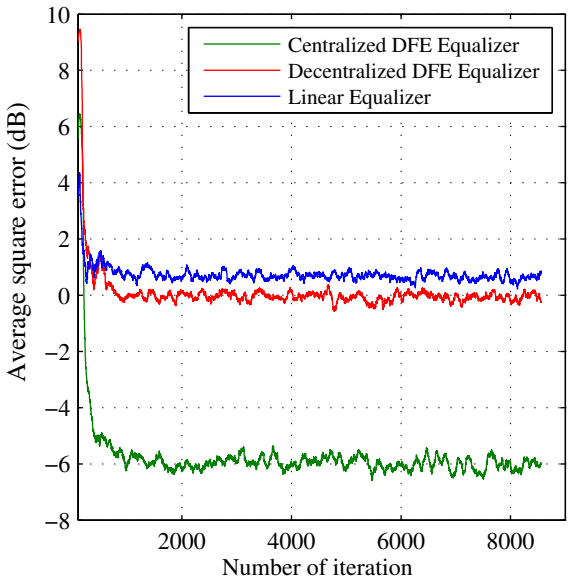


**Figure 6.9:** Average least square error versus iteration number at $E_b/N_0$=10 dB (1 iteration= 1 symbol period).

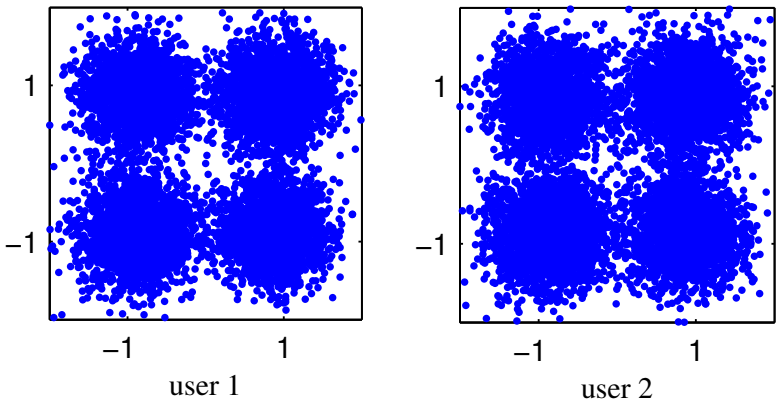


**Figure 6.10:** Scatter plot of the equalized symbols for both users using MDFE at $Eb/N0$=10 dB.

with NLMS adaptation is achieved a performance almost coincides to the performance obtained by MDFE with RLS adaptation when SNR is become higher than 5 dB. The lower feedback error propagation in PIC-DDFE-IDMA compared to MDFE-IDMA is the main reason behind the absence of difference between NLMS and RLS adaptations.

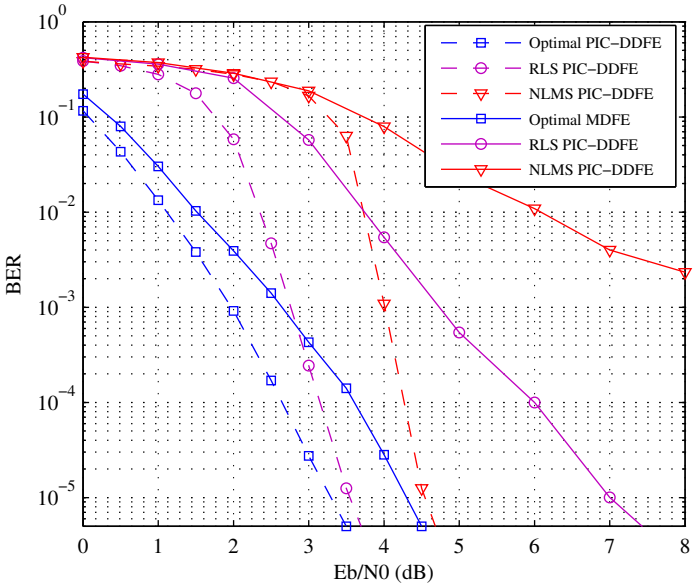


**Figure 6.11:** BER vs. Eb/N0 performance comparison of PIC-DDFE-IDMA and MDFE-IDMA using optimal and adaptive algorithms.

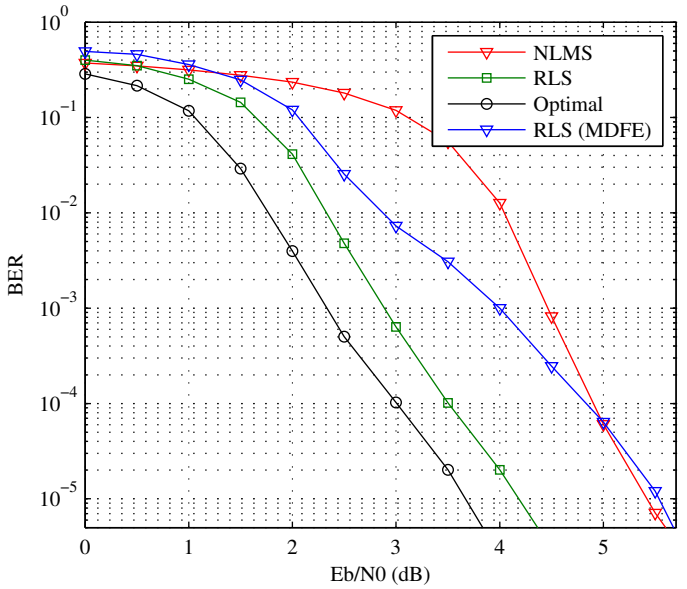


**Figure 6.12:** Performance of PIC-DDFE-IDMA in underwater acoustic shallow channels .

## 6.3 Complexity Analysis

In this section, the computational complexity of PIC-DDFE-IDMA and MDFE-IDMA is compared to the rake IDMA system on the basis of the number of arithmetic operations. The three receivers have the same operation numbers in the APP-DEC, repetition, down-sampling, interleavers, and deinterleavers functions. Therefore, their complexity is not taken into account within comparison procedure. However, the receivers can be compared according to the total operations taken place within PIC (or ESE), DFE equalizer, and channel estimation blocks.

For rake IDMA receiver, the operation number is determined base on the equations given in [10]. The ESE processes include jointly MAI and ISI elimination for all users' signal when channel coefficients are provided. For making a fair comparison between the proposed receivers and the rake IDMA receiver, the same iterative channel estimation technique in PIC-DDFE-IDMA has been adapted for providing ESE with the channel coefficients. The ESE in rake IDMA receiver treats the first $N_t$ training symbols and the remaining $N_s$ data symbols in each received block in a different manner. The received training symbols are extracted from MAI interference based on the equations in PIC processes and then fed to the channel estimation process. While the data symbols are first multiplied by the conjugate of the estimated channel coefficients and then extracted from the effect of the both MAI and ISI interferences simultaneously based on the equations given in [10].

Table 6.1 summarizes the total computational complexity of PIC-DDFE-IDMA, rake IDMA and MDFE-IDMA receivers for NLMS adaptive algorithm. The off diagonal entries of covariance matrix has been set to be zeros without calculation so as to reduce unnecessary mathematical operations. One complex multiplication costs 4 real multiplications and 2 real additions. One complex addition/subtraction costs 2 real additions. Table 6.1 generated based on the following parameters; $K$=8 users, $L$=16 paths, $it$=8 IDMA iterations, $\text{it}_c$=4 channel estimation iteration, and $N_f = N_b = N_c = 16$ filter taps. Obviously, the MDFE-IDMA has a lower complexity than rake IDMA and PIC-DDFE-IDMA

using NLMS adaptive algorithm. This is because there is no complex interference cancellation in cross-over filters to remove MAI as its exit in both PIC and ESE processes. At the same time, the channel estimation operation is taken place just one time before IMDA detection in MDFE-IDMA, whereas for the other two receivers the channel estimation is processed for $it_c$ iterations. Moreover, the MD equalizer complexity rises linearly with the number of the users in MDFE-IDMA, therefore, for the higher number of users the complexity difference between MDFE-IDMA and PIC-DDFE-IDMA will be reduced. On other hand, PIC-DDFE-IDMA provides lower complexity than rake IDMA receiver. In spite of DFE equalizers operations in PIC-DFE-IDMA, the absence of multiplying the channel conjugate with the received symbols, total mean and total covariance of the interference in PIC-DDFE-IDMA makes it lower complex than rake IDMA detection.

The same complexity comparison can be applied by using RLS algorithm. The amount of improvement in BER signal utilizing RLS significantly increases the complexity of the channel estimations and DFE equalizer operations as shown in Table 6.2. Although, MDFE-IDMA became more complex by using RLS, however, it still has lower complexity than the other two receivers. Moreover, it is obvious from the table that there is a hug difference in computation number between MDFE-IDMA and PIC-DDFE-IDMA using NLMS decreases noticeably when RLS is used. This difference in computational complexity becomes lower when higher number of users are employed.

Fig. 6.13 gives another example of comparison between MDFE-IDMA and PIC-DDFE-IDMA for different number of users. A rate 1/2 convolutional code and rate 1/4 spreading code has been used such that the total rate becomes 1/8. As mentioned before, the crossover filters in MDFE-IDMA are need to be fully converged for efficiently removing MAI effects, while the MAI elemination is taken place in PIC processes within PIC-DDFE-IDMA detection. Consequently, PIC-DDFE-IDMA shows higher performance than MDFE-IDMA. It is also clear from the figure that the increase in the number of users has lower effects on PIC-DDFE-IDMA compared to MDFE-IDMA, this shows the power of PIC in reducing feedback error propagation produced by larger number of users.

**Table 6.1:** Complexity comparison between rake IDMA, MDFE-IDMA and PIC-DDFE-IDMA for K=8, L=16, It=8, $\text{It}_c$=4, $N_f$=$N_b$=$N_c$=16 utilizing NLMS algorithm.

| Rake IDMA | | | | |
|---|---|---|---|---|
| Operation | ESE | DFE | Channel Estimation | Number of computations |
| add./sub. | $22 \times \text{L} \times \text{K} \times \text{It}$ | - | $(N_f+ N_b+ 1)\times 6\times \text{It}_c$ | 23320 |
| multiplication | $46 \times \text{L} \times \text{K} \times \text{It}$ | - | $(N_f+ N_b+ 1)\times 8\times \text{It}_c$ | 48160 |
| division | $2 \times \text{L} \times \text{K} \times \text{It}$ | - | $2 \times \text{It}_c$ | 2056 |
| tanh | $2 \times \text{K} \times \text{It}$ | - | - | 128 |
| total | | | | 73664 |
| MDFE-IDMA | | | | |
| Operation | Cross-over Filter | DFE | Channel Estimation | Number of computations |
| add./sub. | $(K-1) \times N_c\times 6 \times \text{It}$ | $(N_f+ N_b+ 1)\times 6\times \text{It}$ | $(N_f+ N_b+(K-1) \times N_c+ 1)\times 6$ | 7830 |
| multiplication | $(K-1) \times N_c\times 8 \times \text{It}$ | $(N_f+ N_b+ 1)\times 8\times \text{It}$ | $(N_f+ N_b+(K-1) \times N_c+ 1)\times 8$ | 10440 |
| division | $2 \times \text{It}$ | $2 \times \text{It}$ | 2 | 32 |
| tanh | - | - | - | - |
| total | | | | 18302 |
| PIC-DDFE-IDMA | | | | |
| Operation | PIC | DFE | Channel Estimation | Number of computations |
| add./sub. | $16 \times \text{L} \times \text{K} \times \text{It}$ | $(N_f+ N_b+ 1)\times 6\times \text{It}$ | $(N_f+ N_b+ 1)\times 6\times \text{It}_c$ | 18760 |
| multiplication | $24 \times \text{L} \times \text{K} \times \text{It}$ | $(N_f+ N_b+ 1)\times 8\times \text{It}$ | $(N_f+ N_b+ 1)\times 8\times \text{It}_c$ | 27744 |
| division | $2 \times \text{L} \times \text{K} \times \text{It}$ | $2 \times \text{It}$ | $2 \times \text{It}_c$ | 2072 |
| tanh | $2 \times \text{K} \times \text{It}$ | - | - | 128 |
| total | | | | 48704 |

**Table 6.2:** Complexity comparison between rake IDMA, MDFE-IDMA and PIC-DFE-IDMA for K=8, L=16, It=8, $\mathrm{It}_c$=4, $N_f$=$N_b$=$N_c$=16, $N_o = N_f + N_b$, $N_\bullet = (K-1)N_c + N_o$ utilizing RLS algorithm.

| Rake IDMA | | | | |
|---|---|---|---|---|
| Operation numbers | ESE | DFE | Channel Estimation | Number of computations |
| add./sub. | $22 \times \mathrm{L} \times \mathrm{K} \times \mathrm{It}$ | - | $(N_o^2 + 3 \times N_o) \times \mathrm{It}_c$ | 27008 |
| multiplication | $46 \times \mathrm{L} \times \mathrm{K} \times \mathrm{It}$ | - | $(N_o^2 + 5 \times N_o + 1) \times \mathrm{It}_c$ | 51844 |
| division | $2 \times \mathrm{L} \times \mathrm{K} \times \mathrm{It}$ | - | $2 \times \mathrm{It}_c$ | 2056 |
| tanh | $2 \times \mathrm{K} \times \mathrm{It}$ | - | - | 128 |
| total | | | | 81036 |
| MDFE-IDMA | | | | |
| Operation numbers | Cross-over Filter | DFE | Channel Estimation | Number of computations |
| add./sub. | $(K-1) \times N_c \times 6 \times \mathrm{It}$ | $(N_o^2 + 3 \times N_o) \times \mathrm{It}$ | $(N_\bullet^2 + 3 \times N_\bullet)$ | 27674 |
| multiplication | $(K-1) \times N_c \times 8 \times \mathrm{It}$ | $(N_o^2 + 5 \times N_o + 1) \times \mathrm{It}$ | $(N_\bullet^2 + 5 \times N_\bullet + 1)$ | 30215 |
| division | $2 \times \mathrm{It}$ | $2 \times \mathrm{It}$ | 2 | 32 |
| tanh | - | - | - | - |
| total | | | | 57921 |
| PIC-DDFE-IDMA | | | | |
| Operation numbers | PIC | DFE | Channel Estimation | Number of computations |
| add./sub. | $16 \times \mathrm{L} \times \mathrm{K} \times \mathrm{It}$ | $(N_o^2 + 3 \times N_o) \times \mathrm{It}$ | $(N_o^2 + 3 \times N_o) \times \mathrm{It}_c$ | 29824 |
| multiplication | $24 \times \mathrm{L} \times \mathrm{K} \times \mathrm{It}$ | $(N_o^2 + 5 \times N_o + 1) \times \mathrm{It}$ | $(N_o^2 + 5 \times N_o + 1) \times \mathrm{It}_c$ | 38796 |
| division | $2 \times \mathrm{L} \times \mathrm{K} \times \mathrm{It}$ | $2 \times \mathrm{It}$ | $2 \times \mathrm{It}_c$ | 2072 |
| tanh | $2 \times \mathrm{K} \times \mathrm{It}$ | - | - | 128 |
| total | | | | 68950 |

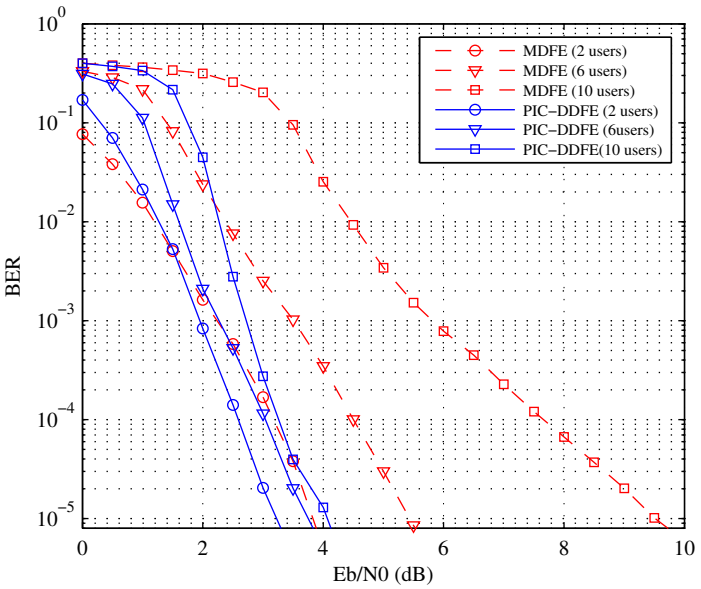


**Figure 6.13:** BER vs. Eb/N0 of PIC-DDFE-IDMA and MDFE-IDMA for different numbers of users.

Fig. 6.14 and Fig 6.15 state the performance comparison of PIC-DDFE-IDMA, MDFE-CDMA and rake IDMA detectors for a 4-users wireless and 2-users shallow water acoustic channels, respectively. From Fig. 6.14, although the process of MAI elimination in MDFE-IDMA requires high values of $E_b/N_0$ to enable the crossover filter taps to converge during training mode, however, it can outperform MDFE-CDMA performance which uses longer training sequence due to spreading by a factor of 4 after modulation. The worse performance of MDFE-CDMA detector comes from the short CDMA codes which provides low auto-correlation property among users' signal. In addition, PIC-DDFE-IDMA outperforms the other three receivers due to the efficient RLS equalizer which results in converge faster at low values of $E_b/N_0$. The same results can be noticed from the performance comparison between the four detectors in shallow water acoustic channels as depicted in Fig 6.15.

## 6.4 Chapter Summary

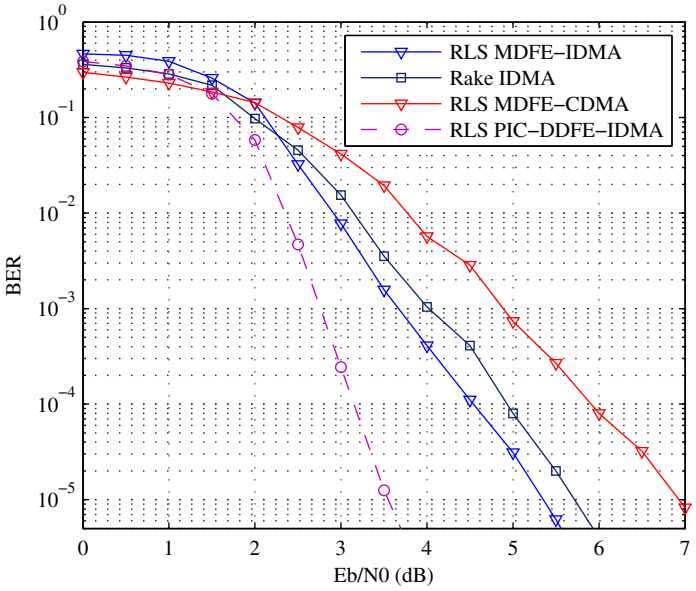


**Figure 6.14:** Performance comparison of optimal multiuser detectors for wireless channels.

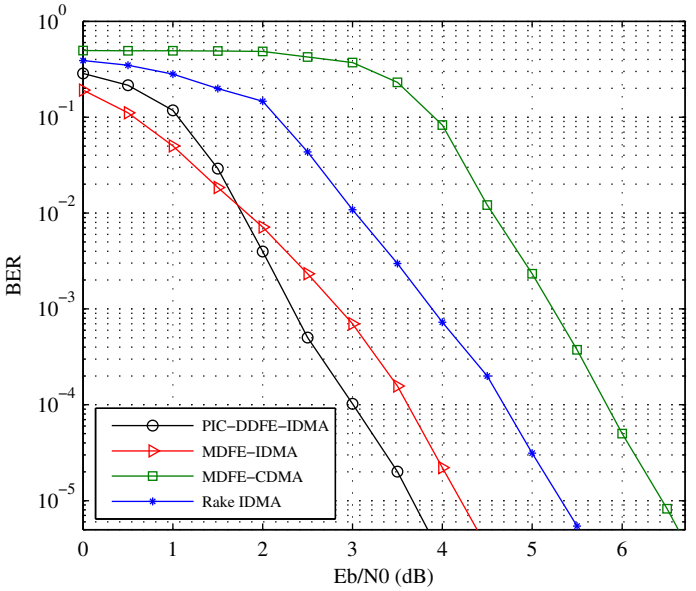


**Figure 6.15:** Performance comparison of optimal multiuser detectors for two-user underwater acoustic channels.

# 7

# Conclusions

Previous equalization techniques for IDMA detection were focused on downlink transmission, where the same channel characteristics was assumed for all users. In turn, it implies that the ISI can be removed with just one DFE equalizer. However, this approach cannot be applied for uplink transmission where the transmitted data for each users arrives at the receiver through different channel characteristics.

The motivation behind this research was to design an equalizer which can be used in conjunction with IDMA detection for uplink transmission. The main objective was to employ a multidimensional equalization with IDMA detection. Multidimensional equalizer basically was designed to remove co-channel interference in the received signal. Then, it employed in conjunction with CDMA to overcome MAI impairments for two users. Moreover, the filter taps of these multidimensional equalizers were determined by using adaptive filters during training mode, hence, there were no derived equations to calculate the optimal filter coefficients.

In this thesis, two types of multidimensional equalizers have been designed for IDMA receiver which are centralized multidimensional equalization and decentralized multidimensional equalization. The centralized multidimensional equalizer depends on crossover filters to remove MAI. However, PIC has been used with decentralized equalizers to eliminate MAI interference in decentralized multidimensional equalizers. Moreover, new equations are derived for centralized

multidimensional equalizers to determine the optimal filter taps. These equations rely on the low correlation property between users' signal, and to this end, it can be used with both IDMA and CDMA detectors.

Centralized multidimensional equalizer is structured as linear and decision feedback equalizer, i.e. MLE and MDFE. The absence of feedback filters in MLE result in a considerable performance degradation, while MDFE shows a consistent efficiency in separating and detecting users' data due to jointly removing MAI and ISI impairments. Simulation results demonstrate improved performance of MDE-IDMA over MDE-CDMA on wireless and shallow water acoustic channels, which is primarily attributed to the use of long interleaver sequence in IDMA that provides lower correlation than the spreading sequence in CDMA. Moreover, the improvement of SINR in crossover filters results in a significant reduction in error propagation during iterative detection that leads to increase the ability of MDE-IDMA in removing MAI effects. Although, the crossover filters provide MDFE with an efficient MAI mitigation, however, these filters are not converged completely during low SNR values. Therefore, an iterative decentralized multidimensional equalizer PIC-DDFE-IDMA has been proposed to resolve this problem.

The proposed PIC-DDFE-IDMA receiver depends on the PIC operations for removing MAI interference. Employing DFE in subtracting ISI and PIC in eliminating MAI provides efficient data detection against channel impairments. The PIC operations require accurate channel coefficients for efficiently removing MAI. For optimal PIC-DDFE-IDMA, LS channel estimation was used for providing the PIC with estimated channel taps, whereas for adaptive equalization the estimated channel taps were obtained by employing RLS and NLMS algorithms during training mode. Although, PIC-DDFE-IDMA was shown to be more robust to the multipath frequency selective channels compared to MDFE-IDMA, MDFE-CDMA and rake IDMA systems, however, it has a higher computational complexity for both NLMS and RLS adaptive algorithms than MDFE-IDMA. Also, the systems robustness against MAI is analyzed by increasing the number of users, PIC-DDFE-IDMA provides higher performance than the other mentioned receivers for up to 10 users. For more than 10 users, the performance of PIC-DDFE-IDMA distinctly decreased as the number of users increased, this is

due to the higher error propagation in feedback filters which significantly affects the efficiency of both PIC and DFE equalizers.

The performance of PIC-DDFE-IDMA could be noticeably improved if further reduction of error propagation through the feedback symbols is obtained. This can be achieved by employing higher coding efficiency such as turbo or LDPC code which results in a significant reduction in the MAI effects.

The processes of equalization and decoding were taking place separately and the feedback symbols from the decoders to the equalizers are converted to hard version symbols before being used by the PIC and the equalizers. However, better performance can be achieved if a soft symbols are returned back to the PIC and the equalizers, such that, the error propagation minimized by using a combination of soft decisions and delayed tentative decisions to cancel ISI at the equalizer and MAI at the PIC. This approach can also be applied to MDFE-IDMA equalizers to provide more reduction in interference effects at the outputs of the equalizers. This idea can be implemented in future works.

# References


[1] John G. Proakis. *Digital Communications*. McGraw Hill, Fourth edition, 2001.

[2] Xiaodong Wang and H.V. Poor. **Blind equalization and multiuser detection in dispersive CDMA channels**. *Communications, IEEE Transactions on*, **46**(1):91–103, Jan 1998.

[3] Thomas A. Edison R. Conot. **A Streak of Luck**. In *DaCapo, New York*, 1979.

[4] S. Verdu. *Multiuser Detection*. Cambridge University Press, 1998.

[5] K.G. Johannsen. **Code division multiple access versus frequency division multiple access channel capacity in mobile satellite communication**. *Vehicular Technology, IEEE Transactions on*, **39**(1):17–26, Feb 1990.

[6] Li Ping, K.Y. Wu, Lihai Liu, and W.K. Leung. **A simple, unified approach to nearly optimal multiuser detection and space-time coding**. In *Information Theory Workshop, 2002. Proceedings of the 2002 IEEE*, pages 53–56, 2002.

[7] Shu Wang, J. Caffery, and B.K. Yi. **Analysis of A Novel Blind Decision-Feedback Interference Cancellation Framework**. In *Global Telecommunications Conference, 2008. IEEE GLOBECOM 2008. IEEE*, pages 1–5, 2008.

[8] Z. Zvonar, D. Brady, and J. Catipovic. **Adaptive detection for shallow-water acoustic telemetry with cochannel interference**. *Oceanic Engineering, IEEE Journal of*, **21**(4):528–536, 1996.

[9] C.C. Tsimenidis, O.R. Hinton, A.E. Adams, and B.S. Sharif. **Underwater acoustic receiver employing direct-sequence spread spectrum and spatial diversity combining for shallow-water multiaccess networking**. *Oceanic Engineering, IEEE Journal of*, **26**(4):594–603, 2001.

[10] S. Houcke, G. Sicot, and M. Debbah. **SPC01-6: Blind Detection for Block Coded Interleaved Division Multiple Access**. In *Global Telecommunications Conference, 2006. GLOBECOM '06. IEEE*, pages 1–5, 2006.

[11] K. Kusume, G. Bauch, and W. Utschick. **IDMA vs. CDMA: Analysis and Comparison of Two Multiple Access Schemes**. *Wireless Communications, IEEE Transactions on*, **11**(1):78–87, 2012.

[12] B. Cristea, D. Roviras, and B. Escrig. **Turbo receivers for interleave-division multiple-access systems**. *IEEE Transactions on Communications*, **57**(7):2090–2097, 2009.

[13] J. Dang, W. Zhang, L. Yang, and Z. Zhang. **OFDM-IDMA with User Grouping**. *IEEE Transactions on Communications*, **61**(5):1947–1955, 2013.

[14] C. Novak, F. Hlawatsch, and G. Matz. **MIMO-IDMA: Uplink Multiuser MIMO Communications using Interleave-Division Multiple Access and Low-Complexity Iterative Receivers**. In *2007 IEEE International Conference on Acoustics, Speech and Signal Processing - ICASSP '07*, **3**, pages III–225–III–228, 2007.

[15] I. M. Mahafeno, C. Langlais, and C. Jego. **OFDM-IDMA versus IDMA with ISI Cancellation for Quasistatic Rayleigh Fading Multipath Channels**. In *Turbo Codes Related Topics; 6th International*

*ITG-Conference on Source and Channel Coding (TURBOCODING), 2006 4th International Symposium on*, pages 1–6, 2006.

[16] C. Novak, G. Matz, and F. Hlawatsch. **IDMA for the Multiuser MIMO-OFDM Uplink: A Factor Graph Framework for Joint Data Detection and Channel Estimation**. *IEEE Transactions on Signal Processing*, **61**(16):4051–4066, 2013.

[17] D. Bai, W. Nam, J. Lee, and I. Kang. **Comments on "A Technique for Orthogonal Frequency Division Multiplexing Frequency Offset Correction"**. *IEEE Transactions on Communications*, **61**(5):2109–2111, 2013.

[18] T. Peng, Y. Xiao, X. He, and S. Li. **Improved Detection of Uplink OFDM-IDMA Signals with Carrier Frequency Offsets**. *IEEE Communications Letters*, **16**(5):646–649, 2012.

[19] Y.K. Won, G.H. Lee, R.-H. Park, J.H. Park, and B.-U. Lee. **Channel equalization techniques for HDTV systems**. *Consumer Electronics, IEEE Transactions on*, **40**(4):903–912, Nov 1994.

[20] J.K. Tugnait, Lang Tong, and Zhi Ding. **Single-user channel estimation and equalization**. *Signal Processing Magazine, IEEE*, **17**(3):16–28, May 2000.

[21] S. Qureshi. **Adaptive equalization**. *Communications Magazine, IEEE*, **20**(2):9–16, March 1982.

[22] M.J. Di Toro. **Communication in time-frequency spread media using adaptive equalization**. *Proceedings of the IEEE*, **56**(10):1653–1679, Oct 1968.

[23] Simon Haykin. *Adaptive Fitler Theory*. Third Edition, 1996.

[24] A. Zaknich. *Principles of Adaptive Filters and Self-Learning Systems*. Springer, 2005.

[25] Ali H. Sayed. *Adaptive Fitlers*. Wiley-IEEE Press, 2008.

[26] A.P. Clark and U.S. Tint. **Linear and non-linear transversal equalizers for baseband channels**. *Radio and Electronic Engineer*, **45**(6):271–283, June 1975.

[27] H.Q. Zhao, X.P. Zeng, J.S. Zhang, Y.G. Liu, and T.R. Li. **Adaptive non-linear filter using a modular polynomial perceptron**. *Signal Processing, IET*, **4**(6):640–649, Dec 2010.

[28] T. Koh and E.J. Powers. **Second-order Volterra filtering and its application to nonlinear system identification**. *Acoustics, Speech and Signal Processing, IEEE Transactions on*, **33**(6):1445–1455, Dec 1985.

[29] J.K. Nelson, A.C. Singer, U. Madhow, and C. S. McGahey. **BAD: bidirectional arbitrated decision-feedback equalization**. *Communications, IEEE Transactions on*, **53**(2):214–218, Feb 2005.

[30] S.K. Wilson and J.M. Cioffi. **Multi-dimensional equalization for adjacent channel interference**. In *Communications, 1991. ICC '91, Conference Record. IEEE International Conference on*, pages 1398–1402 vol.3, 1991.

[31] S.A. Aliesawi, C.C. Tsimenidis, B.S. Sharif, and M. Johnston. **Iterative Multiuser Detection for Underwater Acoustic Channels**. *Oceanic Engineering, IEEE Journal of*, **36**(4):728–744, 2011.

[32] S.N. Qader, C.C. Tsimenidis, M. Johnston, and B.S. Sharif. **Two-way relay network for shallow water channels using CDFE-IDMA detection**. In *Underwater Acoustics internationl conference and exhibition (UAC) , 2013 IEEE*, June 2013.

[33] S.N. Qader, C.C. Tsimenidis, B.S. Sharif, and M. Johnston. **Adaptive detection for asynchronous uplink IDMA shallow-water acoustic channels**. In *Sensor Signal Processing for Defence (SSPD 2012)*, pages 1–5, 2012.

[34] S.N. Qader, C.C. Tsimenidis, M. Johnston, and B.S. Sharif. **Optimization of iterative DFE-IDMA detection for multipath fading channels**. In *Wireless Communications and Networking Conference (WCNC), 2014 IEEE*, pages 1236–1241, April 2014.

[35] S.N. Qader, C.C. Tsimenidis, M. Johnston, and B.S. Sharif. **PIC-DDFE-IDMA Detection for Uplink Shallow Water Acoustic Channels**. In *Underwater Acoustics internationl conference and exhibition (UAC) , 2014 IEEE*, June 2014.

[36] T. S. Rappaport. *Wireless Communications: Theory and Practice*. Prentice-Hall, 2002.

[37] A. Saadani, S. Wendt, P. Gelp, and D. Duponteil. **A tapped delay line model of multipath channel for CDMA systems**. In *Control, Communications and Signal Processing, 2004. First International Symposium on*, pages 783–786, March 2004.

[38] J. Sykora. **Tapped delay line model of linear randomly time-variant WSSUS channel**. *Electronics Letters*, **36**(19):1656–1657, Sep 2000.

[39] Zizheng Li, Lisa M. Zurk, and B. Ma. **Vertical arrival structure of shipping noise in deep water channels**. In *OCEANS 2010*, pages 1–8, Sept 2010.

[40] E. Cheng B. Sun and X. Ou. **Research and simulation on shallow water acoustic channels**. In *Wireless Communication Technology*, pages 11–15 vol.3, 2006.

[41] H. K. Yeo, B.S. Sharif, A.E. Adams, and O.R. Hinton. **Analysis of experimental shallow water network channel and theoretical channel model**. In *OCEANS 2000 MTS/IEEE Conference and Exhibition*, **3**, pages 2025–2029 vol.3, 2000.

[42] Fangkun Jia, En Cheng, and Fei Yuan. **The study on time-variant characteristics of under water acoustic channels**. In *Systems and Informatics (ICSAI), 2012 International Conference on*, pages 1650–1654, May 2012.

[43] D.B. Kilfoyle and A.B. Baggeroer. **The state of the art in underwater acoustic telemetry**. *Oceanic Engineering, IEEE Journal of*, **25**(1):4–27, Jan 2000.

[44] J.M. Hovem, Shefeng Yan, Xueshan Bao, and Hefeng Dong. **Modeling Underwater Communication Links**. In *Sensor Technologies and Applications, 2008. SENSORCOMM '08. Second International Conference on*, pages 679–686, Aug 2008.

[45] C.C. Tsimenidis, B.S. Sharif, O.R. Hinton, and A.E. Adams. **Analysis and modelling of experimental doubly-spread shallow-water acoustic channels**. In *Oceans 2005 - Europe*, **2**, pages 854–858 Vol. 2, June 2005.

[46] W. S. Burdic. *Underwater Acoustic System Analysis*. Prentice Hall, 1991.

[47] R. Urick. *Principles of Underwater Sound*. McGraw Hill, 3rd edition, 1983.

[48] J.A. Catipovic. **Performance limitations in underwater acoustic telemetry**. *Oceanic Engineering, IEEE Journal of*, **15**(3):205–216, Jul 1990.

[49] M. C. Domingo. **Overview of channel models for underwater wireless communication networks**. *Physical Communication*, **1**(3):163–182, 2008.

[50] W. W. Peterson and E. J. Weldon. *Error Correcting Codes*. Cambridge, MA: The MIT Press, Second edition, 1972.

[51] L. Bahl, J. Cocke, F. Jelinek, and J. Raviv. **Optimal decoding of linear codes for minimizing symbol error rate (Corresp.)**. *Information Theory, IEEE Transactions on*, **20**(2):284–287, Mar 1974.

[52] M. Tuchler, A. C. Singer, and R. Koetter. **Minimum mean squared error equalization using a priori information**. *IEEE Transactions on Signal Processing*, **50**(3):673–683, 2002.

[53] W. Koch and A. Baier. **Optimum and sub-optimum detection of coded data disturbed by time-varying intersymbol interference [applicable to digital mobile radio receivers]**. In *Global Telecommunications Conference, 1990, and Exhibition. 'Communications: Connecting the Future', GLOBECOM '90., IEEE*, pages 1679–1684 vol.3, Dec 1990.

[54] J. Erfanian, S. Pasupathy, and P.G. Gulak. **Reduced complexity symbol detectors with parallel structure for ISI channels**. *Communications, IEEE Transactions on*, **42**(234):1661–1671, Feb 1994.

[55] P. Robertson, E. Villebrun, and P. Hoeher. **A comparison of optimal and sub-optimal MAP decoding algorithms operating in the log domain**. In *Communications, 1995. ICC '95 Seattle, 'Gateway to Globalization', 1995 IEEE International Conference on*, **2**, pages 1009–1013 vol.2, Jun 1995.

[56] C. Berrou and A. Glavieux. **Near optimum error correcting coding and decoding: turbo-codes**. *Communications, IEEE Transactions on*, **44**(10):1261–1271, 1996.

[57] C. Douillard. **Iterative correction of intersymbol interference: Turbo equalization**. *European Transactions on Telecommunications*, **6**:507–511, Sep-Oct 1995.

[58] R. Koetter, A.C. Singer, and M. Tuchler. **Turbo equalization**. *Signal Processing Magazine, IEEE*, **21**(1):67–80, Jan 2004.

[59] M. Tuchler and A.C. Singer. **Turbo Equalization: An Overview**. *Information Theory, IEEE Transactions on*, **57**(2):920–952, Feb 2011.

[60] L. Bahl, J. Cocke, F. Jelinek, and J. Raviv. **Optimal decoding of linear codes for minimizing symbol error rate (Corresp.)**. *Information Theory, IEEE Transactions on*, **20**(2):284–287, Mar 1974.

[61] M. Tuchler, R. Koetter, and A.C. Singer. **Turbo equalization: principles and new results**. *Communications, IEEE Transactions on*, **50**(5):754–767, May 2002.

[62] J. HAGENAUER. **The turbo principle: Tutorial introduction and state of the art**. In *Proc. of international Symposium on Turbo Codes*, pages 1–11, Sep 1997.

[63] A. Fertner. **Improvement of bit-error-rate in decision feedback equalizer by preventing decision-error propagation**. *Signal Processing, IEEE Transactions on*, **46**(7):1872–1877, Jul 1998.

[64] R.R. Lopes and J.R. Barry. **The soft-feedback equalizer for turbo equalization of highly dispersive channels**. *Communications, IEEE Transactions on*, **54**(5):783–788, May 2006.

[65] Seongwook Jeong and Jaekyun Moon. **Soft-In Soft-Out DFE and Bi-Directional DFE**. *Communications, IEEE Transactions on*, **59**(10):2729–2741, October 2011.

[66] C. Laot A. Glavieux and J. Labat. **Turbo equalization over a frequency selective channel**. In *Proc. Int. Symp. Turbo Codes, Brest, France*, pages 96–102, Sep. 1997.

[67] Z. Wu and J. Cioffi. **Turbo decision aided equalization for magnetic recording channels**. In *Proc. Global Telecomm. Conf.*, pages 733–738, Dec. 1999.

[68] Xiaodong Wang and H.V. Poor. **Iterative (turbo) soft interference cancellation and decoding for coded CDMA**. *Communications, IEEE Transactions on*, **47**(7):1046–1061, Jul 1999.

[69] H. Poor. *An Introduction to Signal Detection and Estimation*. New York: Springer-Verlag, 1994.

[70] D. Jitsukawa and R. Kohno. **Multiuser equalization using multidimensional lattice filter for DS/CDMA**. In *Universal Personal Communications. 1995. Record., 1995 Fourth IEEE International Conference on*, pages 899–903, 1995.

[71] Xiaodong Wang and H.V. Poor. **Iterative (turbo) soft interference cancellation and decoding for coded CDMA**. *Communications, IEEE Transactions on*, **47**(7):1046–1061, 1999.

[72] Li Ping, Lihai Liu, and W. K. Leung. **A simple approach to near-optimal multiuser detection: interleave-division multiple-access**. In *Wireless Communications and Networking, 2003. WCNC 2003. 2003 IEEE*, **1**, pages 391–396 vol.1, 2003.

[73] Li Ping, Lihai Liu, Keying Wu, and W. K. Leung. **Interleave division multiple-access**. *Wireless Communications, IEEE Transactions on*, **5**(4):938–947, 2006.

[74] R.H. Mahadevappa and J.G. Proakis. **Mitigating multiple access interference and intersymbol interference in uncoded CDMA systems with chip-level interleaving**. *Wireless Communications, IEEE Transactions on*, **1**(4):781–792, 2002.

[75] M.C. Reed, C.B. Schlegel, P.D. Alexander, and J.A. Asenstorfer. **Iterative multiuser detection for CDMA with FEC: near-single-user performance**. *Communications, IEEE Transactions on*, **46**(12):1693–1699, 1998.

[76] S. Moshavi. **Multi-user detection for DS-CDMA communications**. *Communications Magazine, IEEE*, **34**(10):124–136, Oct 1996.

[77] J. Luo, K.R. Pattipati, P.K. Willett, and F. Hasegawa. **Near-optimal multiuser detection in synchronous CDMA using probabilistic data association**. *Communications Letters, IEEE*, **5**(9):361–363, Sept 2001.

[78] Dongning Guo, L.K. Rasmussen, and Teng Joon Lim. **MMSE-based linear parallel interference cancellation in long-code CDMA**. In *Broadband Communications, 2000. Proceedings. 2000 International Zurich Seminar on*, pages 31–38, 2000.

[79] Dongning Guo, L.K. Rasmussen, and Teng Joon Lim. **Linear parallel interference cancellation in long-code CDMA multiuser detection**. *Selected Areas in Communications, IEEE Journal on*, **17**(12):2074–2081, Dec 1999.

[80] L. K. Rasmussen P. H. Tan and J. Luo. **Iterative multiuser decoding based on probabilistic data association**. In *Proc. ISIT, Yokohamma, Japan*, page 301, july 2003.

[81] A. Boariu and R.E. Ziemer. **Multiuser detection in multipath environments for variable spreading-factor CDMA systems**. *Communications, IEEE Transactions on*, **49**(9):1520–1524, Sep 2001.

[82] M. Honig and M.K. Tsatsanis. **Adaptive techniques for multiuser CDMA receivers**. *Signal Processing Magazine, IEEE*, **17**(3):49–61, May 2000.

[83] Junqiang Li, K.B. Letaief, and Zhigang Cao. **Reduced complexity MAP-based iterative multiuser detection for coded multicarrier CDMA systems**. In *Global Telecommunications Conference, 2002. GLOBECOM '02. IEEE*, **1**, pages 916–920 vol.1, Nov 2002.

[84] R. Lupas and S. Verdu. **Near-far resistance of multiuser detectors in asynchronous channels**. *Communications, IEEE Transactions on*, **38**(4):496–508, Apr 1990.

[85] M. Honig, U. Madhow, and S. Verdu. **Blind adaptive multiuser detection**. *Information Theory, IEEE Transactions on*, **41**(4):944–960, Jul 1995.

[86] Xiaodong Wang and H.V. Poor. **Blind multiuser detection: a subspace approach**. *Information Theory, IEEE Transactions on*, **44**(2):677–690, Mar 1998.

[87] H.V. Poor. **Iterative multiuser detection**. *Signal Processing Magazine, IEEE*, **21**(1):81–88, Jan 2004.

[88] M.J. Juntti. **Multiuser detector performance comparisons in multirate CDMA systems**. In *Vehicular Technology Conference, 1998. VTC 98. 48th IEEE*, **1**, pages 31–35 vol.1, May 1998.

[89] J. Boutros and G. Caire. **Iterative multiuser joint decoding: unified framework and asymptotic analysis**. *Information Theory, IEEE Transactions on*, **48**(7):1772–1793, Jul 2002.

[90] M. Moher and P. Guinand. **An iterative algorithm for asynchronous coded multiuser detection**. *Communications Letters, IEEE*, **2**(8):229–231, Aug 1998.

[91] M.C. Reed and P.D. Alexander. **Iterative multiuser detection using antenna arrays and FEC on multipath channels**. *Selected Areas in Communications, IEEE Journal on*, **17**(12):2082–2089, Dec 1999.

[92] Li Ping, Lihai Liu, K. Y. Wu, and W. K. Leung. **Approaching the capacity of multiple access channels using interleaved low-rate codes**. *Communications Letters, IEEE*, **8**(1):4–6, 2004.

[93] H. Wu, L. Ping, and A. Perotti. **User-specific chip-level interleaver design for IDMA systems**. *Electronics Letters*, **42**(4):233–234, Feb 2006.

[94] I. Pupeza, A. Kavcic, and Li Ping. **Efficient Generation of Interleavers for IDMA**. In *Communications, 2006. ICC '06. IEEE International Conference on*, **4**, pages 1508–1513, June 2006.

[95] Zhang Chenghai and Hu Jianhao. **2-Dimension Interleaver Design for IDMA Systems**. In *Circuits and Systems for Communications, 2008. ICCSC 2008. 4th IEEE International Conference on*, pages 372–376, May 2008.

[96] Lihai Liu, W. K. Leung, and Li Ping. **Simple iterative chip-by-chip multiuser detection for CDMA systems**. In *Vehicular Technology Conference, 2003. VTC 2003-Spring. The 57th IEEE Semiannual*, **3**, pages 2157–2161 vol.3, April 2003.

[97] S. Ten Brink. **Convergence behavior of iteratively decoded parallel concatenated codes**. *Communications, IEEE Transactions on*, **49**(10):1727–1737, Oct 2001.

[98] S. Aliesawi, C.C. Tsimenidis, B.S. Sharif, and M. Johnston. **Performance comparison of IDMA receivers for underwater acoustic channels**. In *Wireless Communication Systems (ISWCS), 2010 7th International Symposium on*, pages 596–600, 2010.

[99] C. Berrou, A Glavieux, and P. Thitimajshima. **Near Shannon limit error-correcting coding and decoding: Turbo-codes. 1**. In *Communications, 1993. ICC '93 Geneva. Technical Program, Conference Record, IEEE International Conference on*, **2**, pages 1064–1070 vol.2, May 1993.

[100] Andrej Stefanov and Tolga M. Duman. **Turbo coded modulation for wireless communications with antenna diversity**. *Communications and Networks, Journal of*, **2**(4):356–360, Dec 2000.

[101] D. Divsalar, Marvin K. Simon, and Dan Raphaeli. **Improved parallel interference cancellation for CDMA**. *Communications, IEEE Transactions on*, **46**(2):258–268, Feb 1998.

[102] Kai Li, Xiaodong Wang, and Li Ping. **Analysis and Optimization of Interleave-Division Multiple-Access Communication Systems**. *Wireless Communications, IEEE Transactions on*, **6**(5):1973–1983, 2007.